AD-A039 159 NAVAL POSTGRADUATE SCHOOL MONTEREY CALIF F/G 17/9
IMPLEMENTATION OF A SIDELOBE BLANKING SYSTEM ON THE AN/SPS-12 R--ETC(U)
MAR 77 P P ARANCIBIA

UNCLASSIFIED NL

1 OF 2
ADA
039159

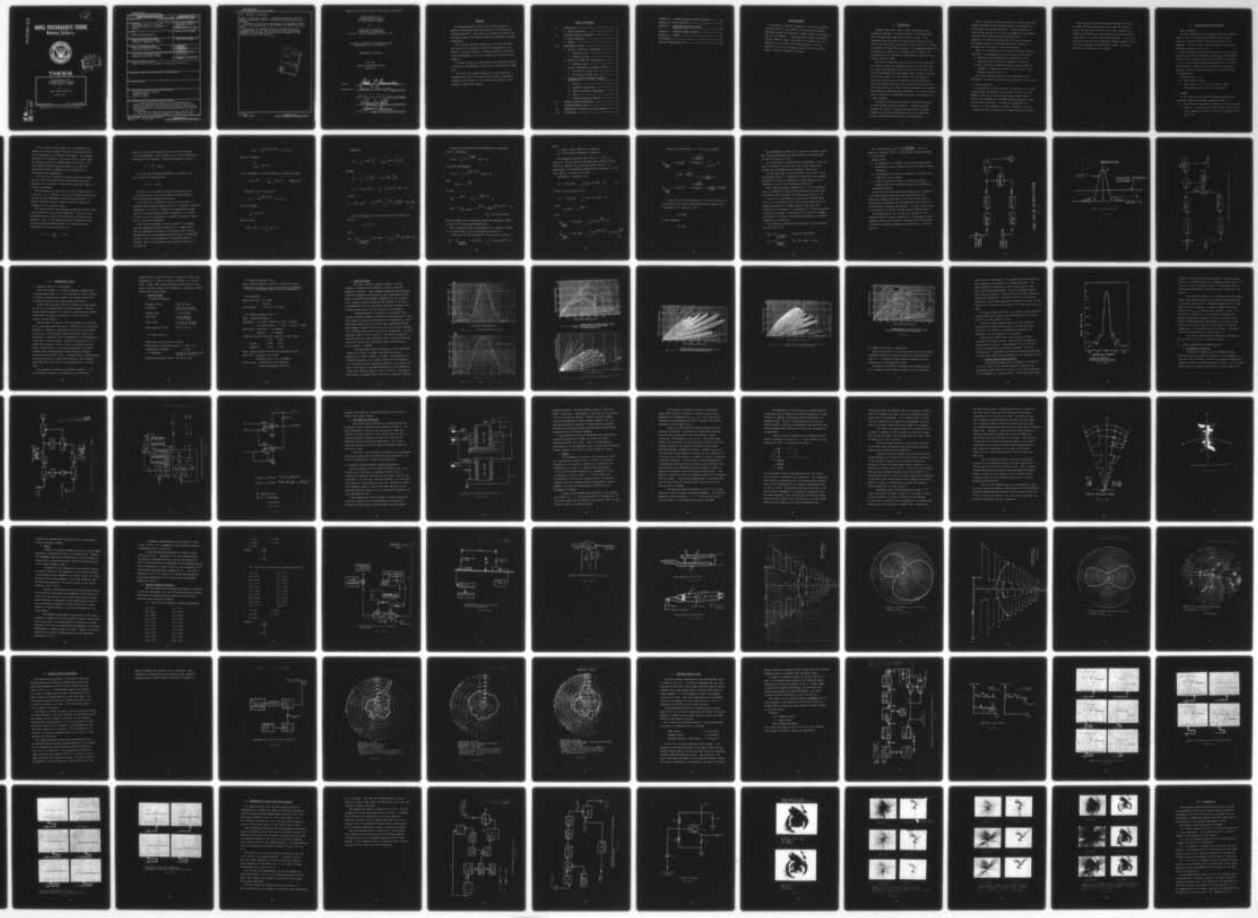

(2) NW

NAVAL POSTGRADUATE SCHOOL
Monterey, California

THESIS

IMPLEMENTATION OF A
SIDELOBE BLANKING SYSTEM
ON THE AN/SPS-12 RADAR

by

Pedro Pablo Arancibia

March 1977

Thesis Advisor: D. B. Hoisington

UNCLASSIFIED

SECURITY CLASSIFICATION OF THIS PAGE (When Data Entered)

REPORT DOCUMENTATION PAGE		READ INSTRUCTIONS BEFORE COMPLETING FORM
1. REPORT NUMBER	2. GOVT ACCESSION NO. (2) Master's thesis,	3. RECIPIENT'S CATALOG NUMBER
4. TITLE (and Subtitle) (6) Implementation of a Sidelobe Blanking System on the AN/SPS-12 Radar.		5. TYPE OF REPORT & PERIOD COVERED Engineer's Thesis; March 1977
		6. PERFORMING ORG. REPORT NUMBER
7. AUTHOR(s) (10) Pedro Pablo Arancibia		8. CONTRACT OR GRANT NUMBER(s)
9. PERFORMING ORGANIZATION NAME AND ADDRESS Naval Postgraduate School Monterey, California 93940		10. PROGRAM ELEMENT, PROJECT, TASK AREA & WORK UNIT NUMBERS
11. CONTROLLING OFFICE NAME AND ADDRESS Naval Postgraduate School Monterey, California 93940 (11)		12. REPORT DATE Mar[illegible]977
		13. NUMBER OF PAGES (12) 144 p.
14. MONITORING AGENCY NAME & ADDRESS(if different from Controlling Office) Naval Postgraduate School Monterey, California 93940		15. SECURITY CLASS. (of this report) Unclassified
		15a. DECLASSIFICATION/DOWNGRADING SCHEDULE

16. DISTRIBUTION STATEMENT (of this Report)

Approved for public release; distribution unlimited.

17. DISTRIBUTION STATEMENT (of the abstract entered in Block 20, if different from Report)

18. SUPPLEMENTARY NOTES

19. KEY WORDS (Continue on reverse side if necessary and identify by block number)

Sidelobe Blanking System
AN/SPS-12 Radar
AN/UPS-1 Radar

20. ABSTRACT (Continue on reverse side if necessary and identify by block number)

A sidelobe blanking system can be looked upon as a method for maximizing main-lobe-detection and minimizing sidelobe detection. The system is intended to provide only main-beam signals and thereby producing unambiguous bearing information.

The sidelobe blanking system turns the video off when the signal in an auxiliary antenna is stronger than the → OVER

DD FORM 1 JAN 73 1473 (Page 1) EDITION OF 1 NOV 65 IS OBSOLETE S/N 0102-014-6601

UNCLASSIFIED

SECURITY CLASSIFICATION OF THIS PAGE (When Data Entered)

251450

(20. ABSTRACT Continued)

signal in the main antenna. Sidelobe blanking is best for pulse interference, and is not suitable for sidelobe noise jamming.

In order to carry out experiments with sidelobe blanking a system was implemented on the AN/UPS-1 and AN/SPS-12 radar sets.

The theory of sidelobe blanking and the design and implementation of the working circuits used is presented, together with pictures of the system and examples of the displayed signals and results.

Approved for public release; distribution unlimited.

Implementation of a Sidelobe Blanking System on the AN/SPS-12 Radar

by

Pedro Pablo Arancibia
Lieutenant, Chilean Navy
M.S.A.E., Naval Postgraduate School, 1977

Submitted in partial fulfillment of the requirements for the degree of

AERONAUTICAL ENGINEER

from the

NAVAL POSTGRADUATE SCHOOL

March 1977

Author Pedro P. Arancibia

Approved by: David B. Horsington
Thesis Advisor

John M. Boudry
Second Reader

Richard W. Bell
Chairman, Department of Aeronautics

Robert R. Fossum
Dean of Science and Engineering

ABSTRACT

A sidelobe blanking system can be looked upon as a method for maximizing main-lobe-detection and minimizing sidelobe detection. The system is intended to provide only main-beam signals and thereby producing unambiguous bearing information.

The sidelobe blanking system turns the video off when the signal in an auxiliary antenna is stronger than the signal in the main antenna. Sidelobe blanking is best for pulse interference, and is not suitable for sidelobe noise jamming.

In order to carry out experiments with sidelobe blanking a system was implemented on the AN/UPS-1 and AN/SPS-12 radar sets.

The theory of sidelobe blanking and the design and implementation of the working circuits used is presented, together with pictures of the system and examples of the displayed signals and results.

TABLE OF CONTENTS

ACKNOWLEDGMENT

The author is sincerely grateful to his thesis advisor, Professor David B. Hoisington, for his patient guidance, dedicated counsel and continual support during the preparation of this thesis. I also received valuable assistance from Mr. Ross M. Seely, Supervisor of the Radar and E.C.M. Laboratory of the Naval Postgraduate School. For the patience and the moral support provided by my wife Maria Elena I reserve my deepest gratitude.

I. INTRODUCTION

Antennas for search radars which continuously scan through 360 degrees in azimuth usually are characterized by a high-gain main lobe and many minor lobes. It is important that the minor lobe gain be very much less than that of the relatively narrow main lobe in order to (a) have an antenna with high main lobe gain, (b) reduce the possibility of detecting a target on a sidelobe, and (c) reduce the susceptibility of the radar to interfering signals arriving through the side lobes.

The field in the main lobe and the first few side lobes of a radar antenna are determined chiefly by the amplitude and phase distributions of the field in the aperture (for both the Fraunhofer and the Fresnel zone); however the rest of the minor lobes in a 360° pattern are influenced by many other factors such as spillover and back radiation from the primary feed horn, edge currents on the reflector, scattering off of the primary feed and supporting structures and leakage through mesh type reflectors. All these factors make it difficult to completely eliminate the sidelobes in a radar antenna.

A method of reducing the effects of sidelobe signals is the sidelobe blanking technique. Sidelobe blanking systems are useful in preventing acquisition of strong targets in the antenna sidelobes and also in rejecting pulsed interference originating in the sidelobes.

With an effective sidelobe blanker one expects that only signals received through the main beam of the antenna will be available for display purposes. Signals received by the rotating antenna of the radar are compared with signals received from an omnidirectional fixed antenna. A comparator is used that blanks the video output whenever the signal received in the omnidirectional channel is stronger than the signal in the main channel.

There are different ways of using the sidelobe blanking technique. Two approaches will be treated in this work.

(a) Sidelobe blanking employing a directional and an omnidirectional antenna as heretofore described,

(b) The technique of sidelobe clutter blanking which is designed to reduce the ground clutter entering the antenna sidelobes [Ref. 1].

This second approach has not been implemented here. The theory and general description are included in Appendix A.

A. THESIS OBJECTIVE

The objective of this work was to eliminate, or at least reduce as much as possible, the display in the PPI of the AN/UPS-1 radar set of any low-duty-cycle signal coming through the sidelobes of the radar antenna, using the sidelobe blanking technique. In order to accomplish this objective it was necessary to design, implement, and test a comparator-blanker system and an omnidirectional antenna.

Both elements and the system were designed and built to match the characteristics of the radar set AN/UPS-1. During the last third of this work it was necessary to switch to the AN/SPS-12 radar because the initial AN/UPS-1 radar went out of service for major overhaul. It was then necessary to build a new comparator-blanker system to work with the parameters of the AN/SPS-12 radar. The omni-directional antenna was not changed.

II. SIDELOBE BLANKING TECHNIQUE

A. BASIC PRINCIPLE

The basic operation of the sidelobe blanking system is shown in Fig. II-1 where the detected outputs of two channels, identical except for antenna patterns, are compared. Typical relative antenna patterns for the two channels are shown in Fig. II-2.

When the target or pulsed interference is in the sidelobes of the acquisition antenna, the output from channel B ideally will be greater than that of channel A (assuming $a > b$) so that the thresholded difference can be used to blank channel A before the final detection circuits or displays, thereby preventing display of sidelobe targets or interference.

Looking at Fig. II-1

(a) gate normally closed

(b) when signal $|B| \geq |A|$ switch must be opened thereby preventing output to the display.

B. THEORY

In the design of the sidelobe blanking system three questions immediately present themselves [Ref. 2],

(1) What loss in performance (compared to a single channel system) is incurred due to the presence of the sidelobe suppression channel in detecting targets in the main lobe?

(2) How should the threshold detectors be set to achieve a specified level of performance?

(3) What antenna gain is required in the sidelobe suppression channel?

A sidelobe blanking system is studied and the relationship between the probability of main lobe detection is given in terms of false-alarm probability, signal-to-noise ratio, and the ratio of gains of the two channels.

A mathematical equivalent to Fig. II-1 with respect to calculating the single-hit detection probability is given in Fig. II-3. The presence of receiver noise in each channel causes a departure from ideal behavior, and it becomes necessary, by proper choice of sidelobe suppression (SLS) antenna gain and threshold levels F and α_o (corresponding to threshold detectors 1 and 2, respectively), to obtain a satisfactory compromise between three conflicting requirements. Namely, for a given false-alarm probability one seeks to maximize probability of detection in the main lobe, to minimize probability of detection in the sidelobes, and to minimize the size of the SLS antenna.

If u and v denote the square-law detected outputs of receivers A and B respectively, looking at Fig. II-3 it can be determined that the probability of u exceeding threshold α_o so that we have output to the detection circuits is given by,

$$P_o = P(u > \alpha_o , \frac{v}{u} < F)$$

The domain of u and v, which result in threshold α_o being exceeded, is shown by the shaded region R in Fig. II-4.

The joint probability density function of u and v for the same P_o is given by,

$$P_o = \iint_R p(u,v)\, du\, dv$$

$$P_o = \int_{\alpha_o}^{\infty} p_u(u) \int_0^{V=Fu} p_v(v)\, dv\, du$$

Assuming that u and v are independent variables, so that,

$$p(u,v) = p_u(u)\, p_v(v)$$

then

$$\int_0^{V=Fu} p_v(v)\, dv = 1 - \int_{V=Fu}^{\infty} p_v(v)\, dv$$

where $p_u(u)$ and $p_v(v)$ are known density functions depending upon signal-to-noise ratio, so that P_o can be rewritten as

$$P_o = \int_{\alpha_o}^{\infty} p_u(u) \left[1 - \int_{V=Fu}^{\infty} p_v(v)\, dv \right] du$$

If the output of the receiver can be observed for a length of time much greater than one correlation period, it is advantageous to integrate the output. The simplest concept of an integrator is a device which linearly adds the voltage output of N samples from the detector. The time elapsing between samplings must be at least one correlation period, in order that the samples may be considered to be independent.

If the sum of N variates of signal-plus-noise exceeds the bias level calculated from the probability density function for N variates of noise alone, then the signal is said to be detected.

The integrator may take the sum of the squares of the N variates, or, in general, the sum of N variates where each variate has been processed by some general function. As long as the same weight is applied to each variate, the integrator will be called linear.

The function which the integrator applies to each variate will be called the law of the integrator. The law of the integrator acts in exactly the same way as the law of the detector. Thus, if the detector output is defined as any device whose instantaneous output is a function of the envelope of the input wave only, with

$$y = f\left(\frac{R}{\sqrt{\psi_o}}\right) = F(v)$$

where ψ_o is the mean square value of the noise voltage, R is the amplitude of the envelope, and v is the normalized amplitude of the envelope. Then the integrator output is

$$Y = \sum_{1}^{N} \phi[F(v)]$$

As far as the theoretical problem is concerned, the only function of importance is,

$$\psi(v) = \phi[F(v)]$$

There will be an infinite number of combinations of ϕ and F functions which will produce the same function ψ and hence the same theoretical results.

It is seen, by a process of trial and error [Ref. 3], that the best possible function for $\psi(v)$ to produce integrable functions is $\psi(v) = Av^2$. Though this represents a square law for the combined detector and integrator, it is usual to think of it as representing a square-law detector coupled with a linear-law integrator.

Now, for the purposes of this analysis it is assumed that the square-law detected output is u = (amplitude)^2 and the predetection outputs of receivers A and B consist, respectively, of nonfluctuating pulsed signals of amplitude s_o and r, each in the presence of independent additive gaussian noise with normalized unit variance, then $p_v(v)$ is given by

$$p_v(v) = \frac{1}{2} e^{-1/2(v + r_o^2)} \quad I_o\ (\sqrt{v}\ \ r_o)$$

Then the integral

$$\int_{v = Fu}^{\infty} p_v(v)\ dv$$

can be expressed in terms of Marcum's Q function, where

$$Q(r_o,\ \sqrt{Fu}\ ) = \int_{V=Fu}^{\infty} p_v(v)\ dv \qquad \text{[Appendix B]}$$

Similarly, $p_u(u)$ is given by,

$$p_u(u) = \frac{1}{2} e^{-\frac{1}{2}(u + s_o^2)} \quad I_o\ (\sqrt{u}\ \ s_o)$$

and the integral

$$\int_{\alpha_o}^{\infty} p_u(u)\ du$$

can be written

$$Q(s_o,\ \sqrt{\alpha_o}\ ) = \int_{\alpha_o}^{\infty} p_u(u)\ du$$

Therefore,

$$P_o = \int_{\alpha_o}^{\infty} p_u(u) \left[1 - \int_{v=Fu}^{\infty} p_v(v)\, dv \right] du$$

becomes

$$P_o = \int_{\alpha_o}^{\infty} p_u(u) \left[1 - Q(r_o, \sqrt{Fu}\,) \right] du$$

$$P_o = Q(s_o, \sqrt{\alpha_o}\,) - \int_{\alpha_o}^{\infty} p_u(u)\, Q(r_o, \sqrt{Fu}\,)\, du$$

so that

$$P_o = Q(s_o, \sqrt{\alpha_o}\,) - \frac{1}{2} e^{-\frac{1}{2} s_o^2} \int_{\alpha_o}^{\infty} e^{-\frac{1}{2} u} I_o(\sqrt{u s_o^2}\,)\, Q(r_o, \sqrt{Fu}\,)\, du$$

Now, the probability of false alarm can be obtained by setting

$$s_o = r_o = 0$$

Then,

$$P_{FA} = P_o\Big|_{\substack{\text{no signal} \\ \text{present}}} = Q(0, \sqrt{\alpha_o}\,) - \frac{1}{2} \int_{\alpha_o}^{\infty} e^{-\frac{1}{2} u}\, Q(0, \sqrt{Fu}\,)\, du$$

Since we are considering the probability of detection with no integration,

$$Q(\alpha,\beta) = \int_{\beta}^{\infty} ve^{-\frac{v^2+\alpha^2}{2}} I_o(\alpha v)\ dv$$

or in this development

$$Q(u,v) = \int_{v}^{\infty} xe^{-\frac{1}{2}(x^2+u^2)} I_o(ux)\ dx$$

Then,

$$Q(0,v) = e^{-\frac{1}{2}v^2}$$

so that

$$P_{FA} = e^{-\frac{1}{2}\alpha_o} - \frac{1}{2}\int_{\alpha_o}^{\infty} e^{-\frac{1}{2}u(1+F)}\ du$$

$$P_{FA} = P_o\Big|_{\text{no signal}} = e^{-\frac{1}{2}\alpha_o} - \frac{1}{1+F}e^{-\frac{1}{2}\alpha_o(1+F)} \qquad \text{(a)}$$

[P_{FA} for noise alone]

which provides the relationship between the threshold levels, α_o, and F, and false-alarm probability.

For a specified false-alarm probability a range of values for α_o exists each with a corresponding value for F.

In the same way the probability of detection is given by

$$P_D = P_o\Big|_{\substack{\text{signal}\\ \text{present}}} = Q(s_o,\sqrt{\alpha_o}) - \int_{\alpha_o}^{\infty} p_u(u)Q(r_o,\sqrt{Fu})\ du$$

where

s_o = pulse signal amplitude in channel A

r_o = pulse signal amplitude in channel B

The assumption has been made that a << 1 and b << 1 (see Fig. II-2) so that for the main-lobe signal-to-noise ratios of interest, the sidelobe channel SNR is << 1. Accordingly, in calculating probability of detection in the main lobe, r_o is taken to be zero.

Therefore, in the main lobe,

$$P_D = Q(s_o, \sqrt{\alpha_o}) - \int_{\alpha_o}^{\infty} p_u(u)\, Q(0, \sqrt{Fu}\,)\, du \qquad (b)$$

while in the sidelobes P_D is,

$$P_D = Q(s_o, \sqrt{\alpha_o}) - \int_{\alpha_o}^{\infty} p_u(u)\, Q(r_o, \sqrt{Fu}\,)\, du.$$

Since

$$Q(0, \sqrt{Fu}\,) = e^{-\frac{1}{2}Fu}$$

then

$$P_D\Big|_{\substack{\text{main}\\ \text{lobe}}} = Q(s_o, \sqrt{\alpha_o}\,) - \int_{\alpha_o}^{\infty} p_u(u)\, e^{-\frac{1}{2}Fu}\, du$$

$$P_D\Big|_{\substack{\text{main}\\ \text{lobe}}} = Q(s_o, \sqrt{\alpha_o}\,) - \int_{\alpha_o}^{\infty} \frac{1}{2}\, e^{-\frac{1}{2}(u + s_o^2)}\, I_o(\sqrt{u}\, s_o)\, e^{-\frac{1}{2}Fu}\, du$$

Making the substitution $\omega = (1+F)u$, P_D becomes

$$P_D\Big|_{\substack{\text{main}\\\text{lobe}}} = Q(s_o, \sqrt{\alpha_o}) - \frac{e^{\left[-\frac{s_o^2 F}{2(1+F)}\right]}}{1+F} \int_{\alpha_o(1+F)}^{\infty} \frac{1}{2} \cdot$$

$$\cdot e^{\left[-\frac{1}{2}(\omega + \frac{s_o^2}{1+F})\right]} \cdot I_o\left[\sqrt{\omega}\,\frac{s_o}{\sqrt{1+F}}\right] d\omega$$

$$P_D\Big|_{\substack{\text{main}\\\text{lobe}}} = Q(s_o, \sqrt{\alpha_o}) - \frac{e^{\left[-\frac{s_o^2 F}{2(1+F)}\right]}}{1+F} \cdot Q\left(\frac{s_o}{\sqrt{1+F}}, \sqrt{\alpha_o(1+F)}\right)$$

If the ratio of the sidelobe gain of the SLS antenna to the sidelobe gain of the acquisition (radar) antenna (ACQ) is denoted by β^2, from Fig. II-2,

$$\beta^2 = \left(\frac{a}{D}\right)^2$$

in the sidelobes

$$r_o = \beta s_o \quad .$$

The performance results for a variety of sidelobe levels and threshold settings have been obtained using equations (a) and (b) [see Fig. II-5].

It is seen that the probability of detection in the main lobe is monotonic with SNR and, for a given false-alarm probability, increases with increasing values of F.

On the other hand, in the sidelobes, for a given ratio of sidelobe gains β^2, probability of detection is no longer monotonic with SNR but possesses a single maximum, which increases in value with increasing values of F.

This latter statement assumes that $F < \beta^2$, a condition that is necessary to obtain sidelobe blanking at high SNR. The maximum also increases with decreasing values of β^2.

Since it is of interest to minimize the maximum value of P_D in the sidelobes, this can be accomplished either by lowering threshold F, thereby reducing the main-lobe probability of detection, or increasing β^2, thereby requiring a larger SLS antenna. Increasing β^2 can allow an increase in threshold F without a corresponding increase in sidelobe probability of detection.

The numerical results can be summarized in the following way (see Fig. II-5)

$$P_{FA} = P_o\Big|_{\substack{\text{no signal}\\ \text{present}}} \qquad [P_{FA} \text{ for noise alone}]$$

$$P_D = P_o\Big|_{\substack{\text{signal}\\ \text{present}}} \qquad [P_D \text{ for signal + noise}]$$

For a specified P_{FA} and $\beta = \frac{a}{b} \left(\frac{\text{SLS GAIN}}{\text{ACQ SLG}}\right)$ P_D can be found as a function of SNR. For main lobe detection assume v is noise alone.

Results show:

(1) As threshold F is lowered, main lobe P_D drops since probability that SLS channel noise will cause blanking increases.

(2) As threshold F is raised, sidelobe P_D increases since blanking is less likely.

(3) Larger F means less chance of blanking, greater possibility that a sidelobe signal will be detected.

Concluding Remarks.

While variation of threshold settings allows a trade-off to be made between maximizing main-lobe detection and minimizing sidelobe detection, it is likely that the two conflicting requirements can be resolved only by choice of a sufficiently high-gain SLS antenna. The gain required can be calculated in terms of the ACQ antenna sidelobe level.

The detectability loss on main-lobe targets in the sidelobe blanking system, relative to a conventional single-channel system, can be found by comparing the SNR required to achieve a specified probability of detection in the two systems.

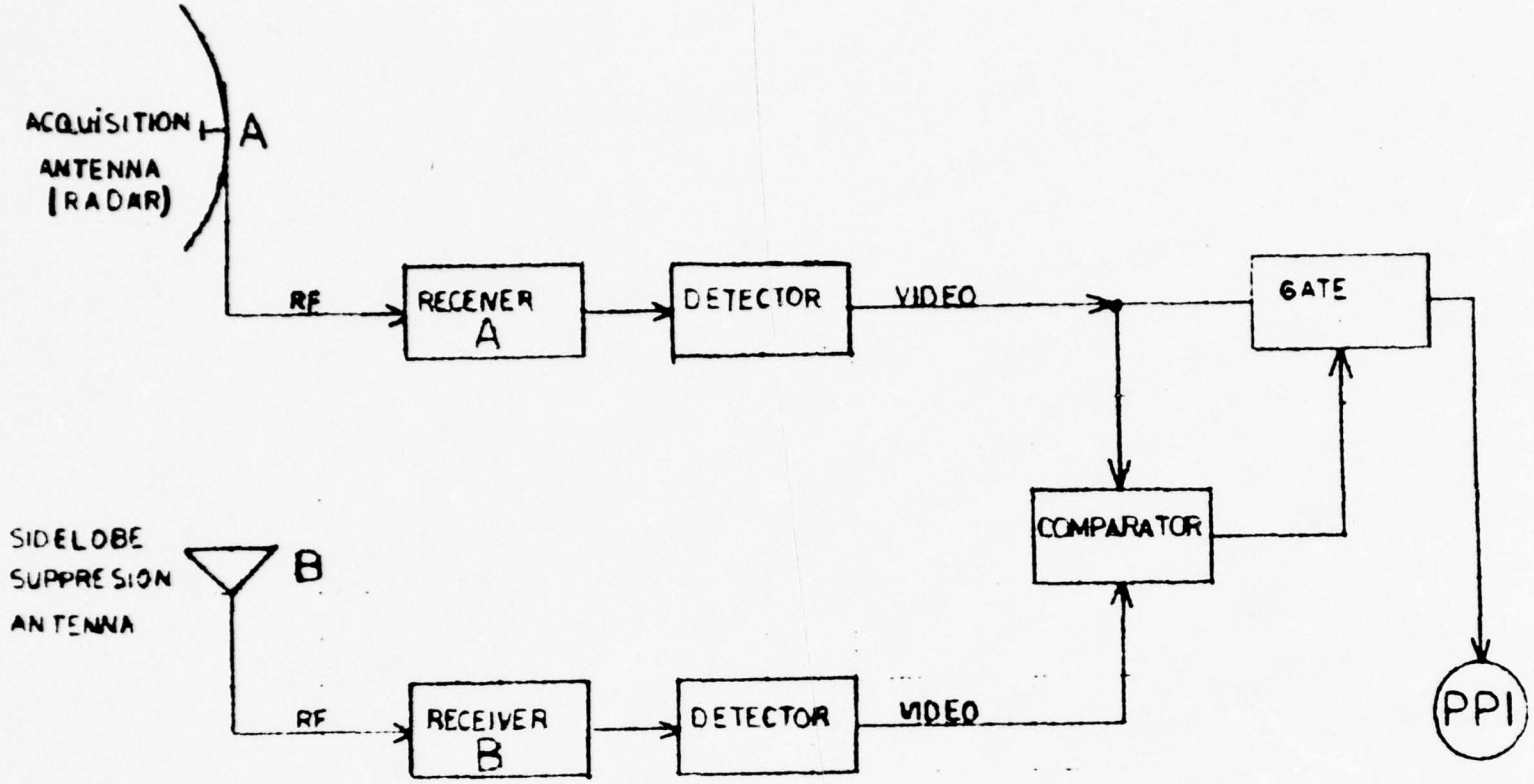

BASIC SIDELOBE BLANKING SYSTEM

FIG. II-1

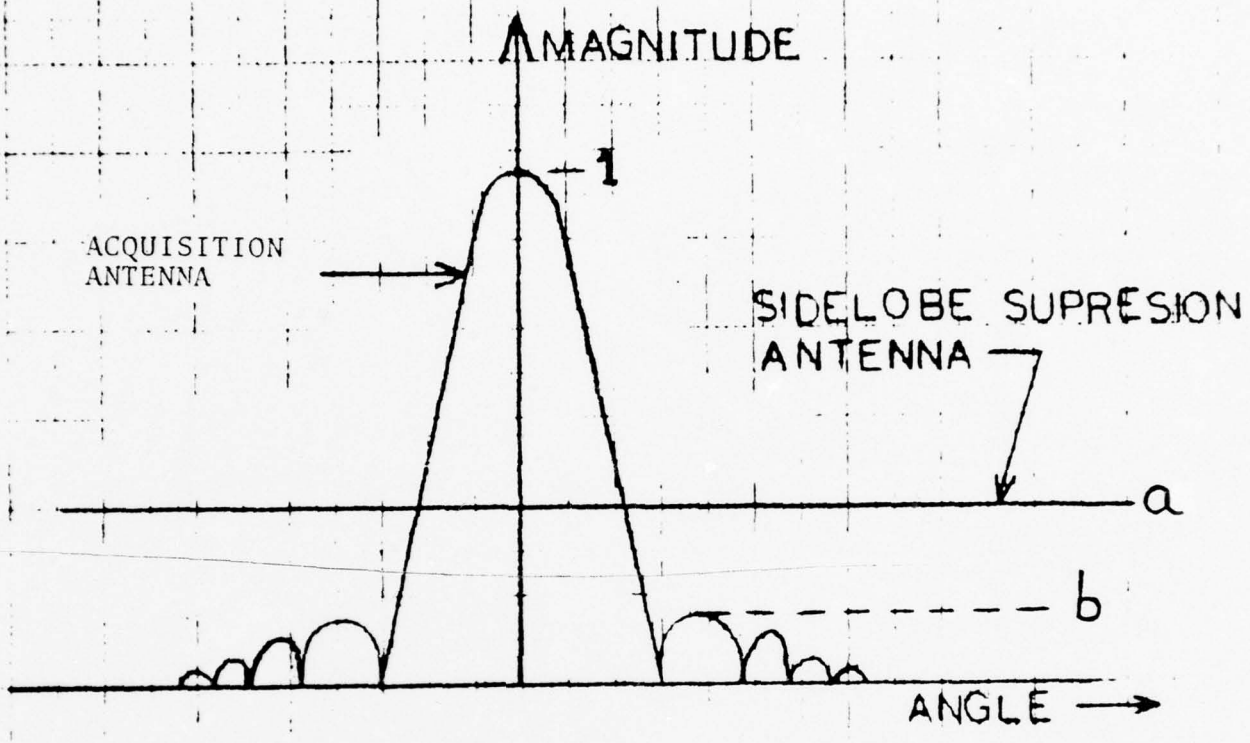

IDEALIZED ANTENNA PATTERN

FIG. II-2

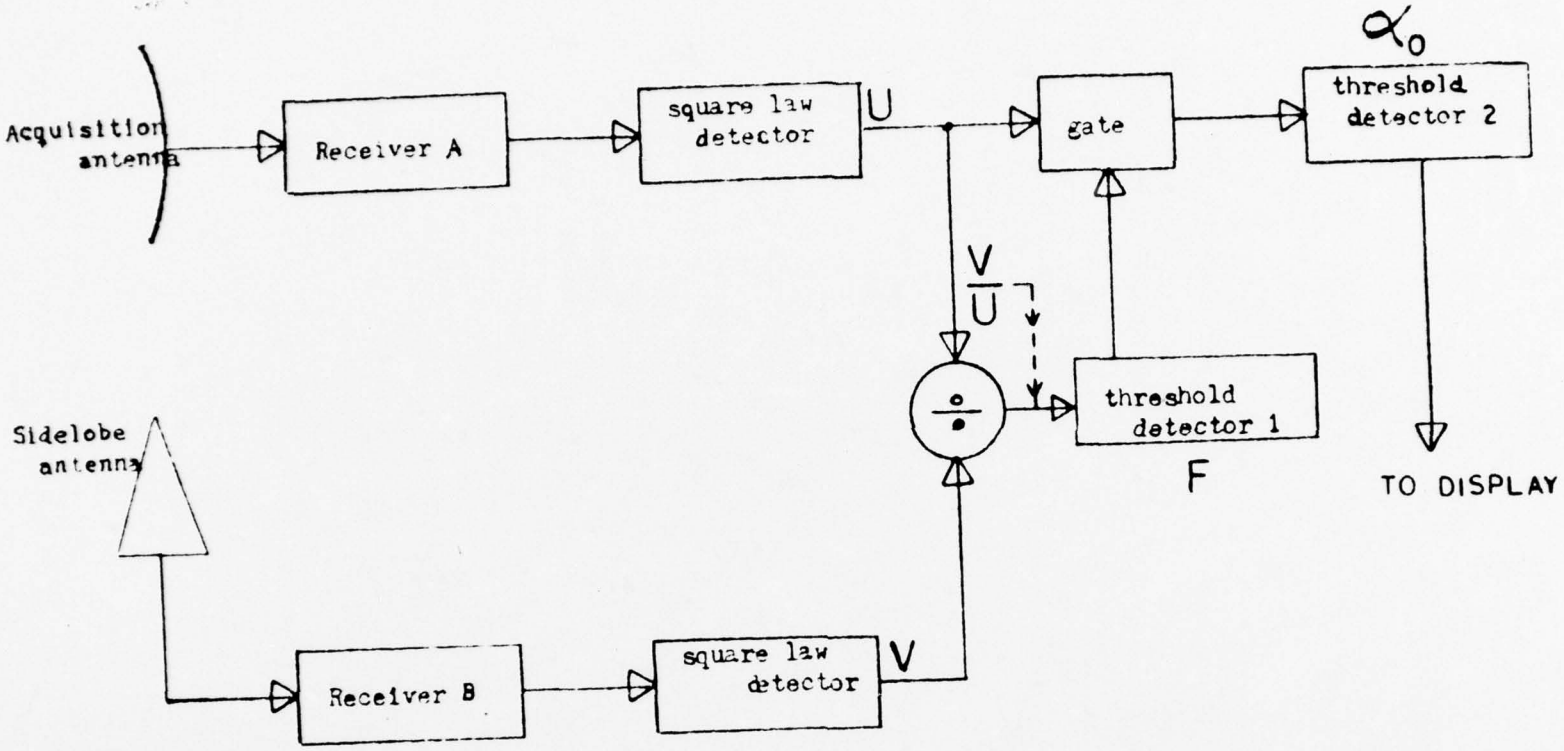

EQUIVALENT CIRCUIT OF SIDELOBE BLANKING SYSTEM

FIG. II-3

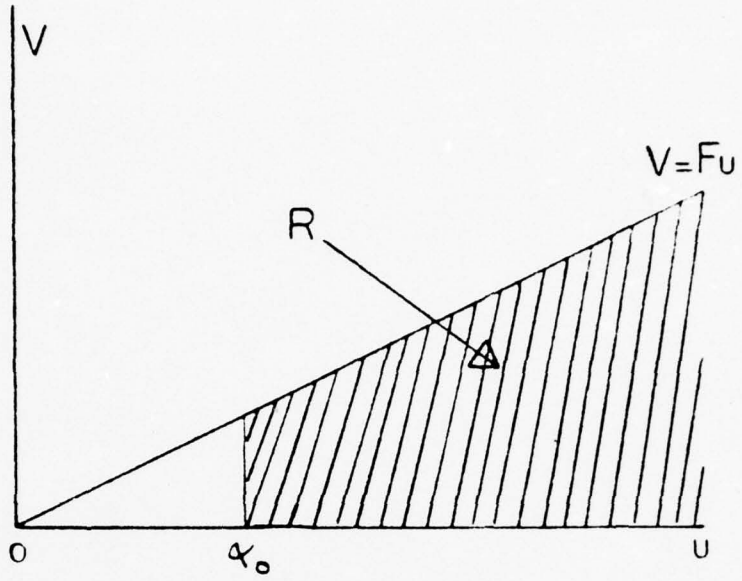

Domain of u and v , which result in threshold α_o being exceeded

FIG. II-4

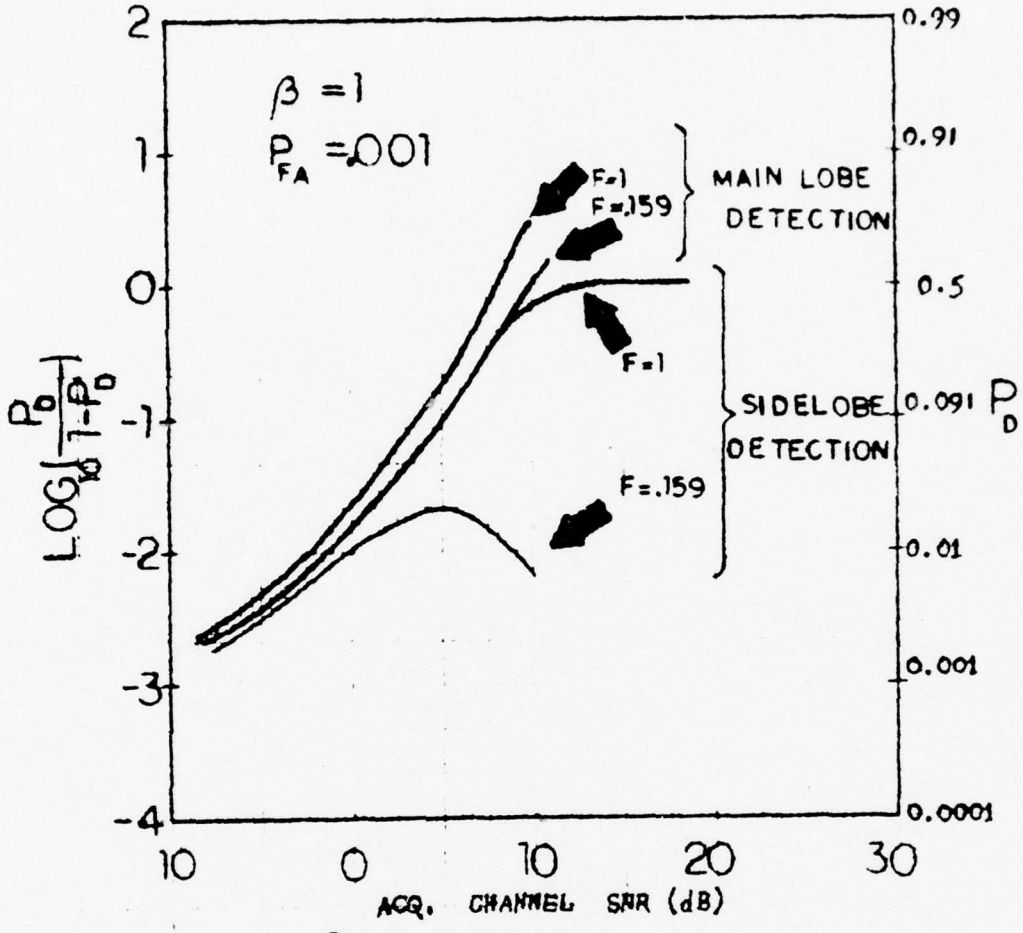

PERFORMANCE RESULTS FOR A VARIETY
OF SIDELOBE LEVELS AND THRESHOLD SETTINGS

FIG. II-5

III. EXPERIMENTAL SET-UP

A. RADAR SET AN/UPS-1, DESCRIPTION

Radar Set AN/UPS-1 is a genral purpose, transportable radar equipment [Ref. 4]. It is designed for tower (assault) or shelter installation to detect air targets and give an accurate determination of their range and bearing.

An MTI (moving target indicator) system is incorporated as an aid to the enhancement of moving targets. This MTI system reduces response to clutter or fixed objects, thereby effectively increasing the ability of the radar set to detect a moving target.

The equipment is capable of being operated at altitudes up to 10000 feet above sea level. Aside from the limitations imposed by atmospheric conditions and physical surroundings of the radar installations (nearby mountains, trees, and buildings), limitations due to dimensions of the transmitted radar beam are also present. Reliable detection on a one square meter target, without relying on ground reflection signal reinforcement, is provided between points having a maximum range corresponding to approximately 10-degree elevation angle at 30000 feet, a maximum range of approximately 100 nautical miles at 30000 feet elevation, and a maximum range near the radar horizon of approximately 80 nautical miles.

The equipment is capable of resolving targets (i.e., discriminating between two reflections) when they are

separated by at least 1500 feet in range at 20 miles and separated by at least 4 degrees in azimuth at a 50 mile range. Under ideal ground reflection conditions or over water, maximum ranges can be expected to increase to almost double those stated above.

1. Technical Data

(a) Radar Transmitter

Frequency range	1200-1350 MHz
Wavelength	24 cm at 1250 MHz 22.2 cm at 1350 MHz
Average power	1.6 KW maximum
Peak power	1.4 MW maximum 1.0 MW minimum
Pulse width	1.4 μsec at 800 pps 4.2 μsec at 267 pps
Pulse repetition rate	800 or 267 pps

(b) Radar Receiver

Stabilized local oscillator (stalo)	
Noise figure (including duplexer)	9 dB or less
Intermediate frequency	30 MHz
I.F. bandwidth	1.5 Mc at 20, 40, 80 miles 0.45 Mc at 275 miles
Minimum discernible signal	-105 dBm or less

(c) Signal Comparator (MTI)

Type; coherent type MTI circuit in receiving channel

Subclutter visibility figure (in searchlight operation); 20 to 30 dB dependent upon stability of magnetron.

(d) Indicators

Types and sizes: PPI scope

A scope

Range scales: 20, 40 80, 275 miles

(e) Antenna Assembly, Type I

Type: modified parabolic

Dimensions: horizontal aperture 16 feet ±2 inches

vertical aperture 4 feet 9 inches ±2 inches

Beam width: horizontal 3.8 degrees

vertical 10 degrees

Side lobe and back radiation relative to main lobe;

	side	back
azimuth	26 dB	30 dB
elevation	20 dB	30 dB

Gain: greater than 27 dB over an isotropic surface

Scan rate: azimuth; 0 to 15 rpm

elevation; tilt -2 to +5 degrees

Drive system: continuous search operation

manual searchlight operation

2. Antenna Pattern

The type I antenna assembly consists of three reflector sections bolted together to form a modified parabolic reflector. This assembly comprises the following: a modified parabolic reflecting surface constructed of wire mesh, an antenna feed assembly composed of a horn radiator with a dipole radiator mounted in the throat of the horn; a transmission line and associated structures necessary for combined radar search and IFF radiation and reception.

The polarization of radiation is horizontal from the horn radiator (radar), and vertical from the dipole (IFF). The antenna is capable of handling 2.0 KW average and 1.4 MW peak power output from the search radar transmitter within the frequency range of 1250 to 1350 Mc, and 50 watts average and 5 KW peak power output from the IFF transmitter. The IFF frequency band is 960 to 1150 Mc. The radiation patterns from the horn and dipole radiators are so oriented that the horizontal axes of the respective beams coincide within plus or minus 1.0 degree.

The horizontal aperture dimension of the reflection surface is 16 feet ±2 inches; the vertical aperture dimension is 4 feet 9 inches ±2 inches. The intensity of sidelobe radiation at all angles (vertical and horizontal) is at least 26 dB down, and back radiation is at least 30 dB down, with respect to maximum radiation, at all frequencies within the frequency range of 1250 to 1350 Mc. The gain of the antenna is greater than 27 dB over an isotropic antenna.

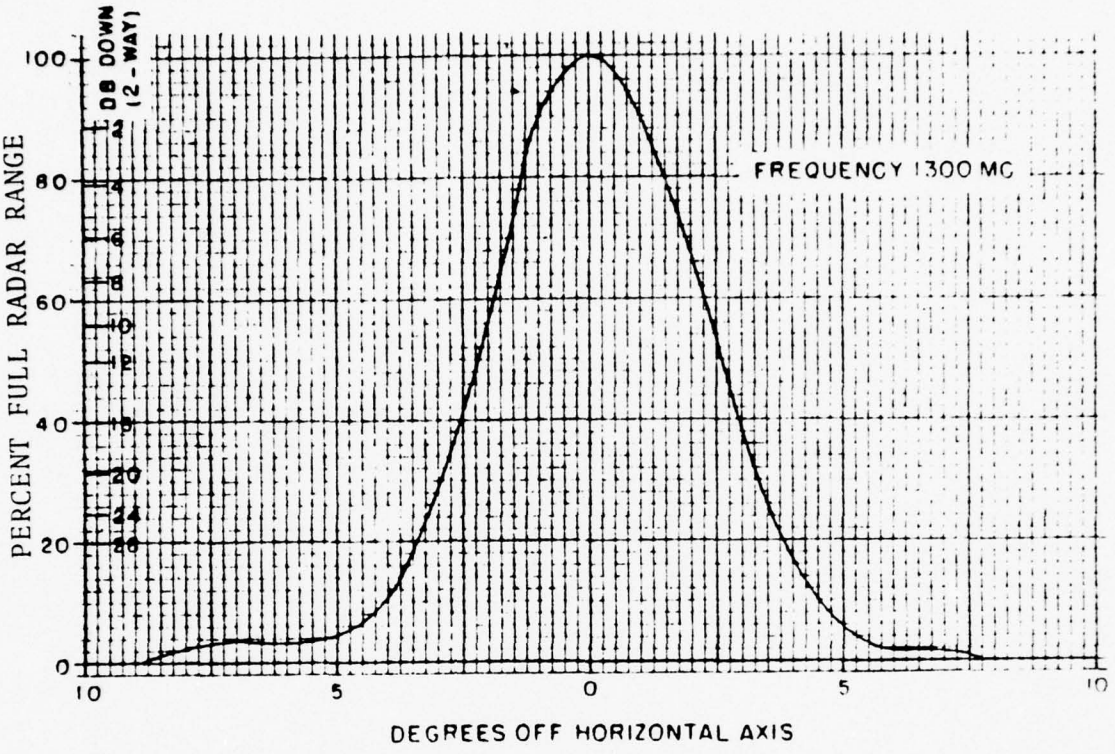

FIG. III-1 Antenna, Horizontal Response Pattern

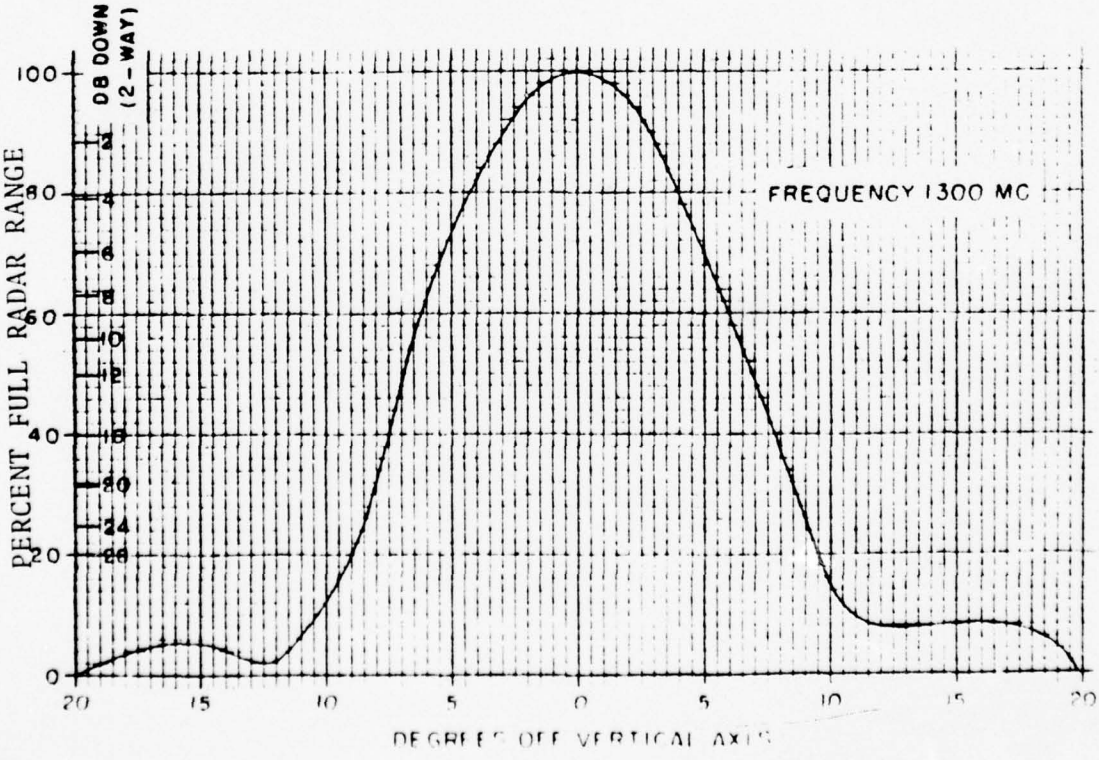

FIG. III-2 Antenna, Vertical Response Pattern

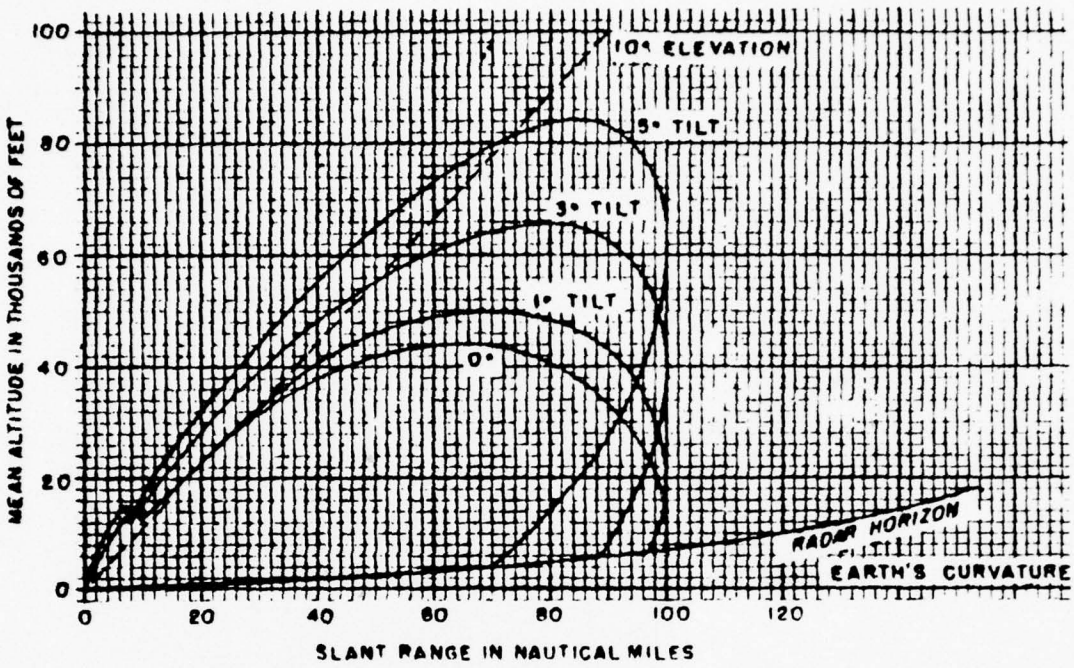

FIG. III-3 **Antenna, Typical Free-Space Vertical Coverage Patterns on an Average Target at 100 Mile Range, for Various Tilting Angles**

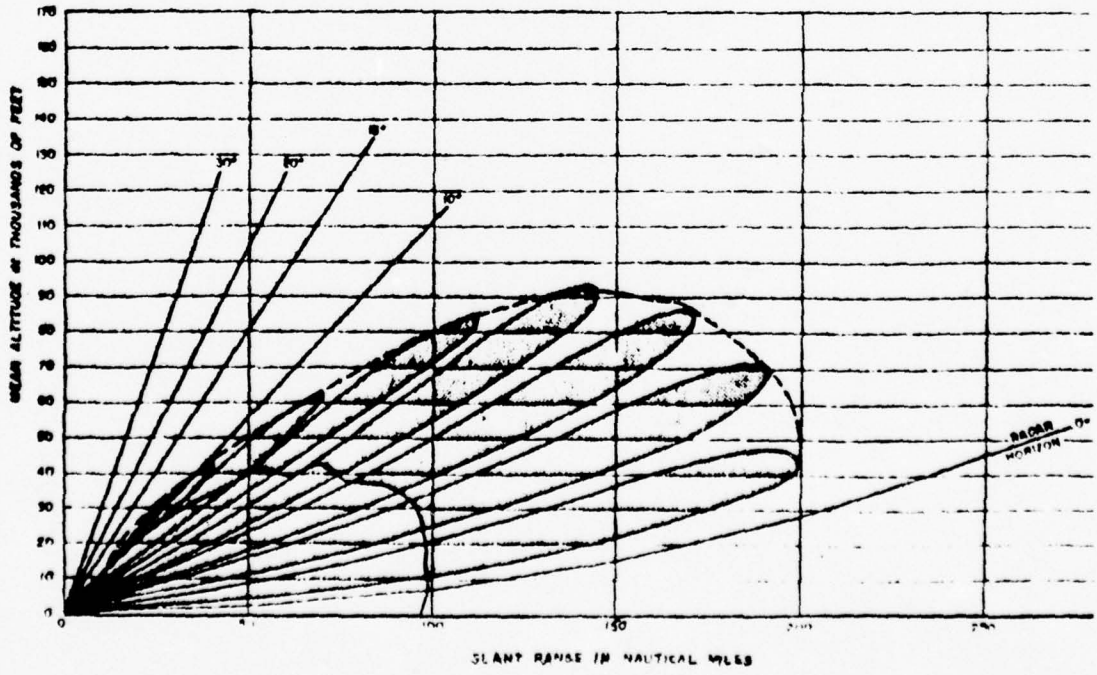

FIG. III-4 **Antenna, Typical Vertical Illumination Pattern at 0° Tilt Showing Lobes Caused by Surface Reflection**

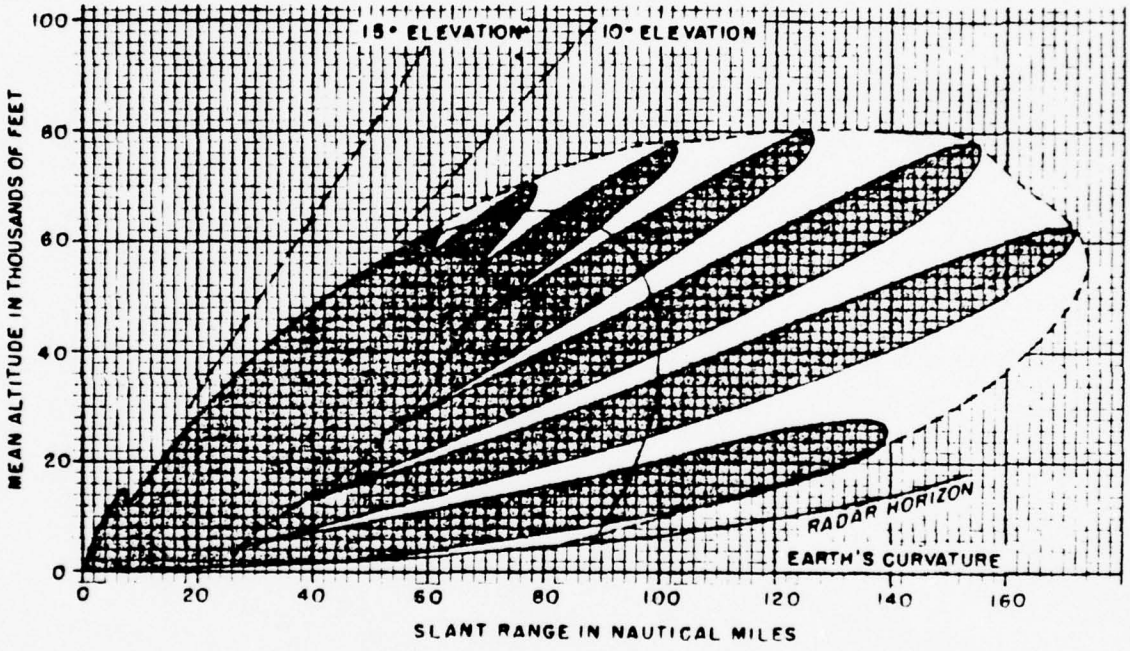

FIG. III-5 **Antenna, Typical Vertical Illumination Pattern at 3° Tilt, Showing Lobes Caused by Surface Reflection**

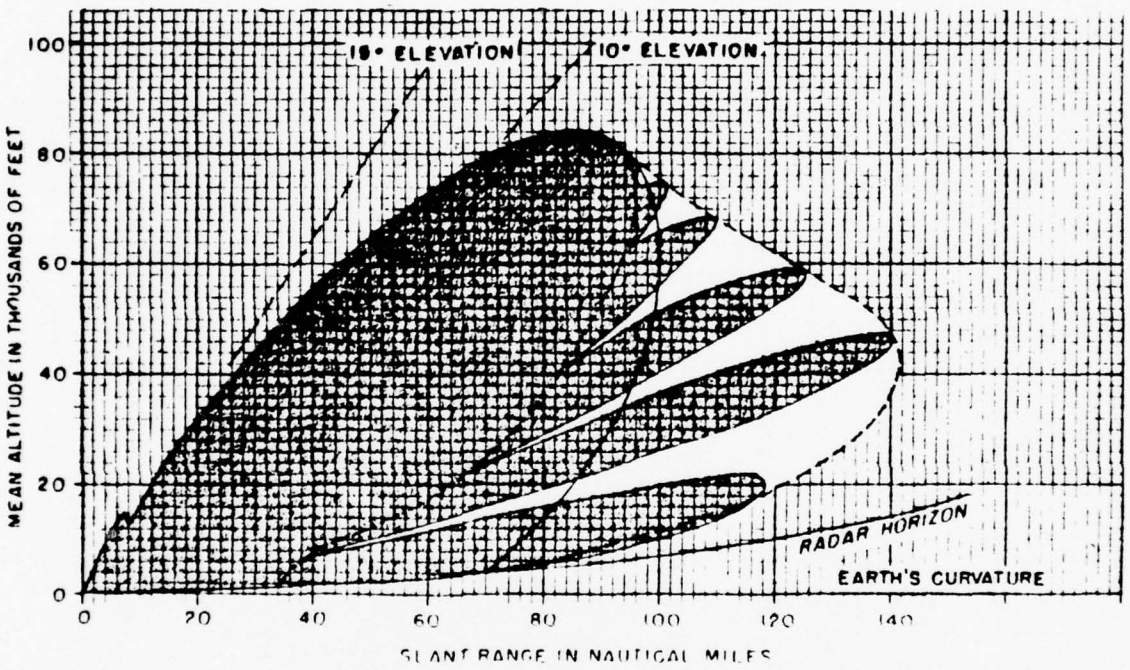

FIG. III-6 Antenna, Typical Vertical Illumination Pattern at 5° Tilt, Showing Lobes Caused by Surface Reflection

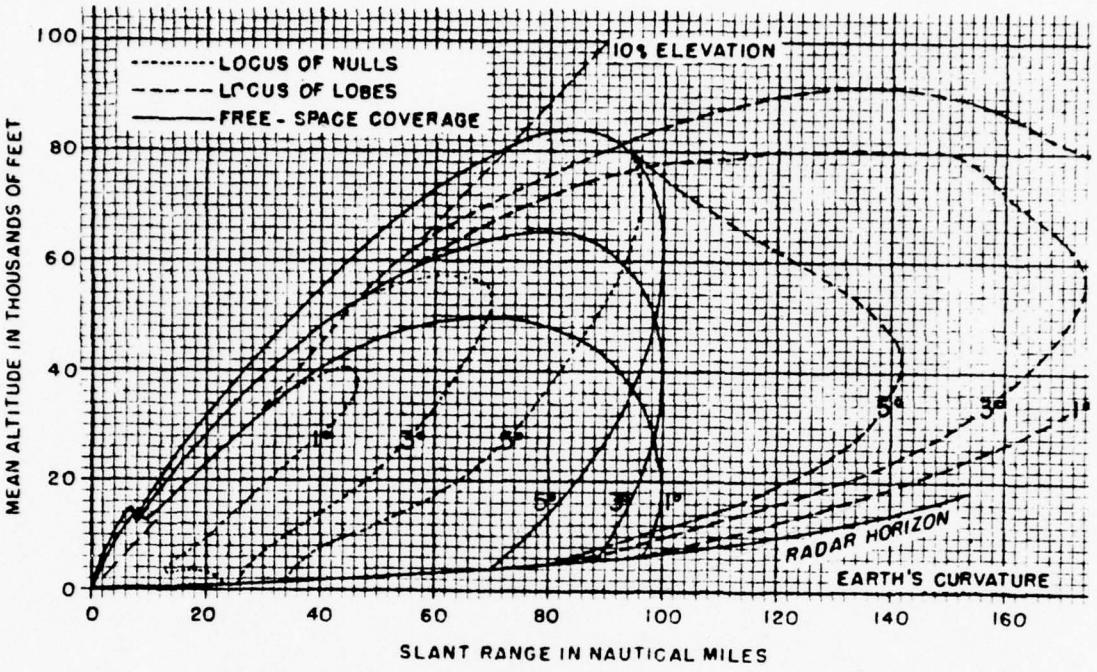

Antenna, Maximum Variations in Vertical Coverage
Due to Surface Reflection for Various Tilting Angles

FIG.III-7

B. RADAR SET AN/SPS-12, DESCRIPTION

Radar set AN/SPS-12 is a medium-range surveillance radar equipment designed to detect aircraft and surface vessels [Ref. 5]. It presents target range and bearing data for presentation on associated PPI units.

The Radar Set AN/SPS-12 transmits and receives pulses of r-f energy in the frequency range of 1250 to 1350 MHz.

These pulses are generated in the radar Receiver-Transmitter and radiated by the antenna in a directional beam. The pulse repetition frequency of the rf pulse may be either 300 or 600 pulses per second. As an anti-jamming measure the prf may be varied ±5% from either of the two fundamental repetition frequencies. The pulse duration is one microsecond for the 600 PRF, and four microseconds for the 300 PRF. Selection of either the long pulse or the short pulse may be made.

The transmitting oscillator is a pulsed tunable magnetron having a peak power output of 500 kilowatts, and covering the 1250 to 1350 megahertz range.

Reflected target energy picked up by the antenna is detected and mixed with the output of a klystron local oscillator to provide an intermediate frequency of 30 megahertz for the receiver i-f amplifier.

Anti-jam STC (sensitivity time control), and AFC (automatic frequency control) circuits are incorporated in the receiving circuits. Four ranges (4, 20, 80 and 200 miles) are provided on the range indicator. The sweep circuits may be calibrated by displaying range markers from an associated radar range calibrator on the indicator screen.

1. Antenna System (AS-603/SPS-12)

The antenna assembly may be rotated in azimuth by the drive motor in the antenna pedestal, either by an adjustable-speed electronic circuit or by direct connection to an emergency dc supply circuit. Under adjustable-speed

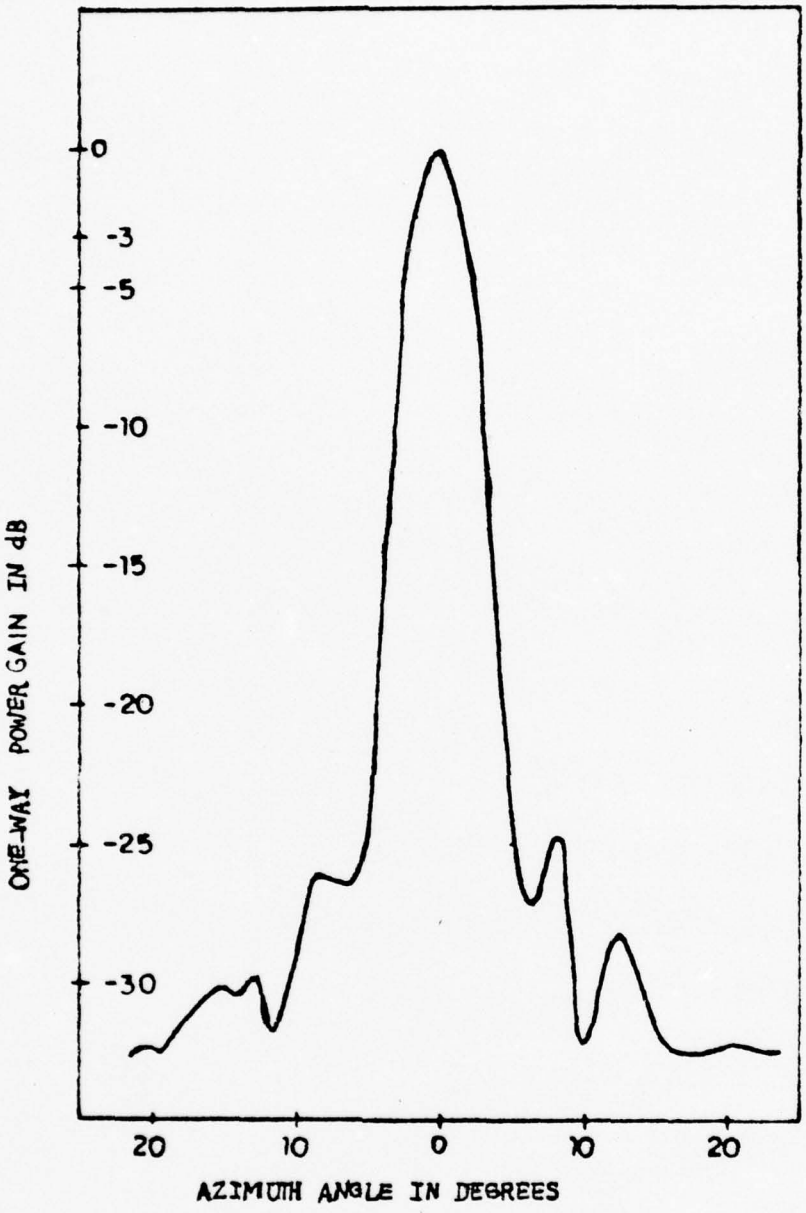

Antenna AS-603/SPS-12
Horizontal radiation pattern

FIG. III-8

control, the antenna can be automatically rotated continuously in a clockwise direction at speeds varying from 2.5 to 15 rpm, or can be manually trained in either direction by the slewing hand wheel on the front panel of the radar set control.

The radiation pattern is a 30-degree cosecant-squared beam in the vertical plane, and a sharp, three-degree beam in the horizontal plane. A cosecant-squared beam is a beam where the field strength (in terms of power) above some minimum angle, θ_o, is proportional to $\csc^2 \theta$, where θ is the angle of elevation. This radiation characteristic permits high-flying aircraft at constant altitude to be tracked continuously over approximately the entire range since returned echo strength in the absence of surface reflections is independent of aircraft range. (Provided aircraft altitude angle is greater than θ_o.)

The gain of AS-603/SPS-12 antenna was calculated to be at least 29 dB over an isotropic antenna.

C. DESIGN COMPARATOR AND BLANKER SYSTEM

1. For Radar Set AN/UPS-1

In order to investigate the Sidelobe Blanking technique using the radar set AN/UPS-1 it was necessary in the first place to design a circuit to compare in amplitude (absolute value), the negative pulses of video (0 to 2.5 volts) coming from the signals received by the radar antenna with

the positive pulses of video (0 to 2.5 volts), received by the sidelobe blanking or auxiliary antenna [Fig. III-11].

In order to compare the two signals it was necessary first to invert the negative video pulse to a positive pulse with the same magnitude. Once the comparison is done the system must be able to blank the output, before the final detection circuits and displays, every time the signal coming from the sidelobe antenna is greater than the main signal coming from the radar antenna.

The circuit was designed in the laboratory with two pulse generators, Data Pulse Model 101 Pulse Generators, simulating the video pulses. The circuit designed works in the following way (see Fig. III-12):

Defining: Radar signal; signal A (video after detection)
Sidelobe signal; signal B (video after detection)

(a) The negative signal A is fed directly into the input port (pin 1) of the analog switch NA4016 [Parameters and characteristics given in Appendix C], which is normally closed, thereby given an output signal identical to the input signal to the final detection circuits and display. The same signal A also is fed into the inverter circuit [transistor 2N3437, parameters and characteristics given in Appendix C].

(b) The output (positive) of the inverter is fed to one of the input ports (pin 4) of the voltage comparator LM319. [Parameters and characteristics given in Appendix C].

(c) The signal B is fed directly into the other input port (pin 5) of the comparator. At this moment the two signals, radar and sidelobe, both with positive polarity, are at the two input ports of the comparator.

The comparator has a supply voltage of +5 volts and works in the following way [see Fig. III-13]:

(d) The output of the comparator (pin 12) is connected to the control port of the switch (pin 13)

(e) The output of the comparator is +5 volts for $C \leq B \leq A$ and 0 volts for $B \geq A$ or $B \leq C$. The input C of the comparator is connected to ground which means it is always less than signal A or B.

With these configurations we have at the output of the comparator (pin 12) and at the control input of the analog switch (pin 13), +5 volts when the radar signal is greater than the sidelobe signal, or 0 volts when the sidelobe signal is greater than the radar signal. The switch is closed or open between the input and output ports (pin 1 and 2) depending on the changes of voltage at its control port. In this way, at the output of the analog switch, we have the original radar signal (negative video pulse), where the radar signal is greater than the sidelobe signal (the switch is closed); or zero (no output), when the sidelobe signal is greater.

The conclusion is then that the system passes signals through the final stages to the display of the radar only when the signal source is in the main lobe of the radar

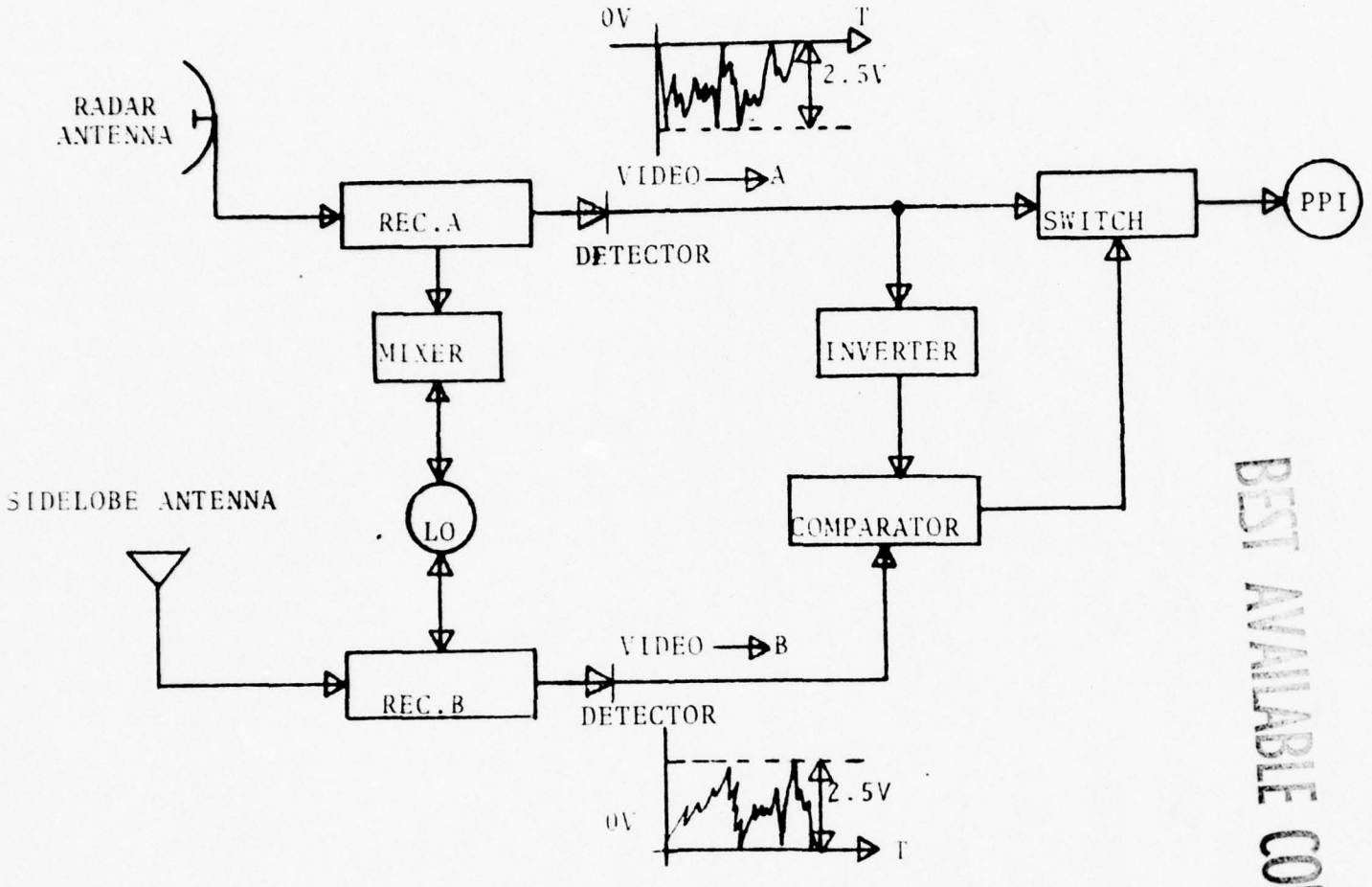

BASIC SIDELOBE BLANKING SYSTEM FOR AN/UPS-1 RADAR

FIG. III-11

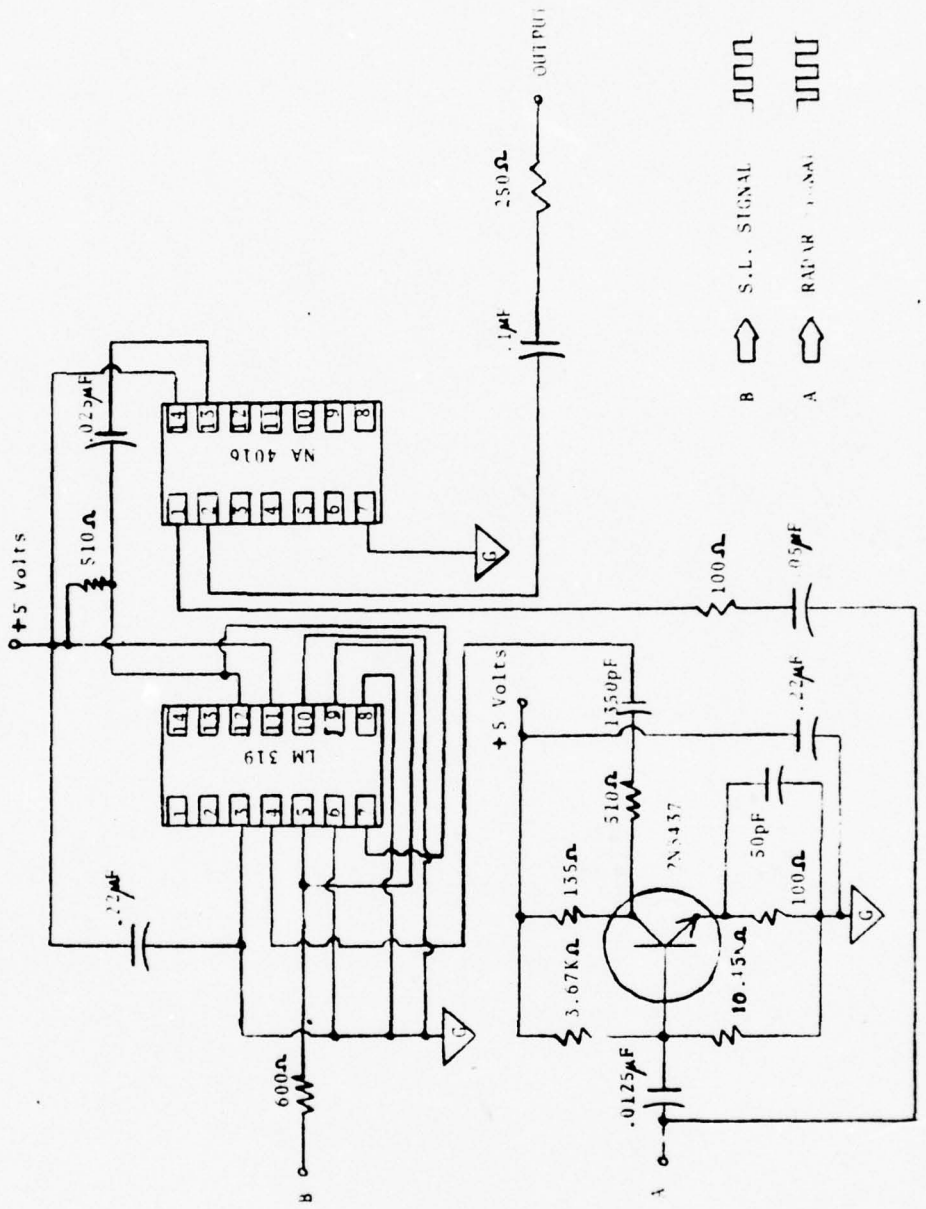

BLANKER SYSTEM FOR RADAR SET AN/UPS-1

FIG. III-12

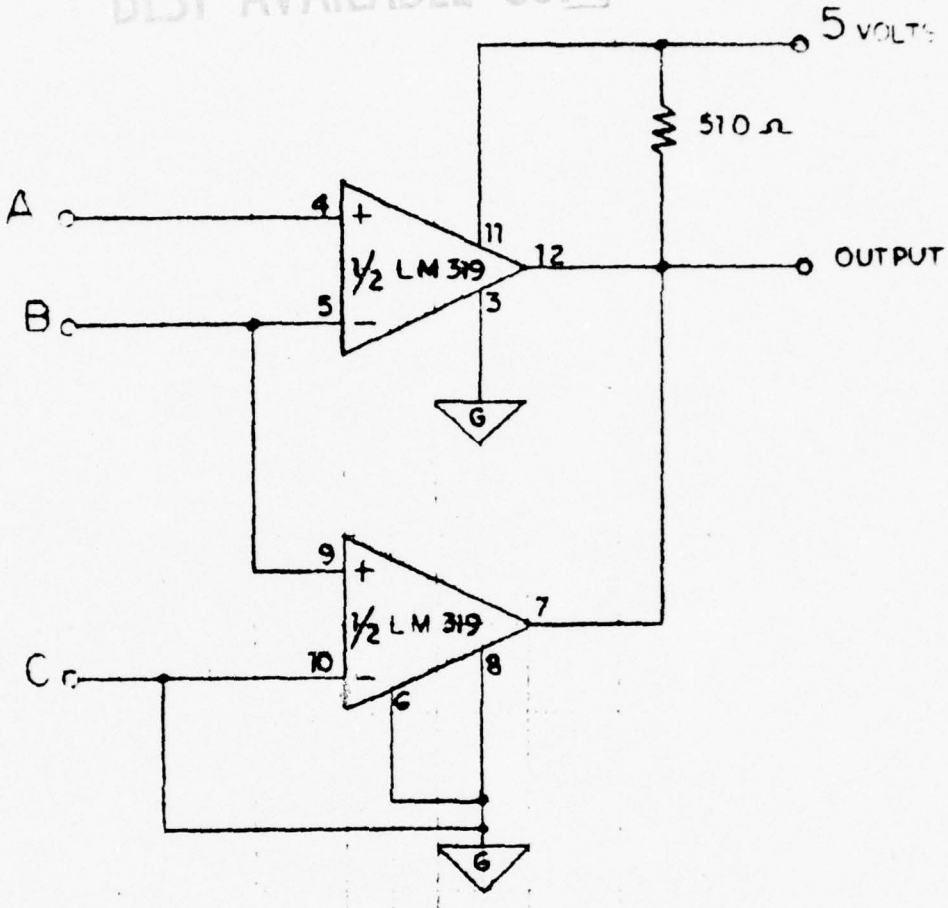

$V_{OUTPUT} = 5$ VOLTS FOR $C \leq B \leq A$

$V_{OUTPUT} = 0$ VOLTS FOR $B \geq A$ OR $B \leq C$

A → RADAR SIGNAL

B → SIDELOBE SIGNAL

COMPARATOR

FIG. III-13

antenna, and blanks all signals originating in the sidelobes of the radar antenna.

2. For Radar Set AN/SPS-12

The system works basically in the same way as the comparator circuit design for the radar set AN/UPS-1. The only difference is that now the two signals, radar and sidelobe are both positive. The circuit [Fig. III-14] is slightly different because the radar set AN/SPS-12 has different PRF and video pulse amplitudes. The circuit shown was designed to fit the specific characteristics of the SPS-12 radar.

The circuit was designed and tested in the laboratory using pulse generators and continuous-wave generators. It also was tested using a random noise generator.

D. SIDELOBE BLANKING ANTENNA, GENERAL DESCRIPTION

Since the antenna of the radar set AN/UPS-1 has a gain greater than 28 dB over an isotropic antenna and the intensity of sidelobe radiation at all angles (vertical and horizontal) is 26 dB down, and back radiation is 30 dB down, with respect to maximum radiation at all frequencies within the frequency range of 1250 to 1350 MHz, the gain of the sidelobe blanking antenna is not a restrictive parameter for this experimental work.

It was determined to be desirable to have a relatively wide-band antenna with an omnidirectional pattern and horizontal polarization (same as radar) for the sidelobe

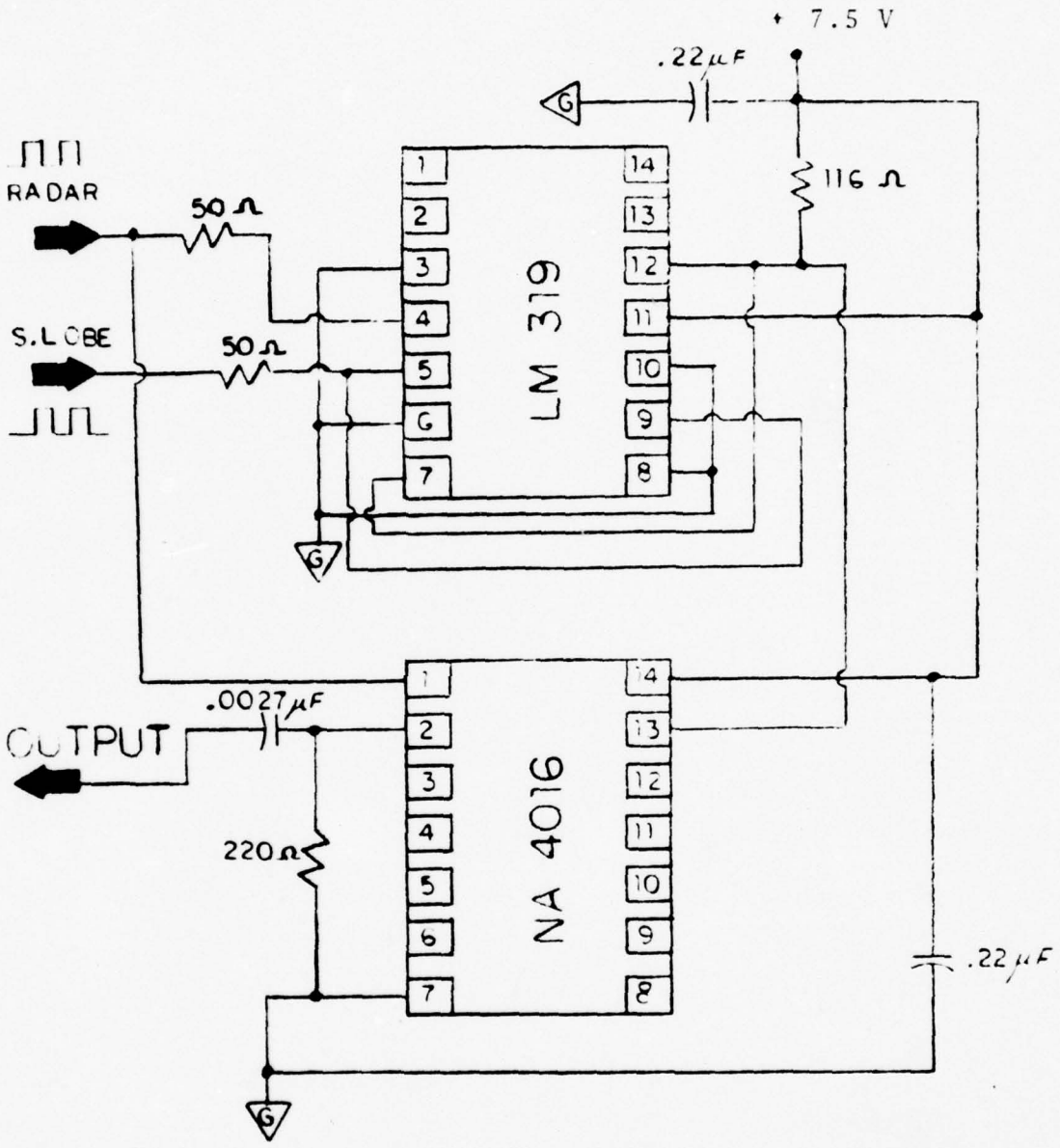

BLANKER SYSTEM FOR RADAR SET AN/SPS-12

FIG. III-14

blanking purposes. The most common antenna to date that tends to meet such a requirement is the vertically polarized discone or biconical antenna. However, pattern breakup limits the bandwidth of these antenna normally to 2 to 1. The desirability of designing a logarithmically periodic structure with omnidirectional and horizontal polarization characteristics was readily apparent.

It was decided to build an omnidirectional horizontally polarized log-periodic antenna to be able to handle frequencies from .8 to 4 GHz. Later, for the antenna AS-603/SPS-12 it was determined that the same omnidirectional antenna already built could be used without any change.

1. Theory

The fundamental principle that governs the design of a log-periodic antenna (LPA), is that if a structure becomes equal to itself by a particular scaling of its dimensions, by a ratio "τ" (usually less than unity), it will have the same properties at a frequency "f" and a frequency τf [Refs. 6 and 7]. In other words, the characteristics of the two antennas such as the pattern radiation and the impedance remains unchanged if antenna geometry and feed are appropriately scaled from one frequency to another.

Hence, if we decrease the dimensions of an antenna by a factor of $\tau < 1$, and the frequency is increased by τ^{-1}, the fields about the two antennas are similar; that is, they differ at most by a constant factor.

The problem is reduced to finding a geometrical shape which remains invariant to scaling at least for a sequence of p frequencies $f_1, f_2, \ldots, f_p$. With appropriate excitation the performance of such an antenna will remain unchanged in the range f_1 to f_p.

There is a very close relationship among the log-periodic structures. The majority of them may be derived from the basic trapezoidal tooth or triangular tooth structures, illustrated in Fig. III-15. These structures satisfy the conditions of the scaling principle and the log-periodic approach; the spectrum coverage is continuous provided rotation accompanies scaling. Another aspect of the practical design problem is related to the truncation to a finite size of the infinite structure in order to construct a practical antenna. The end effect (higher concentration of charge near the ends of the elements which represent that near the ends the capacitance per unit length is greater), should be negligible over the desired frequency band. (The physical truncation should not adversely affect the performance of the antenna). This may be accomplished by requiring that the currents along the antenna decay sufficiently by the time the end is reached.

The basic structure described in Fig. III-15 can be defined in terms of angles and some parameters. The defining parameters are the angles α, β, γ, δ; the scaling factor τ and the factor σ, which defines the tooth width $\overline{AE}$.

The dimensions of significance are logarithmically related and when an antenna is designed according to these criteria it appears electrically similar throughout its operating band. The only dissimilarities are near the limiting points, which are delineated by the structure size and the accuracy and fineness with which the structure can be fabricated.

A wide variety of shapes may be obtained from this general structure by letting α, β, δ take different values. Starting with $\overline{OA} = 1$, there can be defined:

$$\tau = \overline{OH} \quad , \quad 0 < \tau < 1$$

$$\tau^{\sigma} = \overline{OE} \quad , \quad 0 < \sigma < 1$$

$$\tau^{\sigma/2} = \overline{OD} \quad , \quad 0 < \tau < 1 \, , \quad 0 < \sigma < 1$$

$$\tau^{\sigma/2} = \overline{OC}/\overline{OB}$$

$$\tau = \overline{OG}/\overline{OB}$$

$$\sigma = \overline{OF}/\overline{OB}$$

It was decided to begin the construction of the antenna with the basic trapezoidal tooth structure. The parameters were chosen in accordance with the optimum design criteria found in the literature for the range of frequencies from 0.8 GHz to 4 GHz. The periodic discontinuities are in the form of teeth connected to a triangular conducting strip. The upper frequency limit is given for the smallest teeth near the origin (apex) while the radius R1, and the angles alpha and beta determine the lowest frequency limit.

Increasing alpha and reducing beta (to maintain a constant sum of 90 degrees) the lower limit was increased and the upper limit was decreased. It is required that in order for the structure to be equal to its complement that the sum of the angles alpha and beta be equal to 90 degrees.

The ratio σ was taken equal to the square root of τ in order to provide a ratio of tooth to slot width equal for all rows of teeth. The antennas were cut from a sheet of aluminum of 1/16" thickness.

For this planar structure horizontally polarized it was found that the pattern was bidirectional and had almost equal principal plane beamwidths.

Since two dipoles arranged in a turnstile and fed ninety degrees out of phase give omnidirectional patterns, it was decided to arrange the two planar, sheet metal structures (which have approximate dipole patterns), in a turnstile as shown in Fig. III-16. Since the planar sheets were actually soldered together where they crossed, it is apparent that the two sheet structures could not be identical or the same result would occur as when feeding two crossed dipoles in phase (a bidirectional pattern with maximum lobes occurring at an angle of 45°).

Therefore, one of the structures was made $(\tau)^{1/N}$ times the size of the other (where N is the number of arms of the structure), in order to obtain the 90° phasing. An easy way to visualize such a structure is to imagine two cones placed apex to apex on a common axis. Starting at

the apex of each cone, an equiangular spiral is placed on the slant side of the cone with the axis of the spiral coinciding with the axis of the cone. The spiral on one cone is made to rotate clockwise; the spiral on the other cone is made to rotate counterclockwise as the two cones are viewed simultaneously from the point where their respective apexes meet. Actually, these spirals are the openings of grooves which become progressively wider and deeper as they spiral away from the apex of the cones. The outlines of four arms of a four-arm structure would be the lines of intersection of the cones and two planes perpendicular to each other and intersecting on the axis of the cones. Figure III-16 is the visualization of the structure with four arms.

Then, an omnidirectional horizontally polarized antenna was constructed by placing at right angles each half antenna of the planar structure form. This is readily accomplished since each planar structure produces approximately a figure of eight pattern and the scaling of one structure provides the 90 degrees phase shift to give an omnidirectional pattern.

The use of a broadband balun was necessary in order to achieve good performance. This antenna has a horizontally polarized omnidirectional pattern and the measured VSWR in a 50 ohm line does not exceed 3 to 1 from 500 to 1000 MHz, and should be reasonably low to 4 gigahertz.

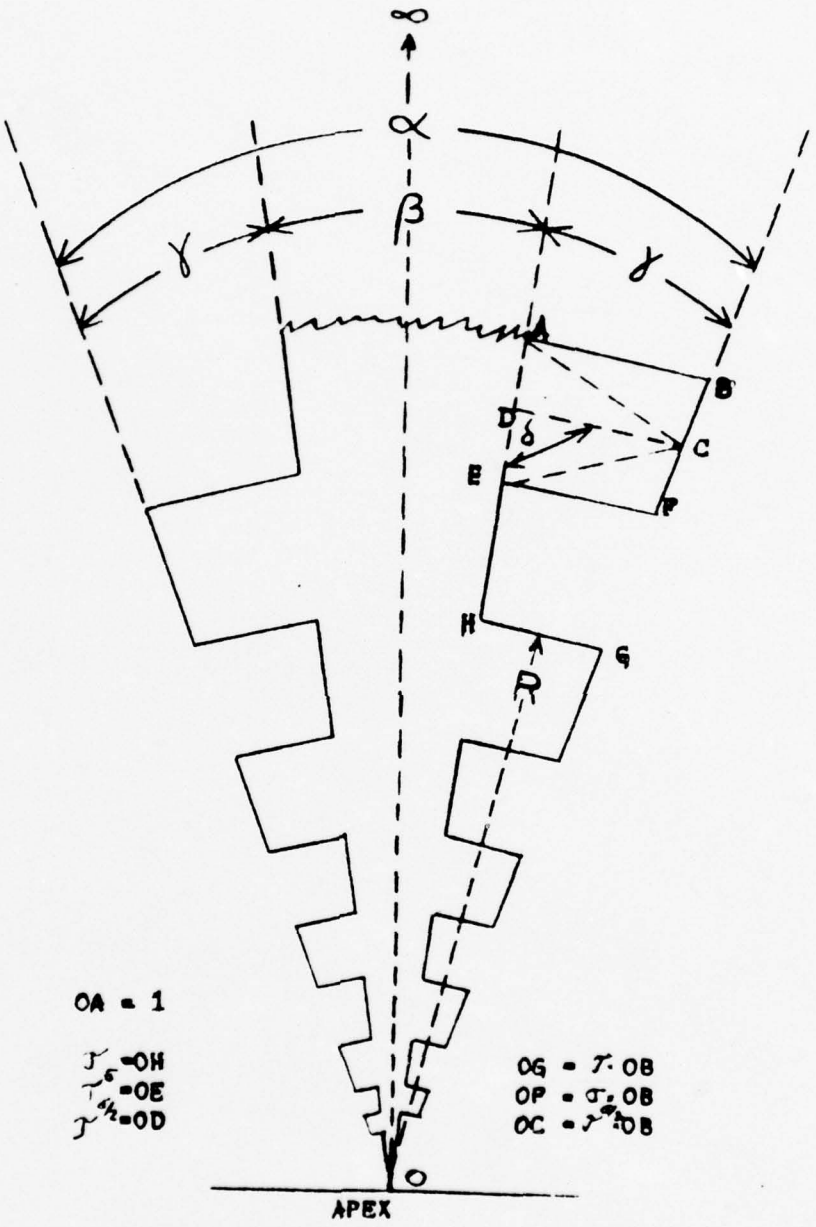

PRACTICAL LOG-PERIODIC ELEMENT

FIG. III-15

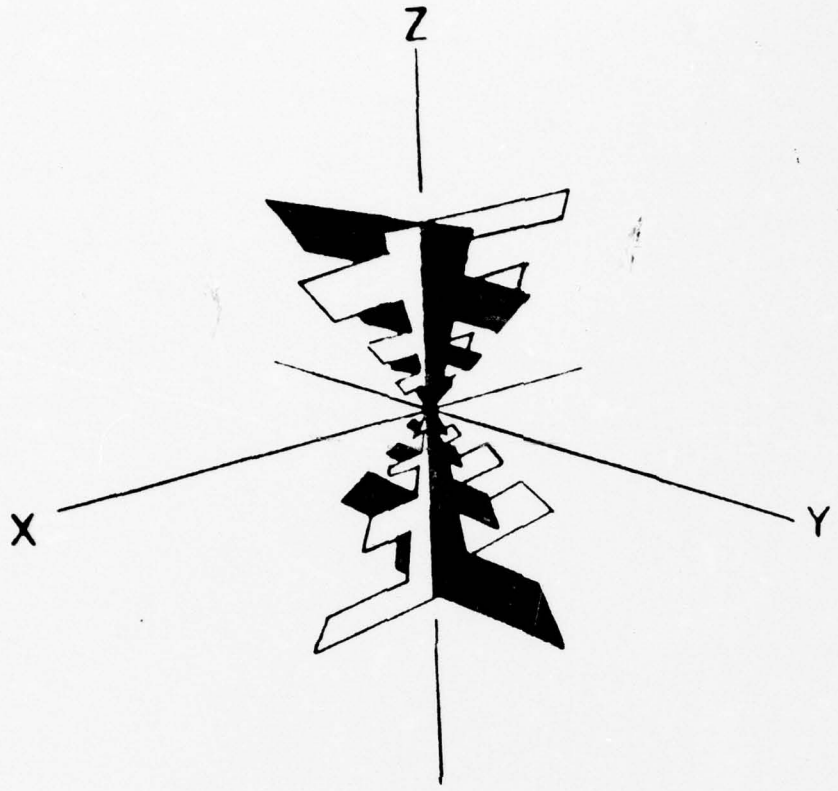

OMNIDIRECTIONAL LOG-PERIODIC ANTENNA

FIG. III-16

2. Impedance Measurement

The input impedance of the antenna was measured as a function of frequency using the experimental set up shown in Fig. III-17. The basic considerations for use of this system were to have a stable frequency source, enough power, and to have available to the measurement system a reference signal for phase measurement.

The equipment used were VHF signal generator H.P. Model 8640A and H.P. Model 608C, an H.P. Model 11536 dual directional coupler, an H.P. Model 11536 adjustable line, an H.P. Model 8405 Vector Voltmeter and a Tektronic DC502 frequency counter. An H.P. 11549 type N power splitter was used to divide the output from the signal generator. One output was connected to the dual directional coupler and the other output to the frequency counter. The counter was monitored to assure frequency stability over the period of measurement.

The H.P. Model 8405 Vector Voltmeter directly measures the amplitude and phase relationship of the fundamental components of two RF voltages.

The ratio of signals at channels A and B, contains information concerning the magnitude and phase of the coefficient of reflection of the antenna.

Prior to each measurement of the magnitude and phase of the coefficient of reflection, the reference signal was obtained from the attenuated output of the dual

directional coupler and applied to channel A of the vector voltmeter. This was done by removing the antenna under test from L_1 and terminating L_1 with a short circuit. With the short circuit in place the tunable line was adjusted so that the vector voltmeter indicated zero phase.

The gain of the signal generator was then adjusted until the reading of the amplitude of the coefficient of reflection read one. The antenna was then replaced and the measurement made. Each time that frequency was changed the line adjustments mentioned above were repeated.

The data representing a series of such measurements was then plotted on a Smith Chart [See Fig. III-26], which shows the input impedance variations with frequency.

3. Pattern Radiation Measurement

The patterns (E-Plane) were obtained with the experimental set-up shown in Fig. III-18. The H.P. 91598-2 tunable horizontal dipole at 100 MHz was used as the transmitting element.

The antennas were tested like receiving elements in the roof-top range above Spanagel Hall. In order to obtain accurate far-field radiation measurements, it is necessary that the distance between the transmitting antenna and the antenna under test be much greater than three wavelengths at the frequency of operation. The length of the range is 30 meters, thus satisfying the requirement.

The pattern radiation plots are shown in Figs. III-23, III-25, III-27, and III-28. The gain of the omnidirectional

antenna was theoretically calculated to be 4 dB maximum over an isotropic antenna.

4. Balun

A balun is a device designed to act as a transformer, matching an unbalanced circuit to a balanced one. Normally for broadband log-periodic structures it is quite advantageous to use a balun transformer capable of operating over a very large frequency range.

Unbalance of the transmission line currents results if current returns to the generator on the outside surface of the coaxial cable, because in a coaxial cable, the total current on the inside surface of the outer conductor must be equal and opposite to the total current on the center conductor (Fig. III-19).

The balun functions by isolating the outside surface of the coaxial cable from the transmission line junction so that all of the current on the inside surface of the coax outer conductor is delivered in the proper phase to one of the two balanced conductors, so that there will be equal currents of opposite phase in the line conductors at any cross section.

The length of the balun is determined by the lowest frequency of operation and the maximum reflection coefficient which is to occur in the pass-band; the balun has no upper frequency limit and the characteristic impedance of the balun transformer is tapered along its length. Normally the balun provides near perfect impedance matching over frequency bandwidths of 100:1.

A schematic representation of the balun is shown in Fig. III-19. It is composed of two lengths of coaxial transmission line, "a" and "b".

A more detailed configuration is shown in Figs. III-20 and III-21. The point "H" is the connection for the external unbalanced section, while the terminals "F" and "G" are the points of attachment of the balanced section. Center conductors of lines "a" and "b" are connected at "D", while outer conductors are connected at "C". The center conductor of line "b" ends at "E", which corresponded to one quarter wavelength (at 1000 MHz) from the balanced terminals F and G.

5. Pattern Radiation Graphics

Here are shown the dimensions and pattern radiations of the two independent sides of the omnidirectional antenna, and finally the omnidirectional pattern which resulted once the whole antenna was tested.

(a) Side one of the antenna, physical dimensions

R_1 = 10"	r_1 = 9.0"
R_2 = 8.1"	r_2 = 7.29"
R_3 = 6.56"	r_3 = 5.90"
R_4 = 5.31"	r_4 = 4.78"
R_5 = 4.3"	r_5 = 3.87"
R_6 = 3.48"	r_6 = 3.13"
R_7 = 2.82"	r_7 = 2.53"
R_8 = 2.28"	r_8 = 2.05"
R_9 = 1.85"	r_9 = 1.66"
R_{10}= 1.49"	r_{10}= 1.35"

$\psi = 60°$ $\tau = 0.81$

$\alpha = 60°$ $\sigma = 0.9$

$\beta = 30°$

where: $\tau = \frac{R_2}{R_1}$

$\sigma = \frac{r_1}{R_1}$

(b) Side two of the antenna, physical dimensions

$R_1 = 10"$	$r_1 = 9.0"$
$R_2 = 8.1"$	$r_2 = 7.29"$
$R_3 = 6.56"$	$r_3 = 5.90"$
$R_4 = 5.31"$	$r_4 = 4.78"$
$R_5 = 4.3"$	$r_5 = 3.87"$
$R_6 = 3.48"$	$r_6 = 3.13"$
$R_7 = 2.82"$	$r_7 = 2.53"$
$R_8 = 2.28"$	$r_8 = 2.05"$
$R_9 = 1.85"$	$r_9 = 1.66"$
$R_{10} = 1.49"$	$r_{10} = 1.35"$

$\psi = 60°$ $\tau = 0.81$

$\alpha = 70°$ $\sigma = 0.9$

$\beta = 20°$

where:

$\tau = \frac{R_2}{R_1}$

$\sigma = \frac{r_1}{R_1}$

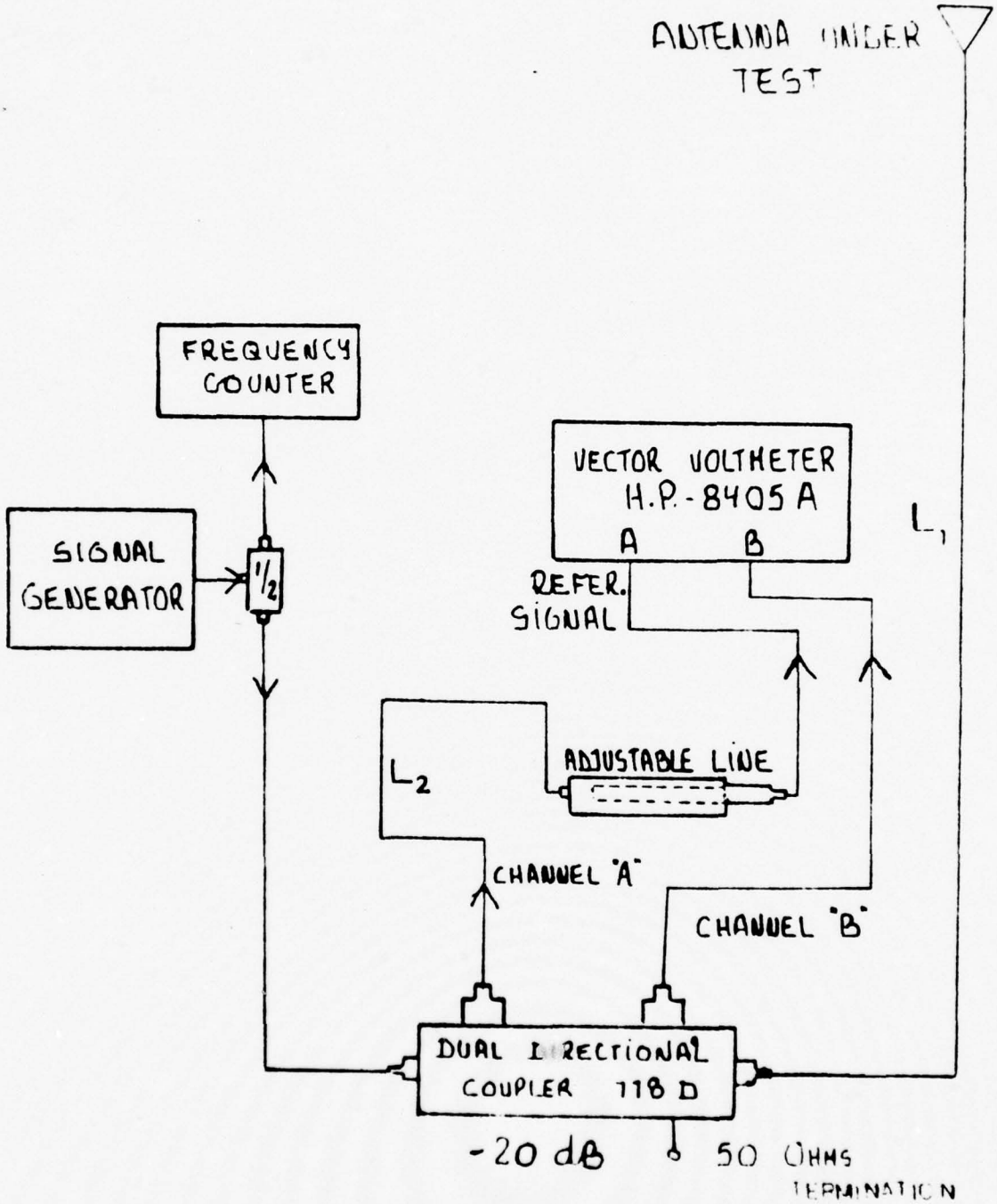

EXPERIMENTAL SET-UP FOR IMPEDANCE MEASUREMENT

FIG. III-17

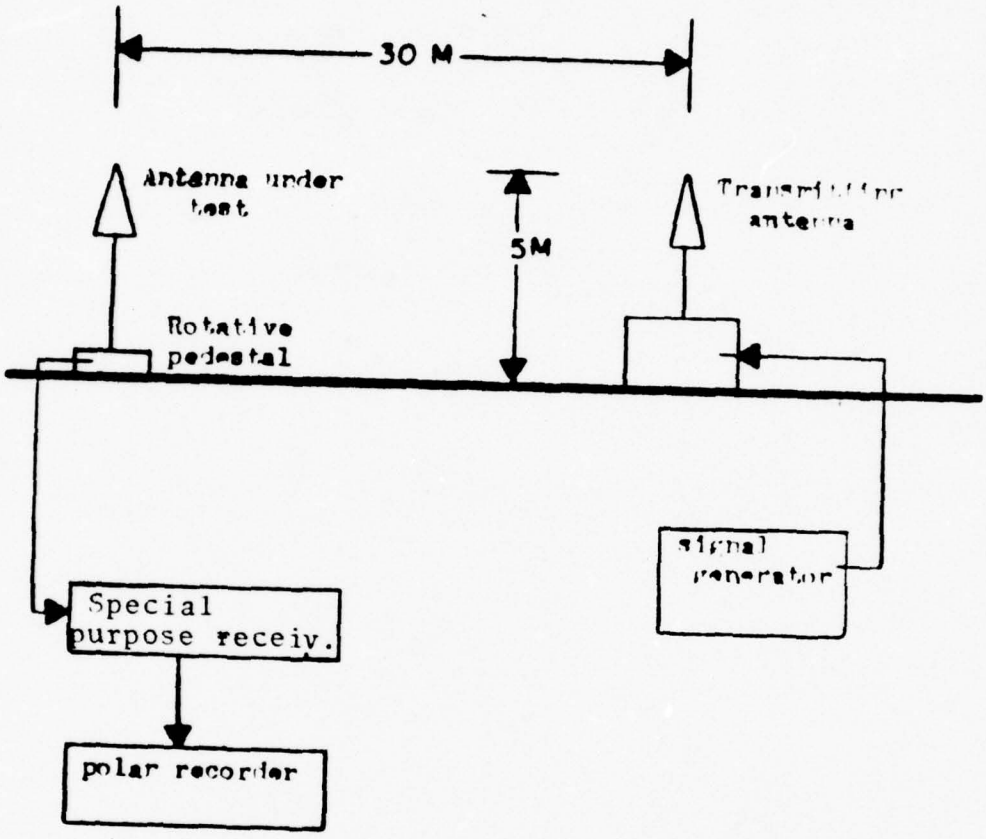

EXPERIMENTAL SET-UP FOR PATTERN RADIATION MEASUREMENT

FIG. III-18

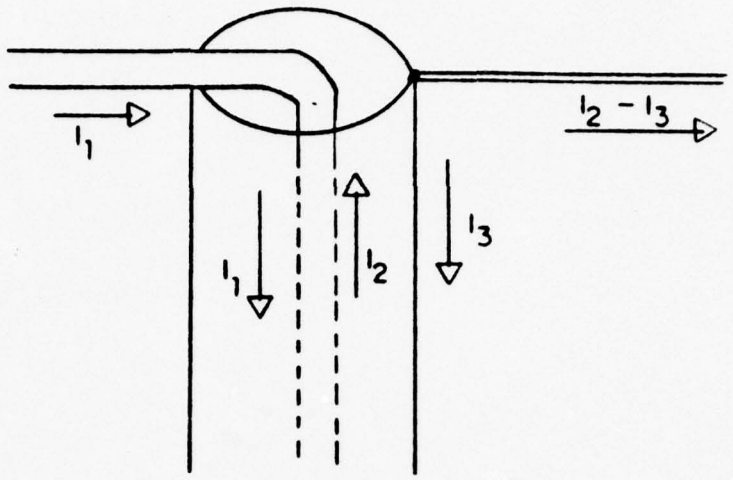

SCHEMATIC REPRESENTATION OF THE BALUN

FIG. III-19

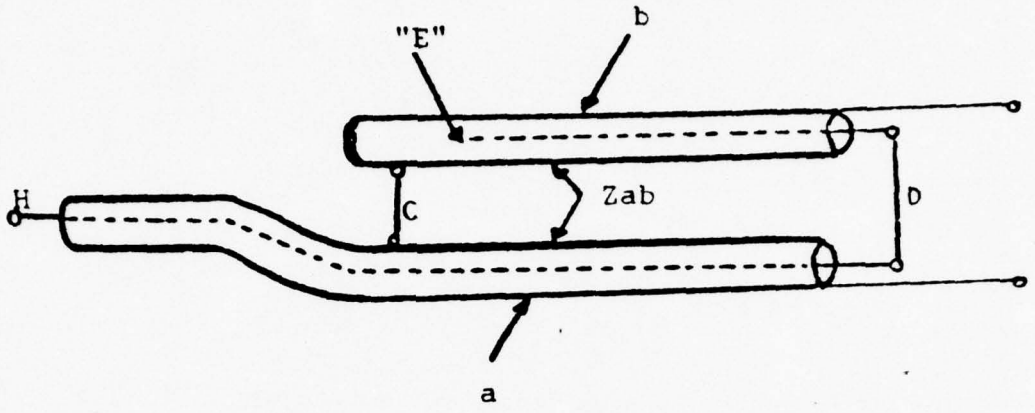

CONFIGURATION OF THE BALUN

FIG. III-20

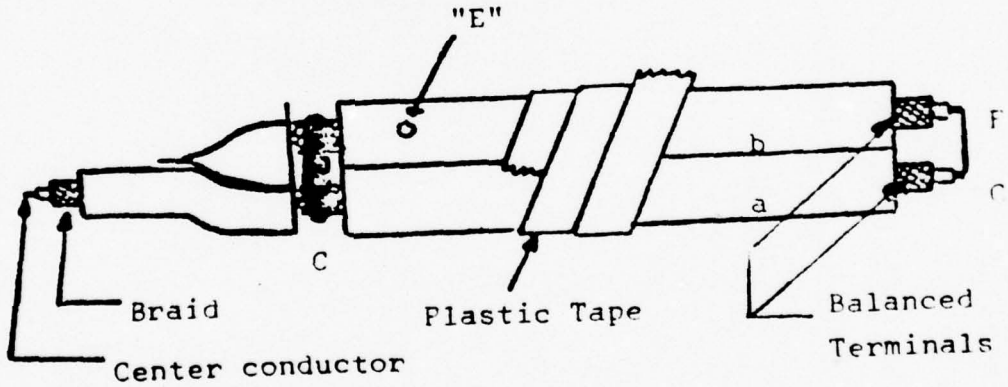

CONFIGURATION OF THE BALUN

FIG. III-21

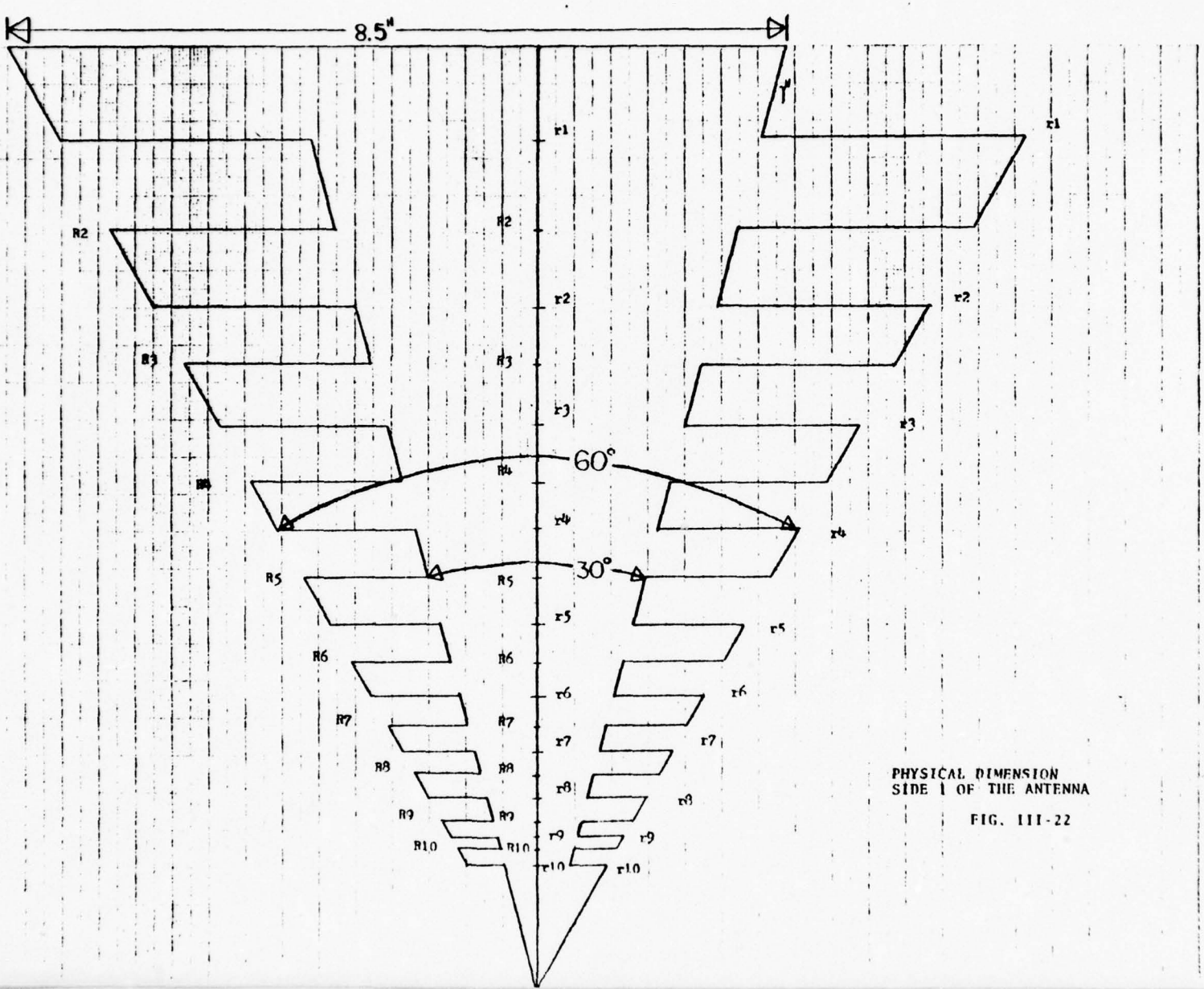

PHYSICAL DIMENSION
SIDE 1 OF THE ANTENNA

FIG. III-22

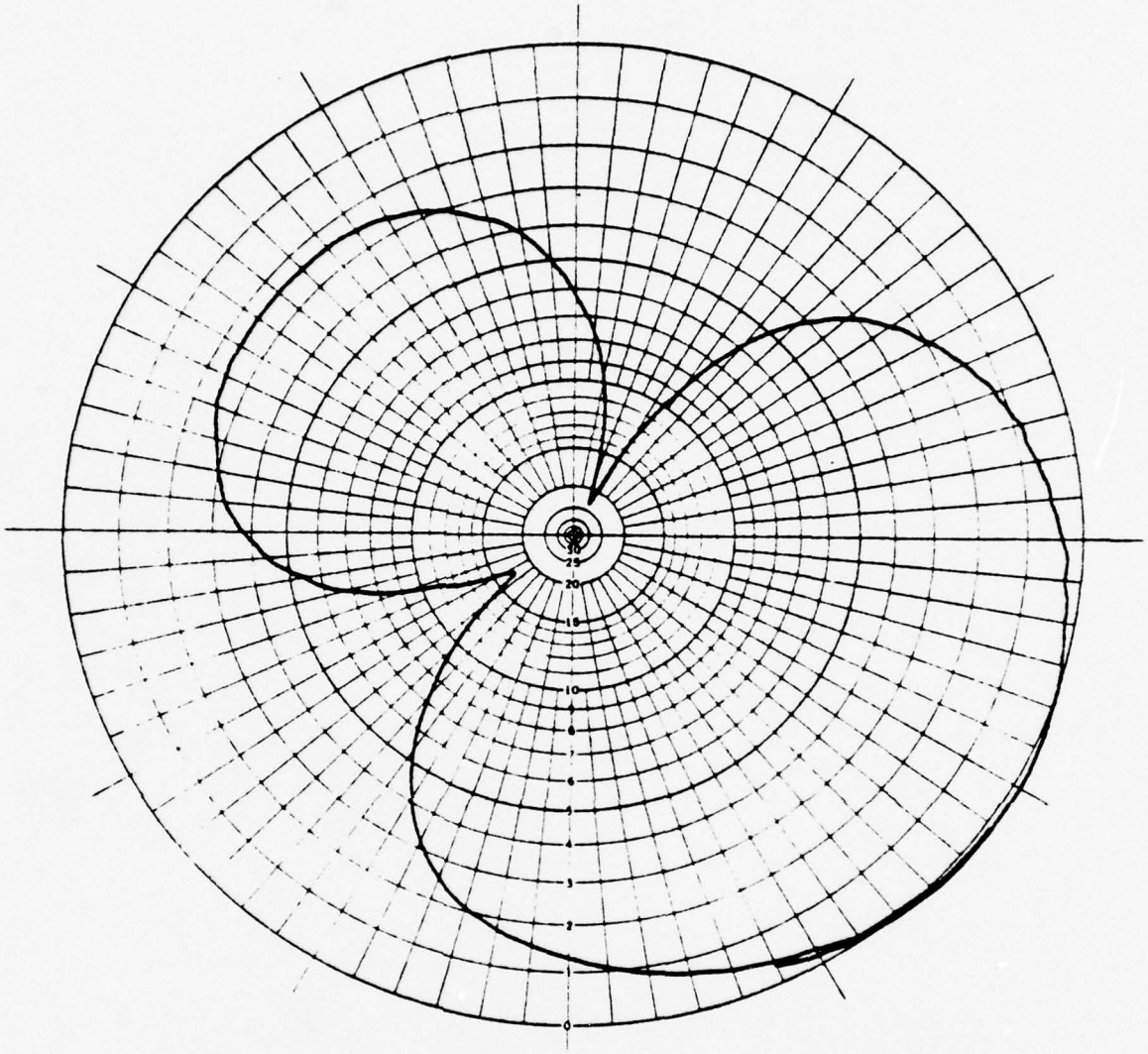

HORIZONTAL PATTERN RADIATION SIDE 1 OF THE ANTENNA

FRECUENCY: 900 MHZ

FIG. III-23

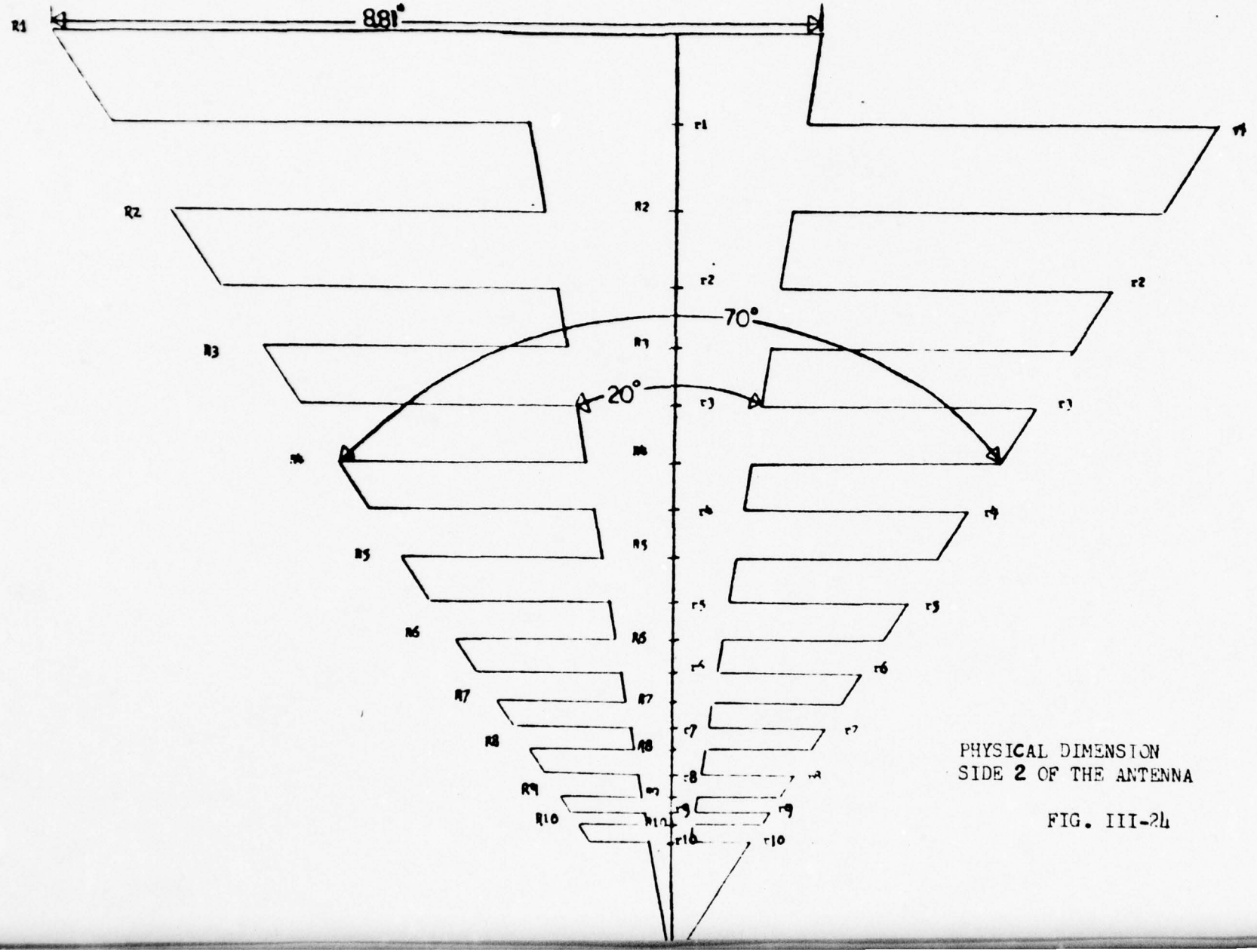

PHYSICAL DIMENSION
SIDE 2 OF THE ANTENNA

FIG. III-24

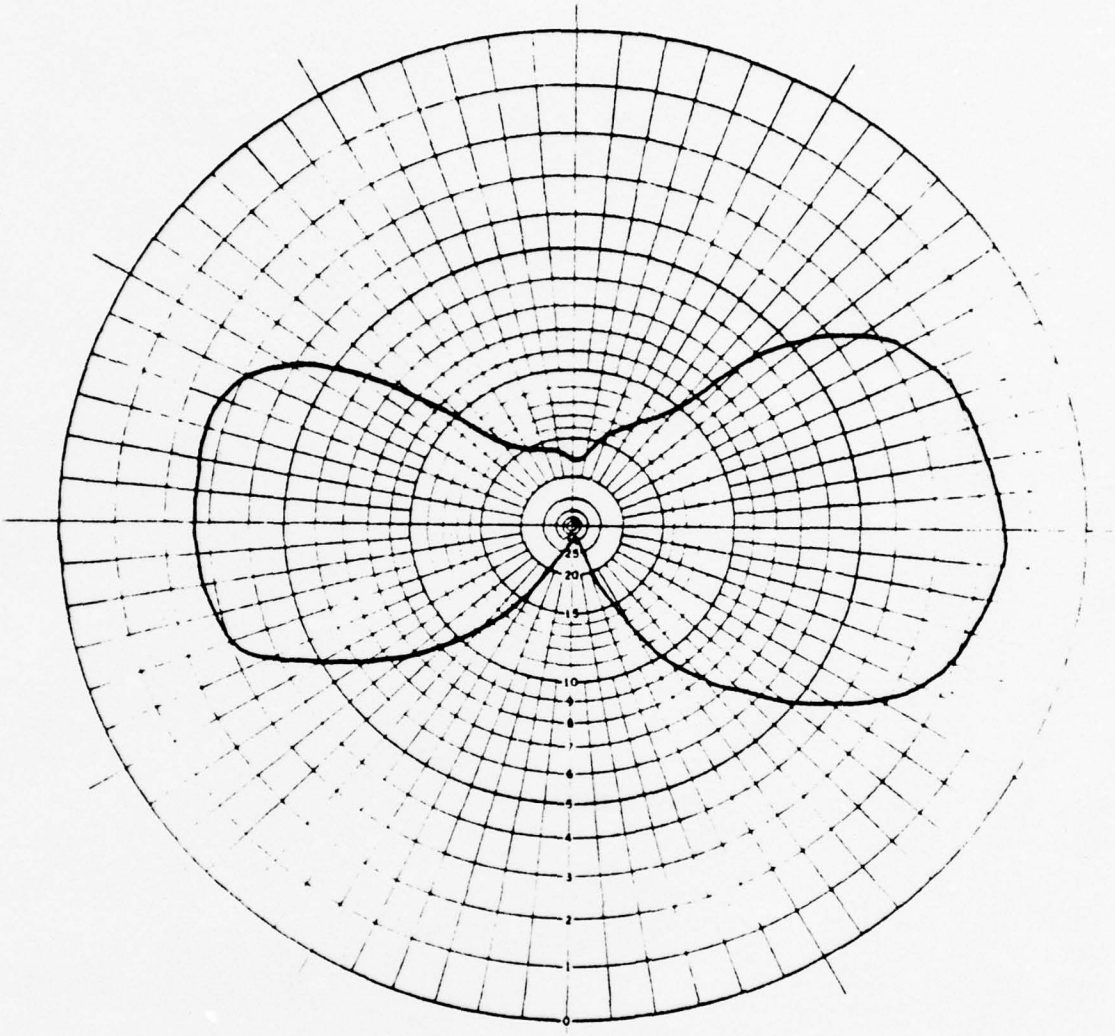

HORIZONTAL PATTERN RADIATION SIDE 2 OF THE ANTENNA

FRECUENCY: 900 MHZ

FIG. III-25

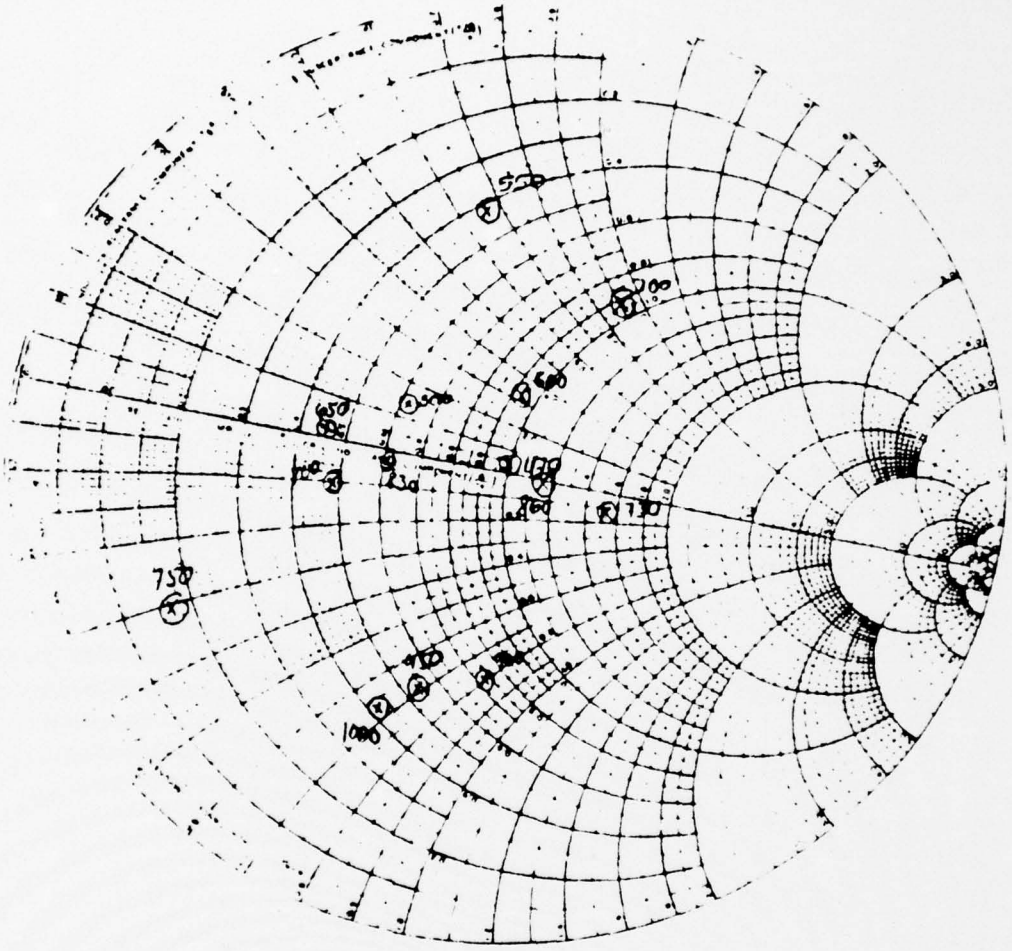

IMPEDANCE PLOT OF THE OMNIDIRECTIONAL ANTENNA

$Z_o = 130\,\Omega$ (500 to 1000 MHZ)

FIG. III-26

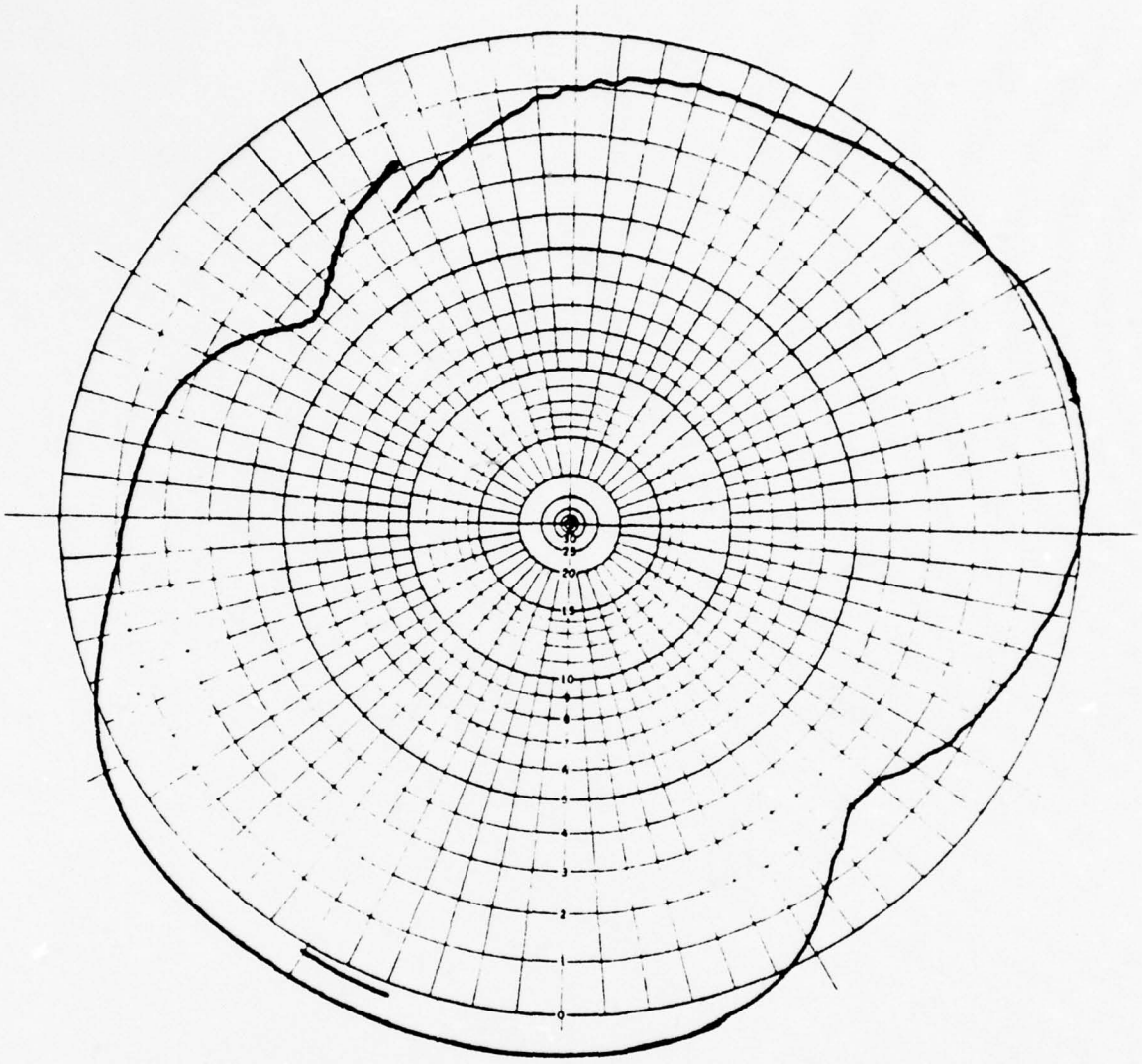

HORIZONTAL PATTERN RADIATION OF THE OMNIDIRECTIONAL ANTENNA

FRECUENCY: 900 MHZ
GAIN OVER ISOTROPIC ANTENNA: 4dB maximum

FIG. III-27

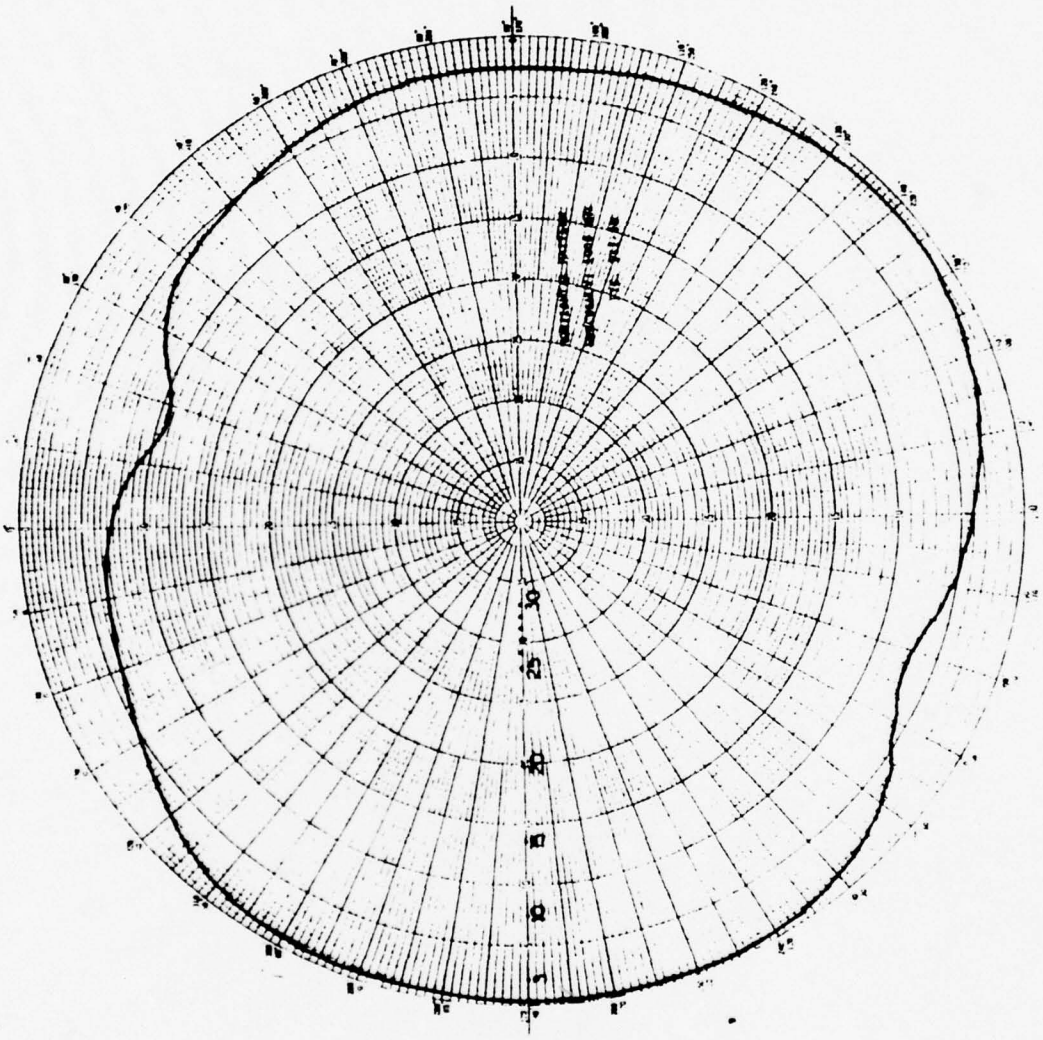

HORIZONTAL PATTERN RADIATION
OMNIDIRECTIONAL ANTENNA
FRECUENCY : 1000 MHZ
GAIN : 4dB maximum

FIG. III-28

IV. ANTENNA PATTERN MEASUREMENT

For measuring the patterns of the radar antenna and the omnidirectional antenna, the experimental array and associated equipment used for the test transmitter are shown in Fig. IV-1. A transmitting antenna was mounted at the top of Herrmann Hall at about 250 meters from the radar antenna, and approximately at the same level. The horizontally polarized echo box antenna AT-43/SPS-12 with a reflector behind it was used. The transmitter output was 1.5 Watts at 1320 MHz.

The change in signal strength in dB with antenna rotation for both receivers, radar and sidelobe, was determined every two degrees for one complete revolution of the antennas using a Narda Step Attenuator (0 to 125 dB) Model 30-0432D positioned directly at the bottom of the transmission line from each antenna to its receiver. The attenuation in dB necessary to maintain constant power at the output of each receiver was determined.

The antenna patterns of the radar antenna and of the log-periodic omnidirectional antenna measured at the bottom of the transmission line from the antenna are plotted in Figs. IV-2, IV-3 and IV-4. The sensitivity of both the radar and auxiliary receiver for a 2 to 1 (S+N)/N ratio is almost the same (106 dBm and 105 dBm). For the two sets of measurements the same attenuator (Narda DC-1GHZ, $Z_o = 50\Omega$,

Model 30-0432D) and voltmeter (H.P.) were used. Some theoretical considerations with respect to the cosecant-squared antenna (radar antenna) are given in Appendix D.

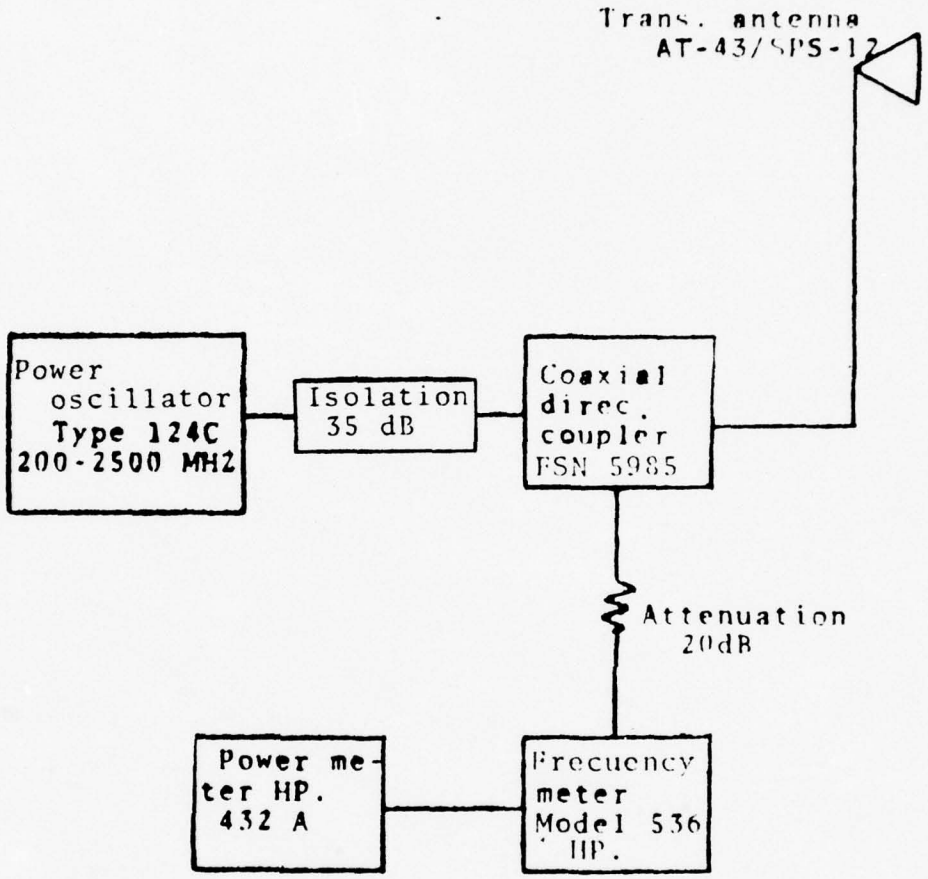

EQUIPMENT USED FOR THE TEST TRANSMITTER

FIG. IV-1

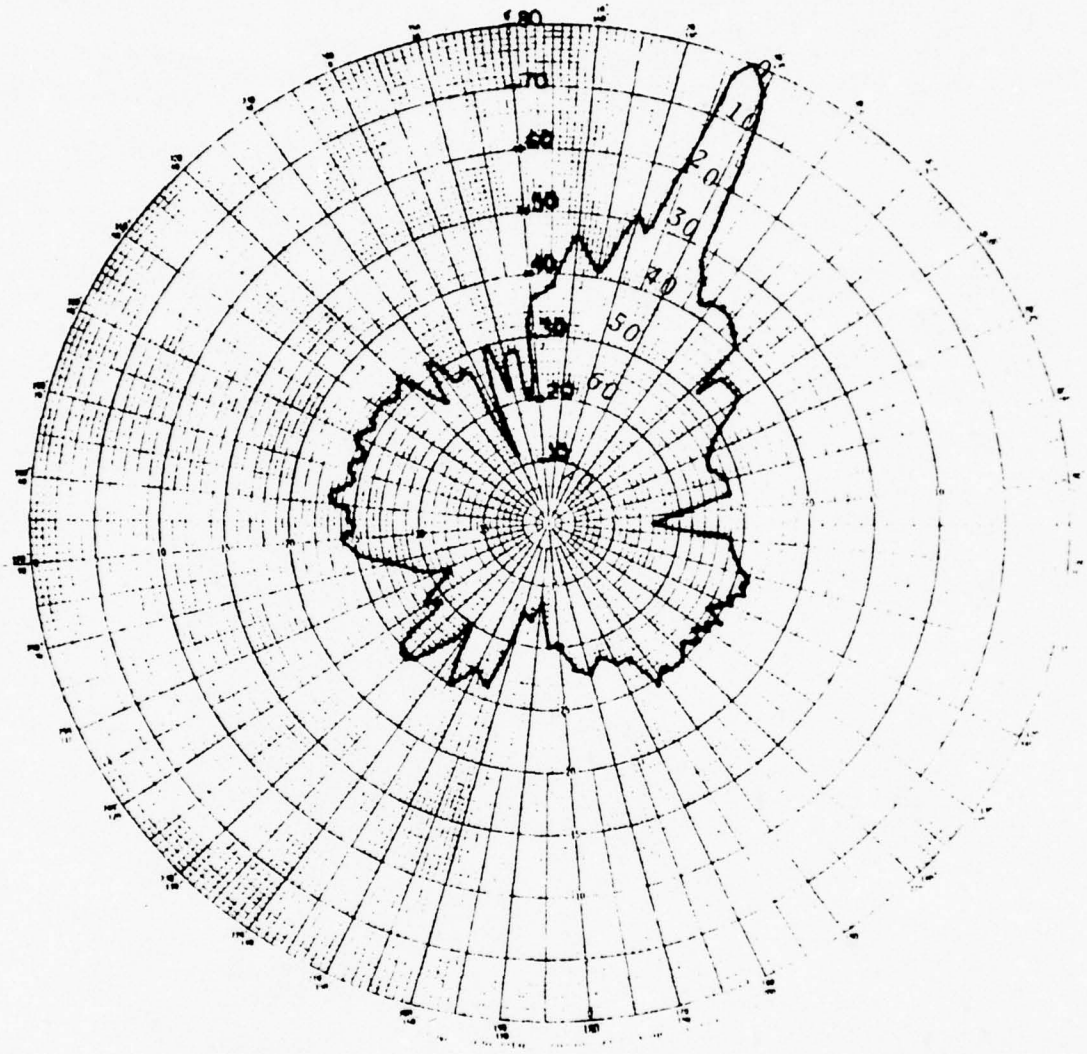

HORIZONTAL PATTERN
RADAR ANTENNA (AN-SPS/12)
HORIZONTAL POLARIZATION
FRECUENCY : 1320 MHZ
(Scale in dB of attenuation to maintain constant output at the receiver, and normalized to 0 dB at the pattern peak)

FIG. IV-2

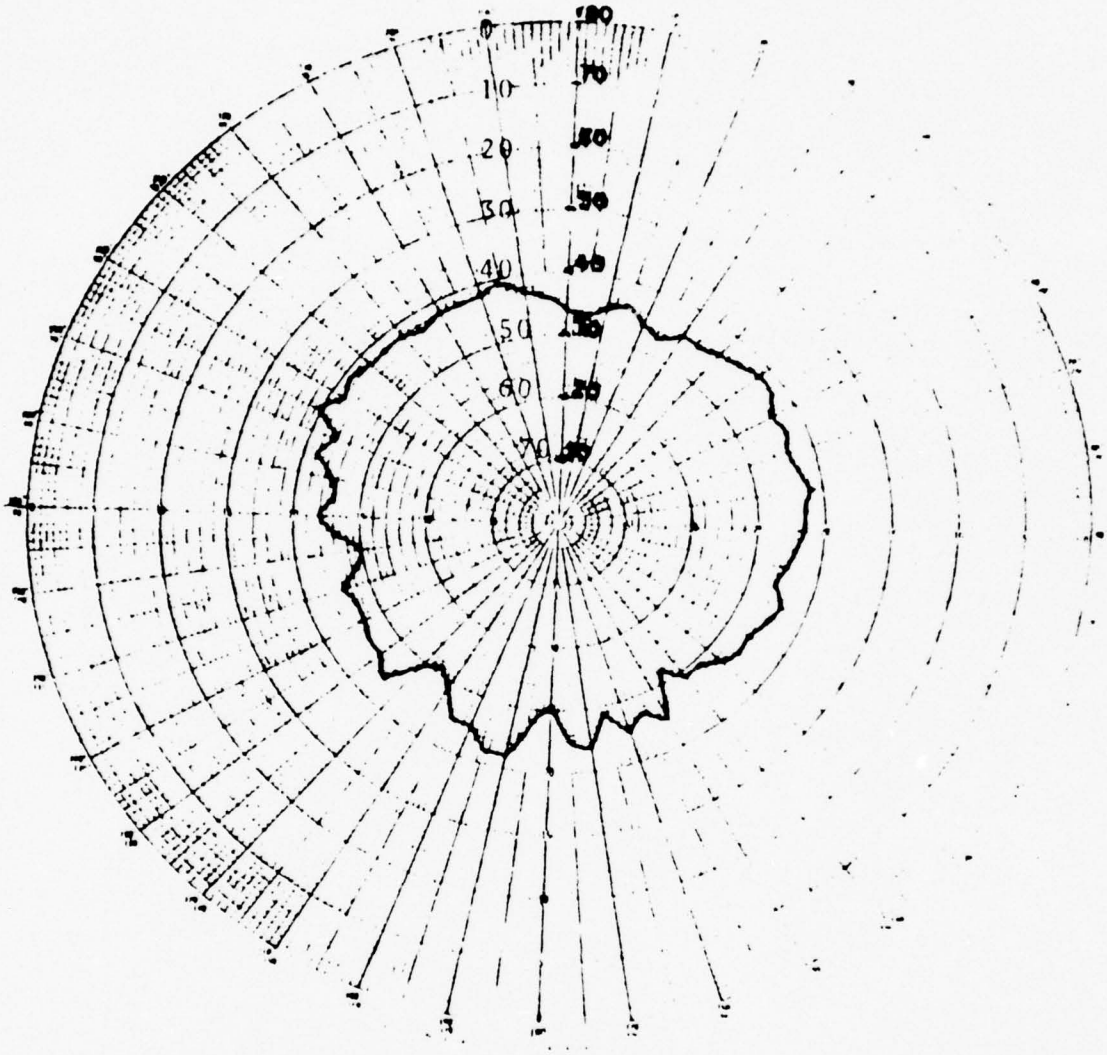

HORIZONTAL PATTERN
OMNIDIRECTIONAL ANTENNA(LOG-PERIODIC)
HORIZONTAL POLARIZATION
FREQUENCY : 1320 MHZ
(Scale in dB of attenuation to maintain constant output at the receiver,and normalized to 0 dB at the pattern peak for the radar antenna)

FIG. IV-3

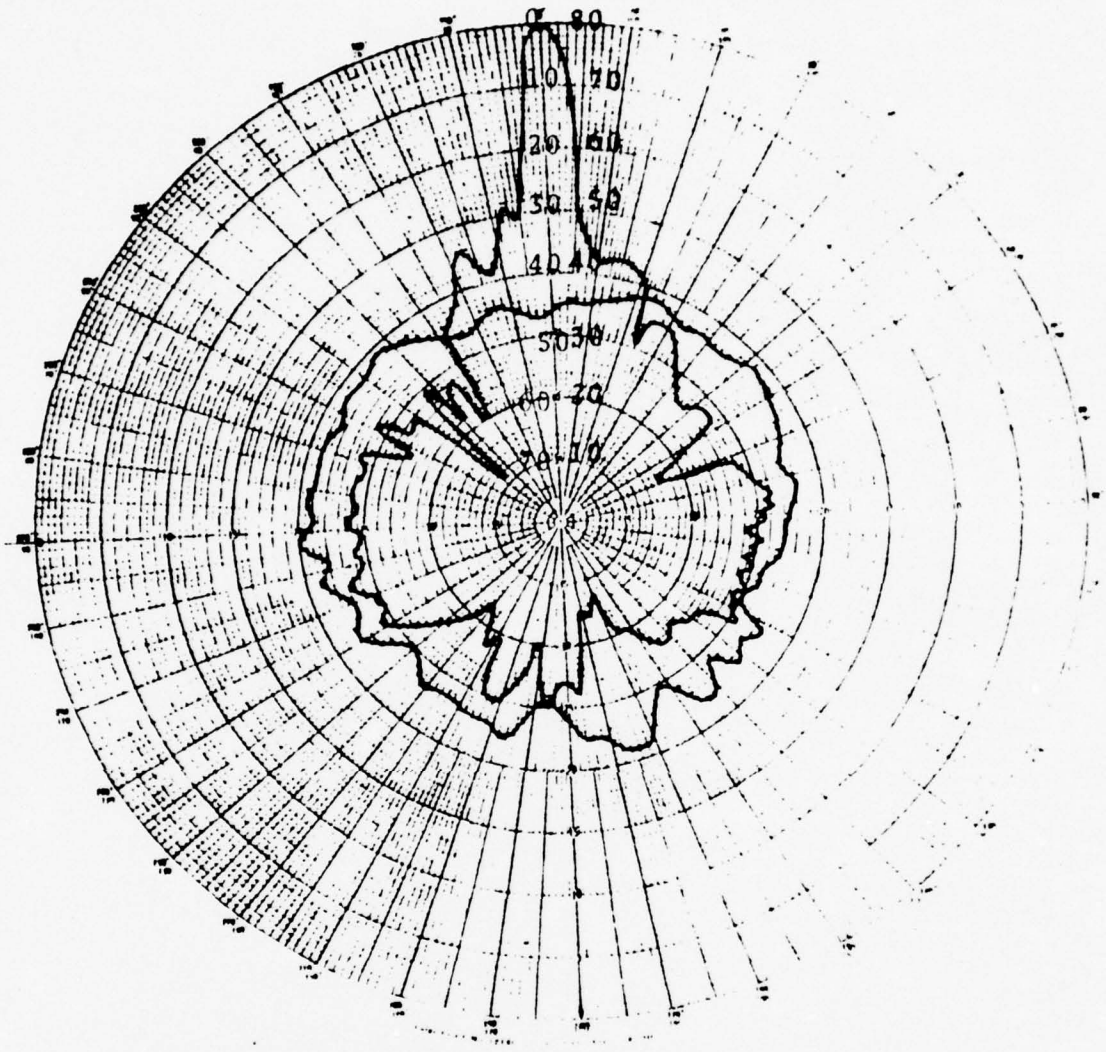

HORIZONTAL PATTERN
RADAR AND OMNIDIRECTIONAL ANTENNA(SUPERIMPOSED)
HORIZONTAL POLARIZATION
FRECUENCY : 1320 MHZ
(Scale in dB of attenuation to maintain
constant output at the receivers,and
normalized to 0 dB at the pattern peak
for the radar antenna)

FIG. IV-4

V. SIDELOBE BLANKING TEST

For the sidelobe blanking test, the experimental setup is shown in Fig. V-1. In order to compensate for the long line used to feed the radar signal into the blanking system together with other system delays (normally they would be close together), it was necessary to delay the sidelobe signal by 2.5 μsec. The total sensitivity of the sidelobe receiver was measured to be 105 dBm for 2 to 1 (S+N)/N compared with 106 dBm for the radar receiver.

It was determined that the sidelobe blanking signal must be 0.2 to 0.25 volts larger than the signal in the main channel in order for the blanker system to blank the video output to the display circuits.

For clarity the displayed signals on the oscilloscopes are shown at different scales as follows:

Radar signal	:	0.5 Volts/Div
Sidelobe signal	:	1.0 Volts/Div
Sidelobe blanking system output	:	0.5 Volts/Div.

In Fig. V-2 are shown simulated video signals. The pictures on the left side show in the upper trace the main channel (radar signals) and in the lower trace the auxiliary channel (sidelobe blanking signal). The picture on the right side shows the output of the sidelobe blanking system. The trace is expected to be essentially the same as the main

channel signal but blanked at some ranges where the sidelobe blanking signal is stronger than the radar signal.

In order to correlate signals in the two channels in time, it was found to be convenient to introduce large attenuation in the main channel (76 dB). A large number of echos could then be correlated, and the delay line length was adjusted for time coincidence. The video pictures obtained are shown in Figs. V-5 and V-6.

The output of the sidelobe blanking system shows very neat blanking at the beginning of the trace, where the strong clutter around the radar antenna is often stronger in the side lobes.

Defining:

SL = sidelobe signal

R = radar signal

SLB = sidelobe blanking

The results are shown in Figs. V-3 to V-8 for different test signals (different widths and amplitudes).

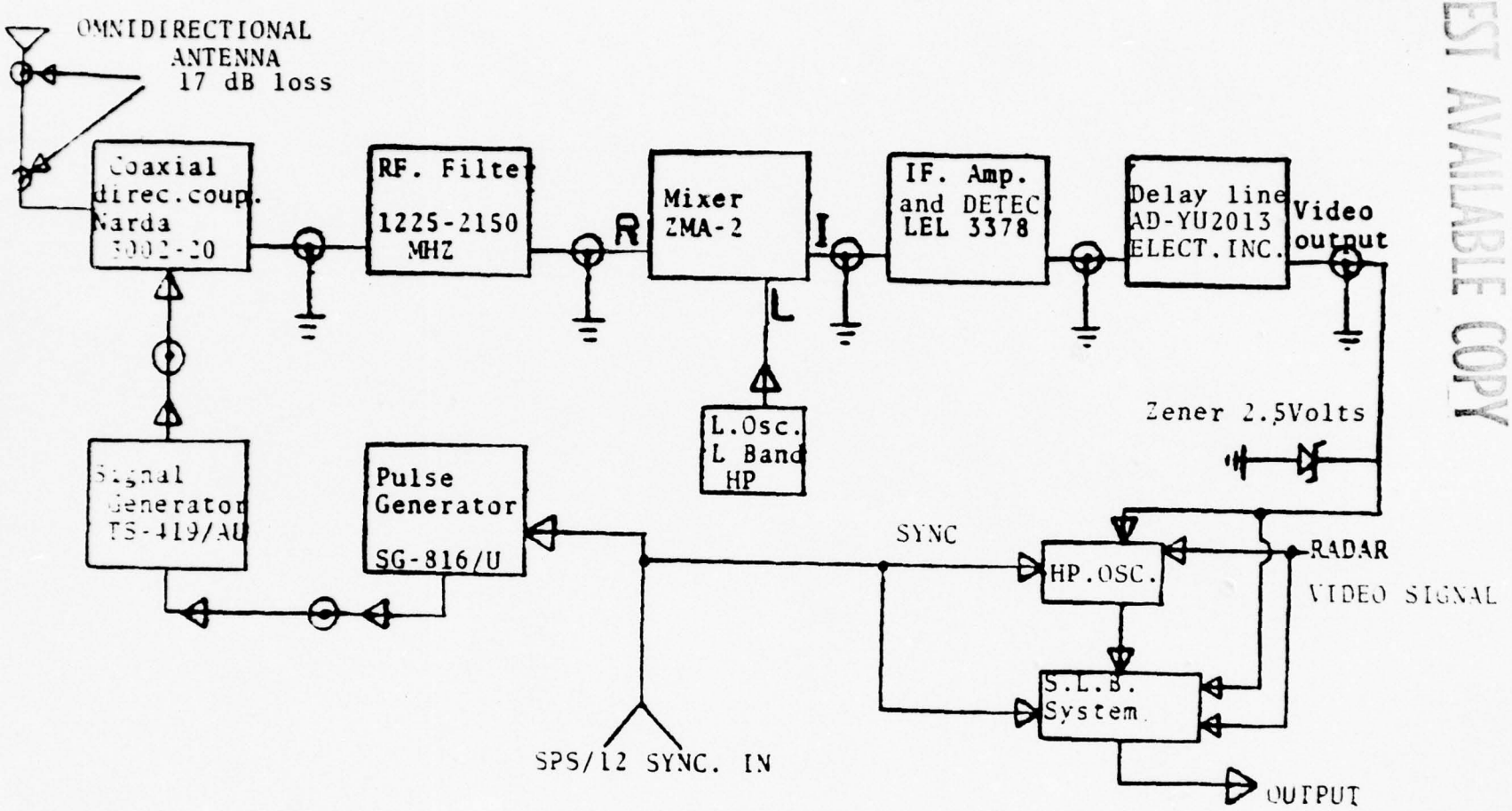

EXPERIMENTAL SET-UP FOR THE SIDELOBE BLANKING TEST

FIG. V-1

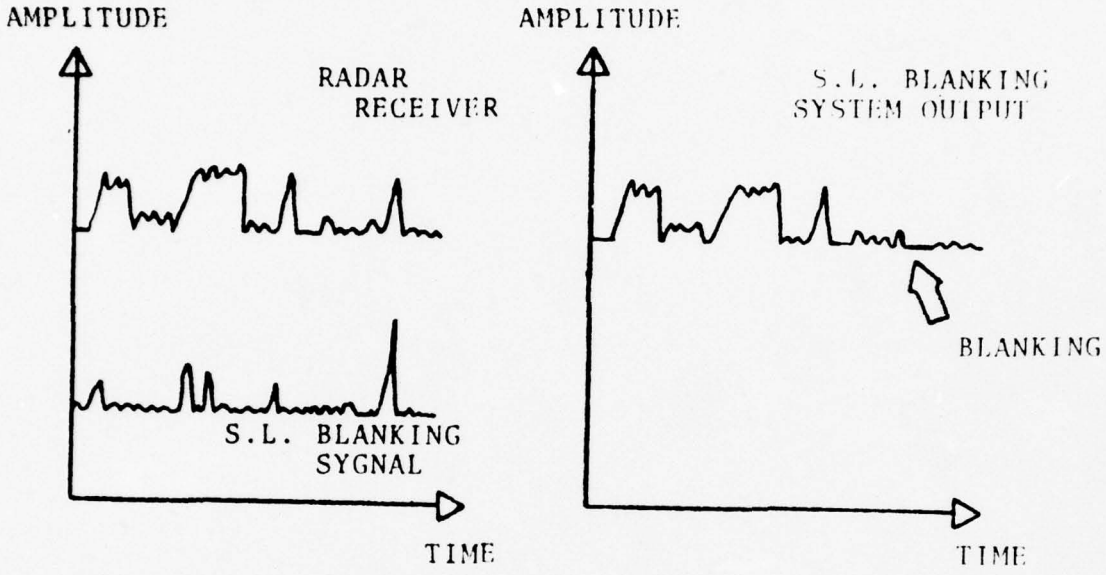

SIMULATED VIDEO SIGNALS

FIG. V-2

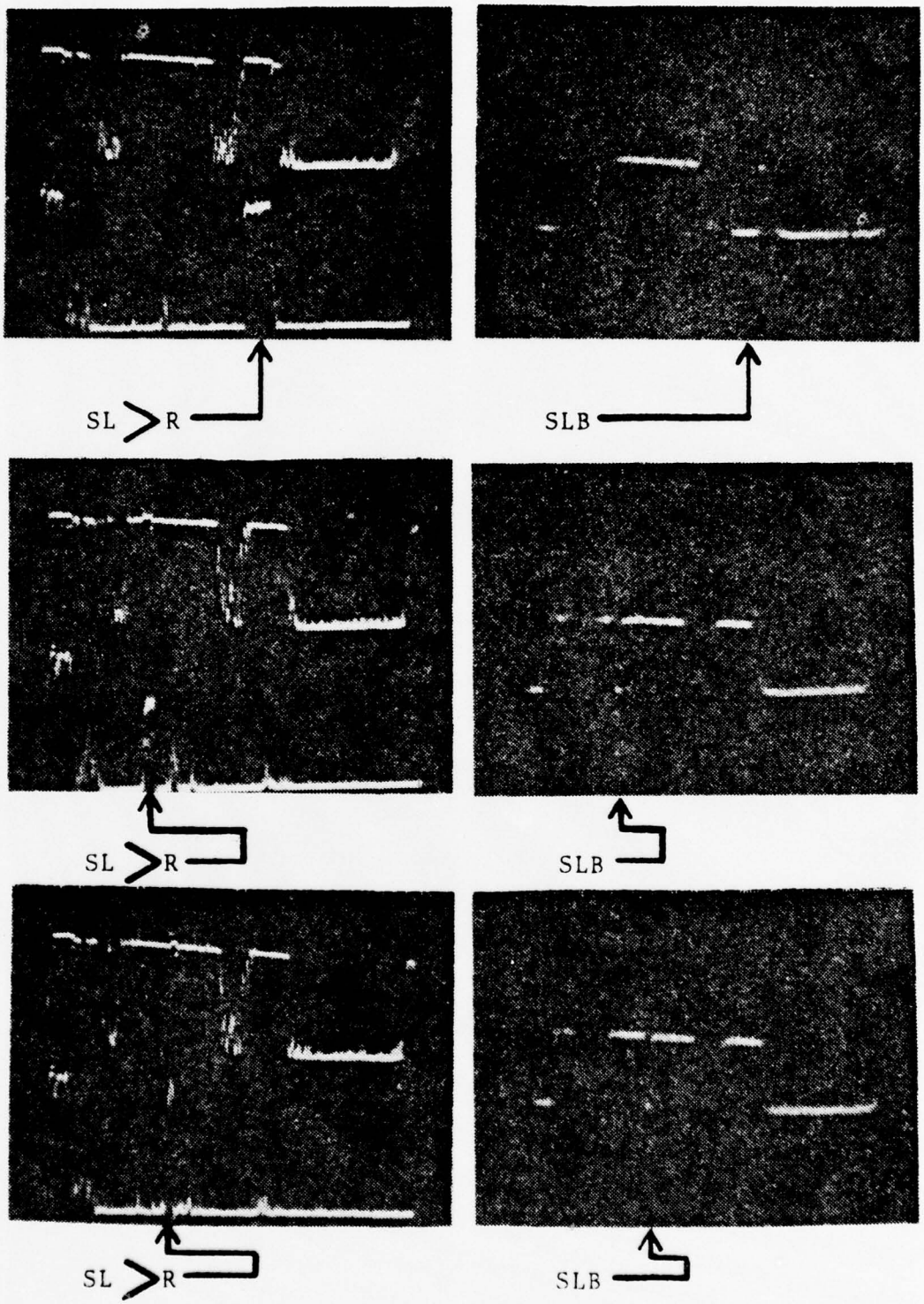

RADAR RECEIVER, NORMAL OPERATION

FIG. V-3

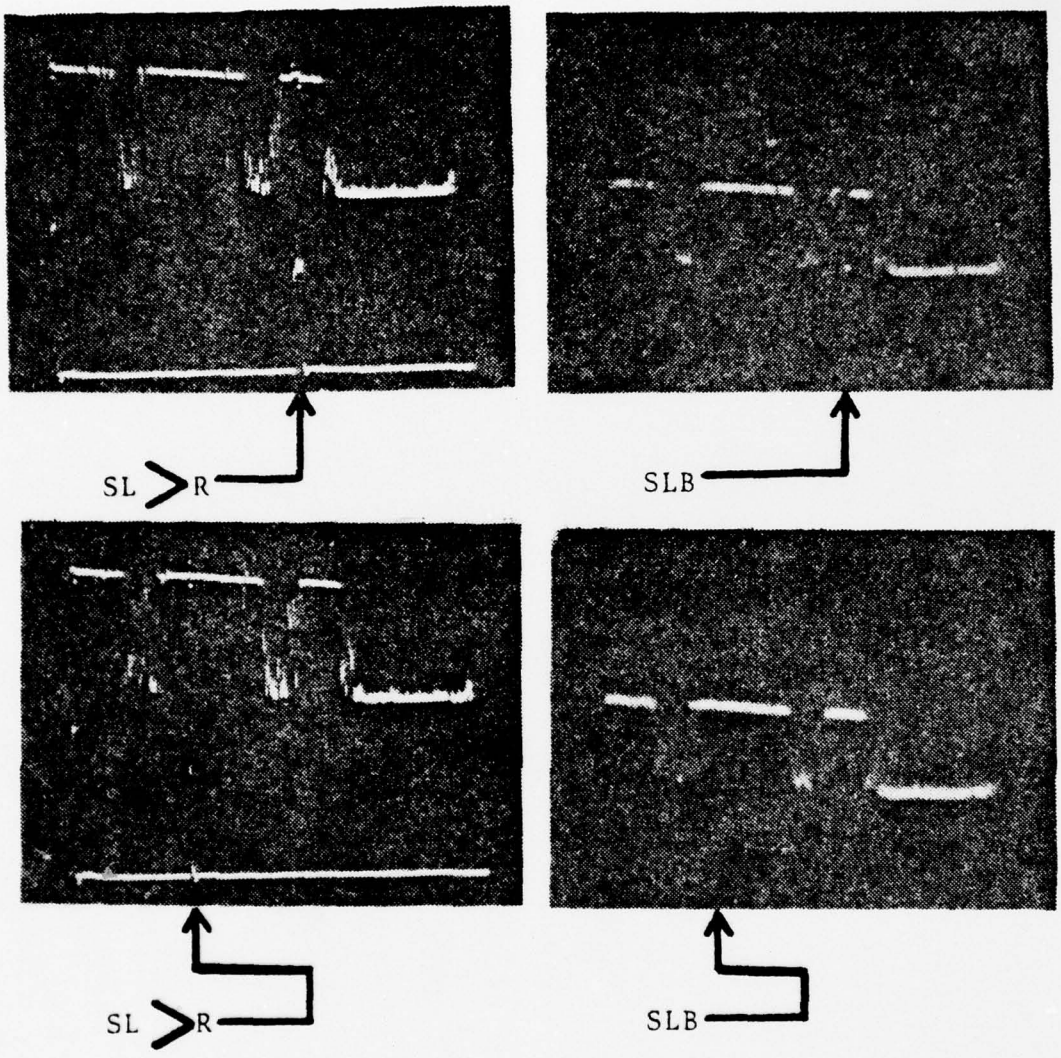

EFFECT OF REDUCED GAIN IN SIDELOBE CHANNEL

FIG.V-4

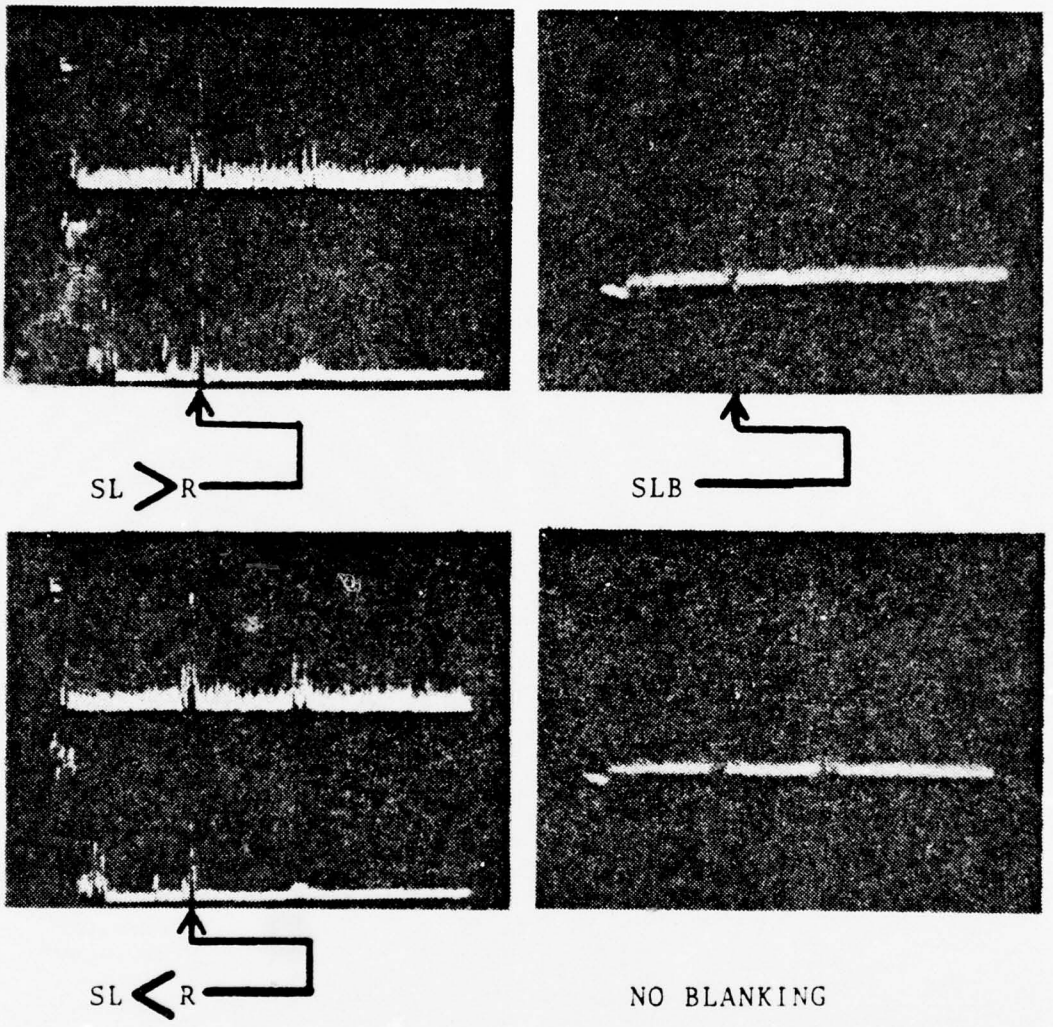

EFFECT OF 76 dB OF ATTENUATION BETWEEN
THE ANTENNA AND MIXER AT THE RADAR RECEIVER

FIG. V-5

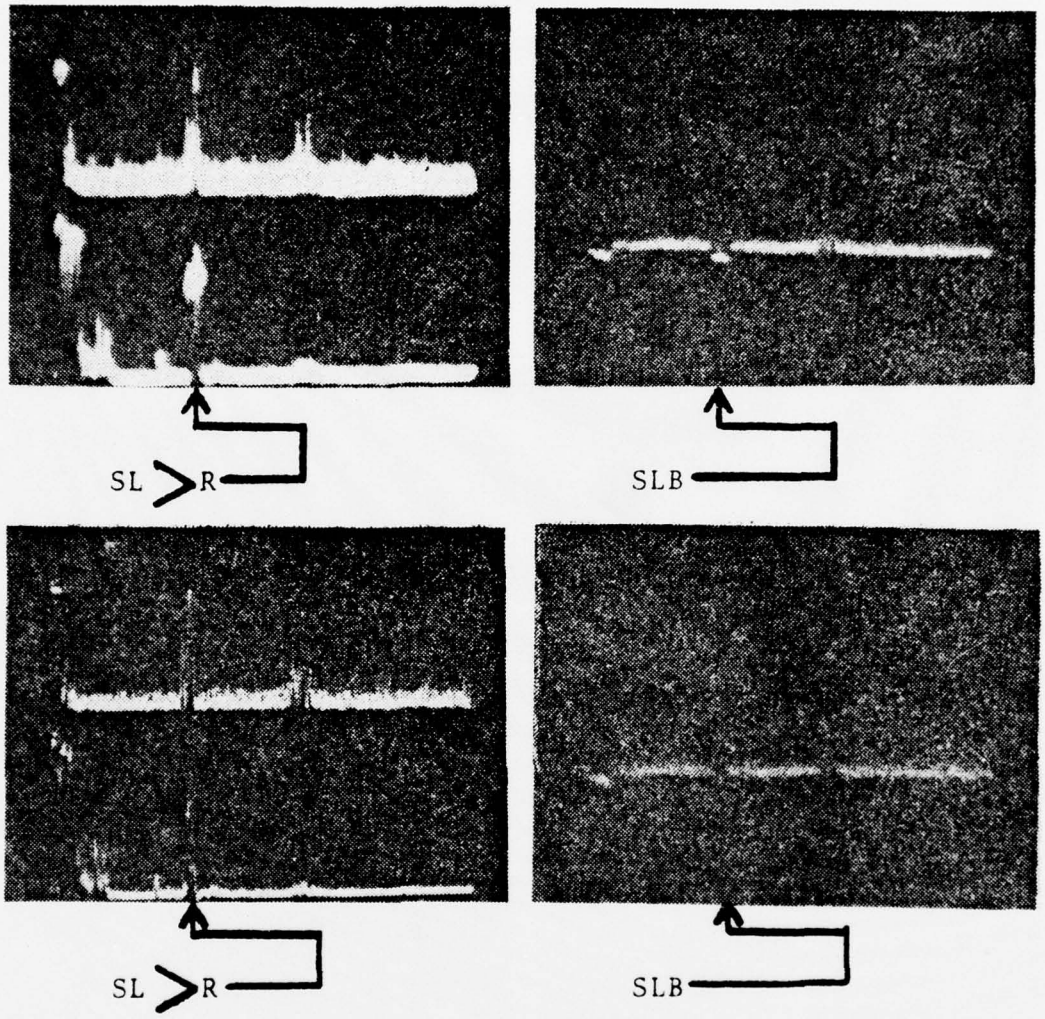

EFFECT OF 76 dB OF ATTENUATION BETWEEN
THE ANTENNA AND MIXER AT THE RADAR RECEIVER

FIG. V-6

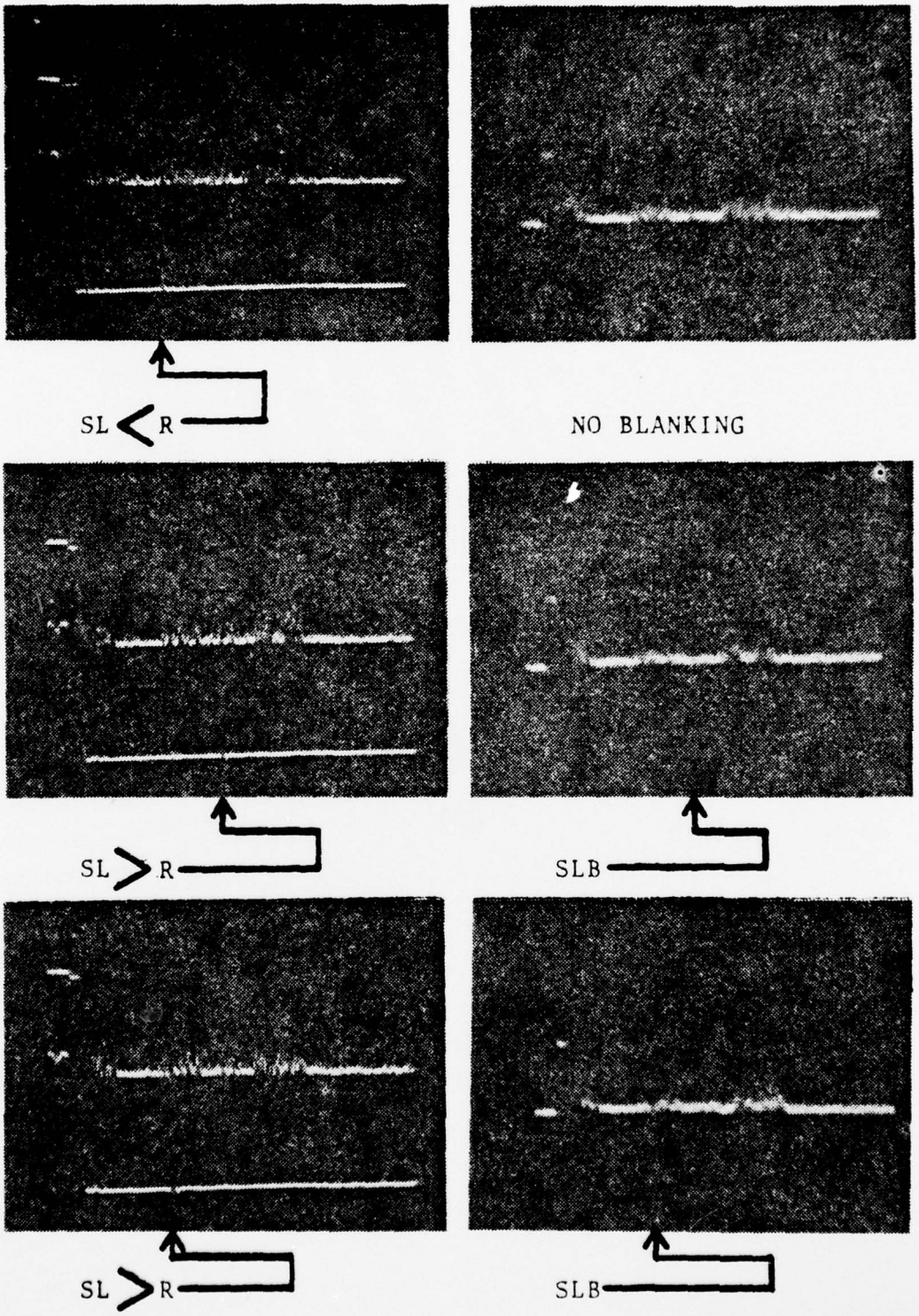

RADAR RECEIVER, NORMAL OPERATION
(DIFFERENT WIDTH AND AMPLITUDE TEST SIGNAL)
FIG. V-7

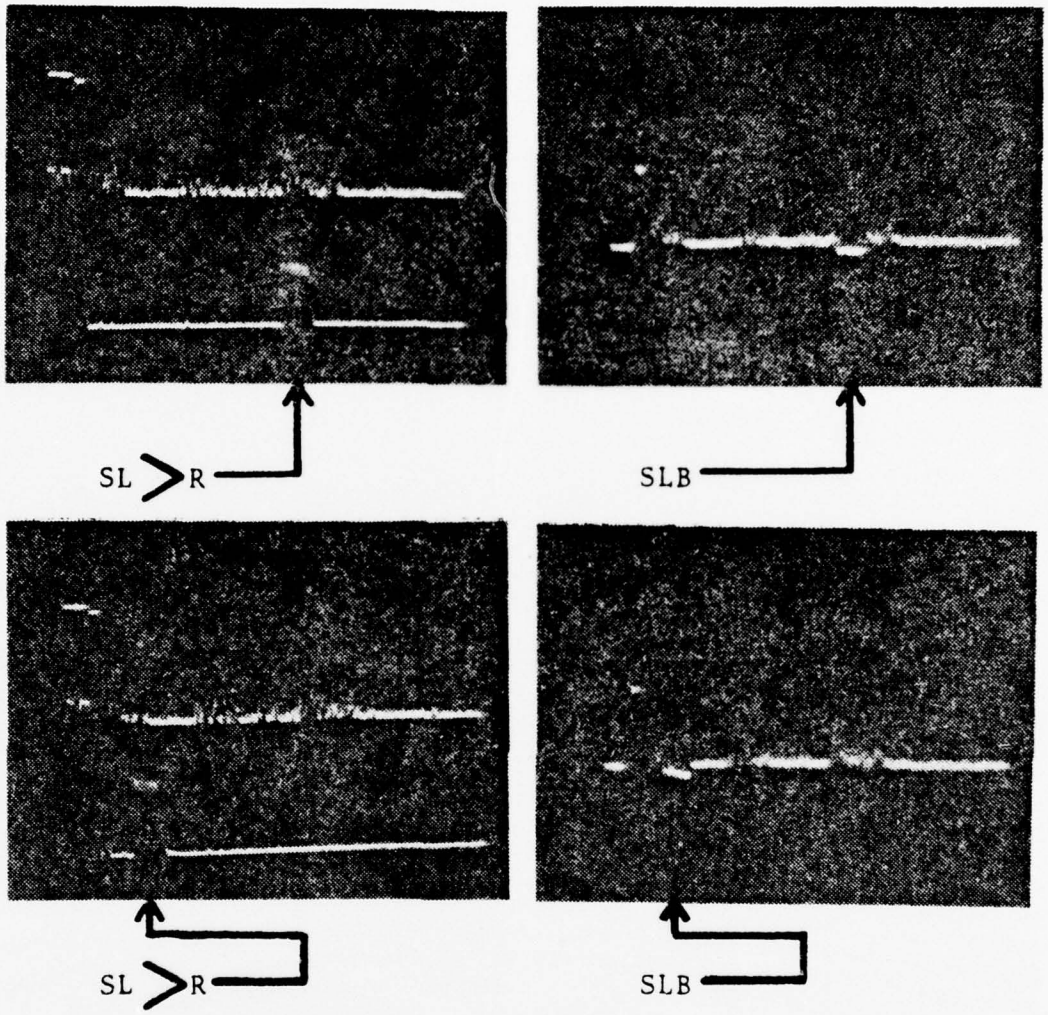

RADAR RECEIVER, NORMAL OPERATION
(DIFFERENTS WIDTH AND AMPLITUDE TEST SIGNAL)

FIG. V-8

VI. PERFORMANCE OF RADAR WITH PULSE JAMMING

An overall test of the sidelobe blanking system was accomplished by jamming the radar from the same transmitter used for antenna pattern measurement, first with a 10 μsec wide pulse signal at a prf of 3 kHz (duty cycle = 0.03) 100 mW power, and then with a 17 μsec wide pulse signal at a prf of 4 kHz (duty cycle = 0.068) 100 mW output power.

The horizontally polarized echo box antenna AT-43/SPS-12 with an estimated gain of 2 dB over an isotropic antenna was mounted at the same level and about 50 meters from the radar and sidelobe antenna on the roof-top range above Spanagel Hall, and was used for the jamming purposes. The experimental array and associated equipment are shown in Figs. VI-1 and VI-2.

The output of the sidelobe blanking system was fed into a PPI (SPA-8A) for display purposes. In order to match the high output impedance of the SLB system with the low input impedance of the SPA-8A (50 Ω), an emitter follower configuration was used, Fig. VI-3.

For the test and measurements with pulse jamming the zener diode shown in Fig. V-1 limiting the amplitude of the radar video signal, was removed, leaving the video signal with normal amplitude.

For each of the two jamming signals the pattern of the radar receiver was changed by varying the radar transmitter

prf ± 5 percent. The test was conducted first with the high pass video of the radar "on" and finally with the radar working in normal conditions.

The results are shown in Figure VI-4 to VI-7. All the pictures are on the same range scale, 50 miles. In Figure VI-4 true North is indicated by the cursor position. These two pictures with no jamming show that there is no apparent loss in performance incurred due to the presence of the sidelobe suppression channel in detecting targets.

With the sidelobe blanking system "on" the pictures show jamming in the main beam and a reflection probably produced by one of the antennas around the SPS-12 radar antenna. Other jamming signals entering the radar antenna through the side lobes have been eliminated.

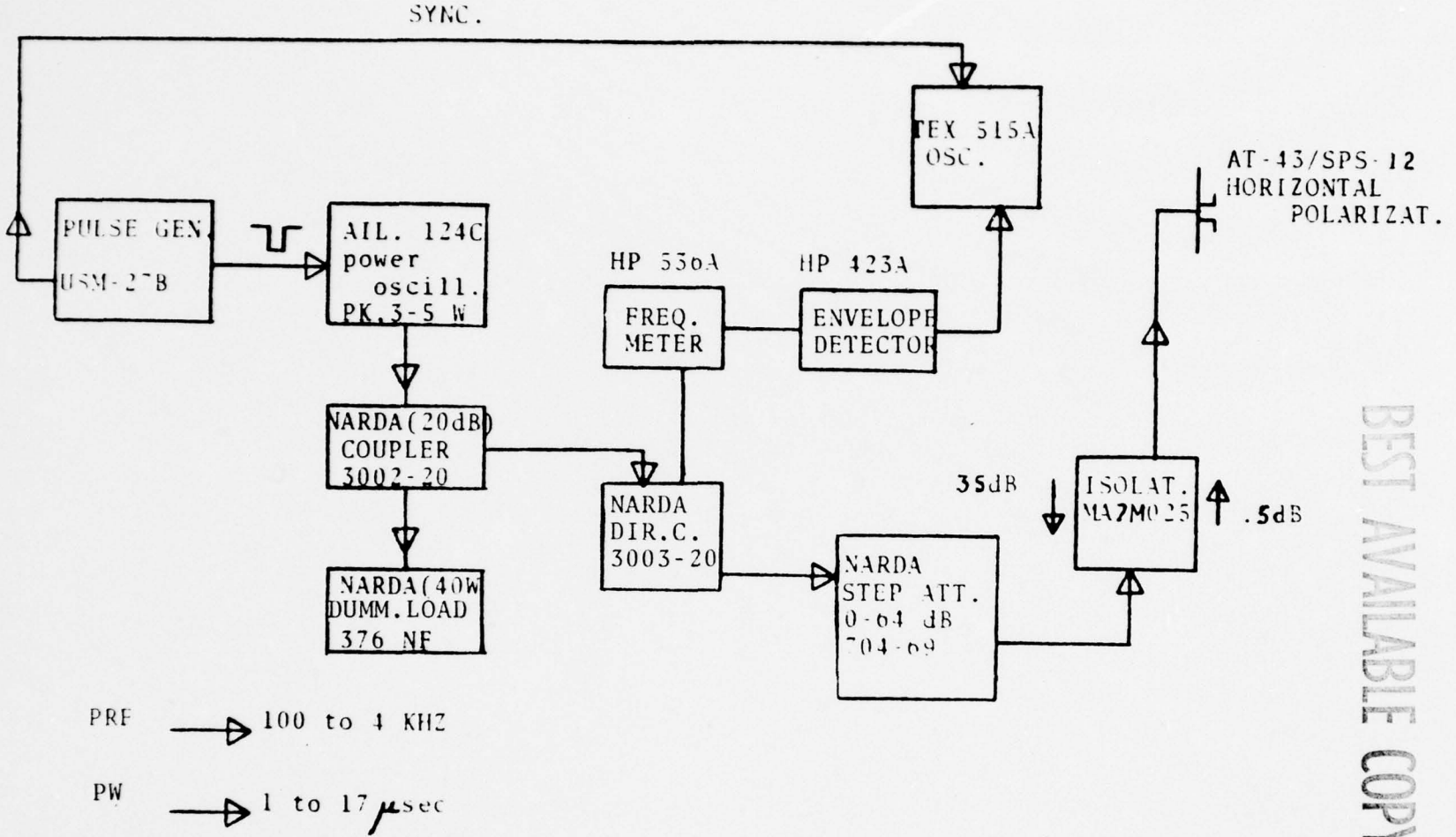

PULSE JAMMER TRANSMITTING SYSTEM

FIG. VI-1

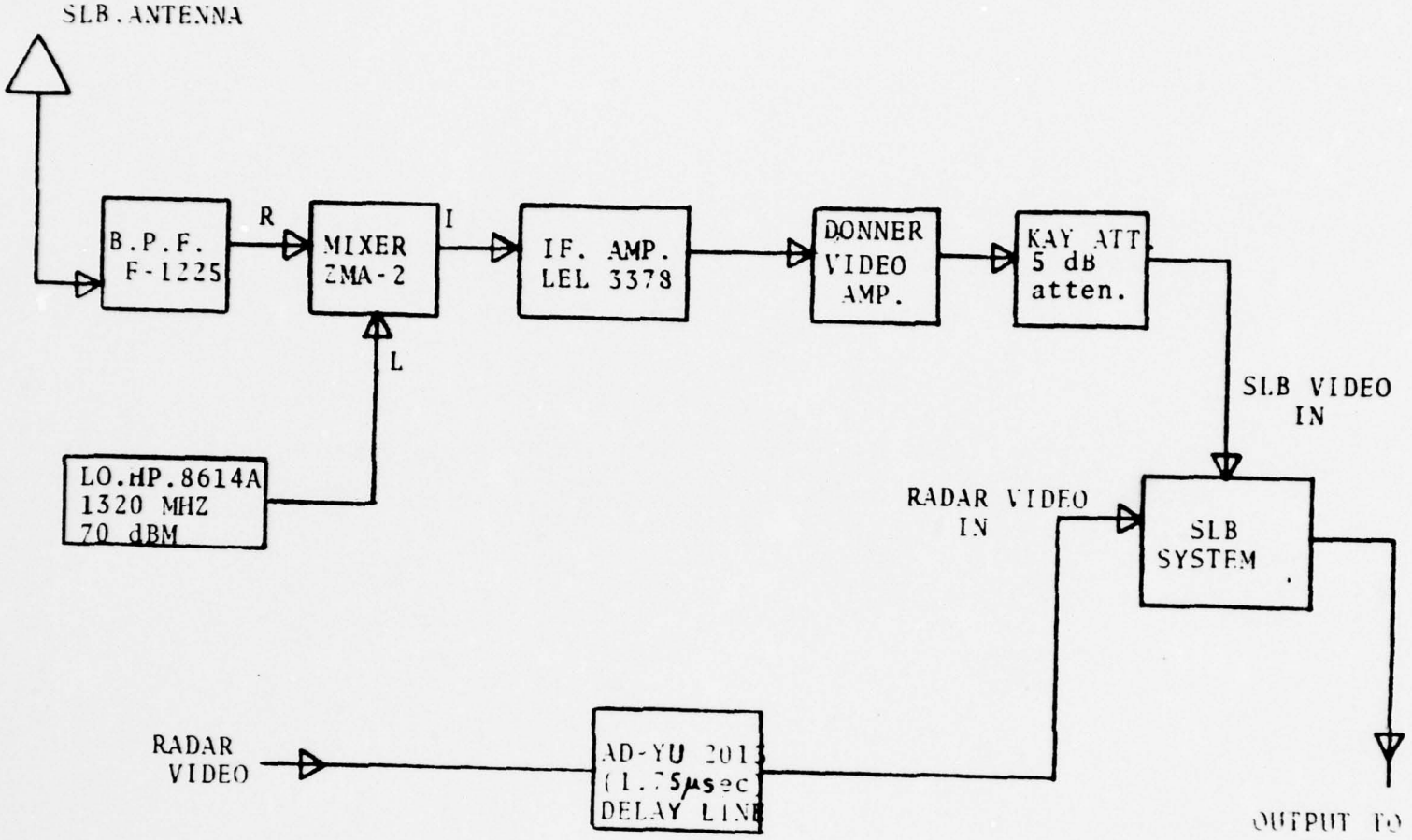

EXPERIMENTAL ARRAY FOR THE TEST AND MEASUREMENTS
WITH PULSE JAMMING

FIG. VI-2

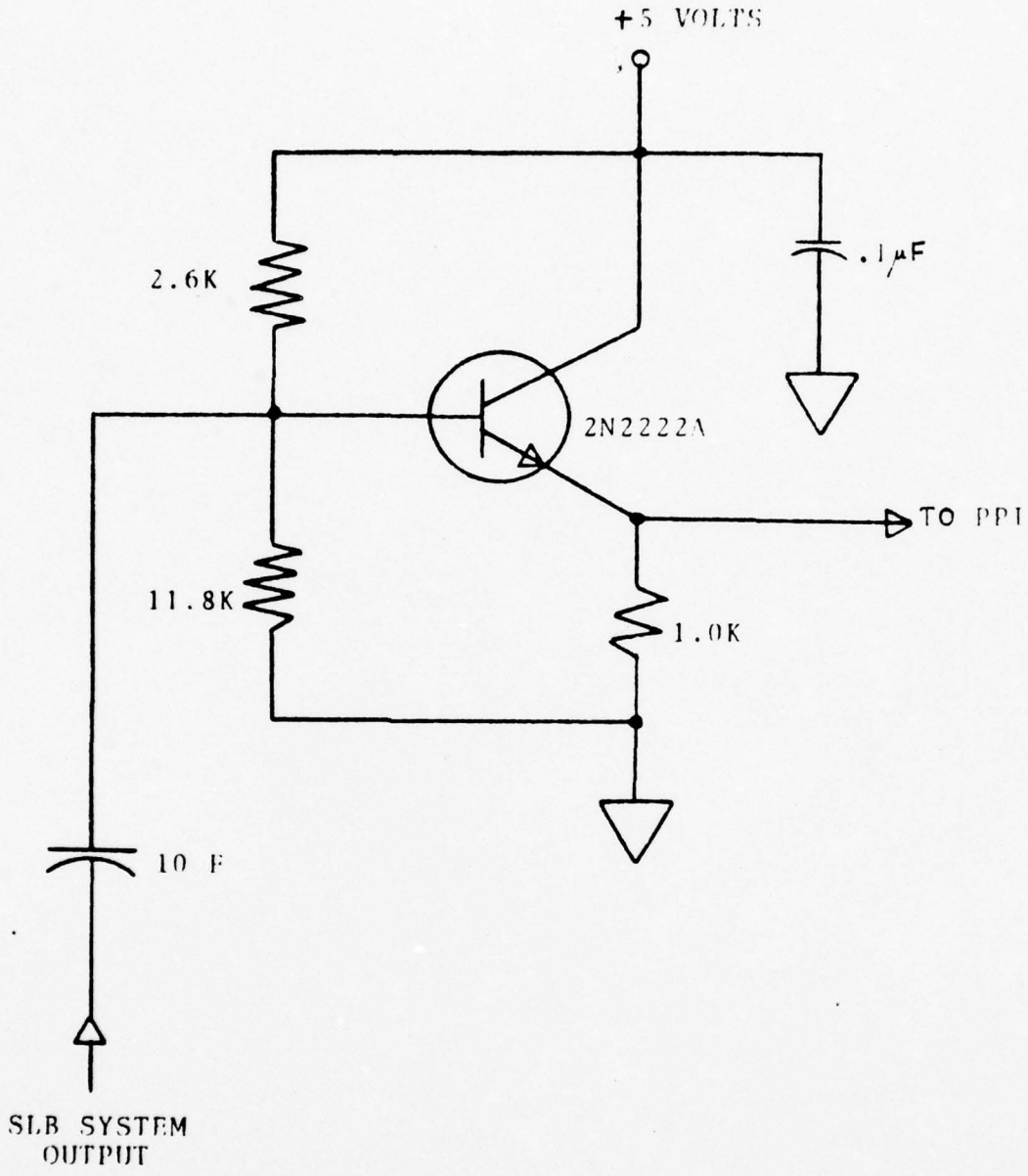

EMITTER FOLLOWER

FIG. VI-3

RADAR AN/SPS-12 VIDEO
CURSOR AT 000°, RANGE 50 MILES

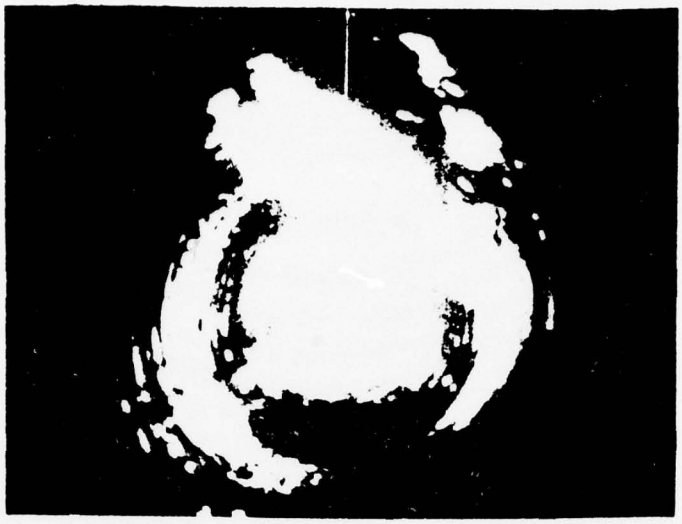

STRAIGHT SPS-12 VIDEO
SLB "OFF"
NO JAMMING

SPS-12 VIDEO
SLB "ON"
NO JAMMING

FIG.VI-4

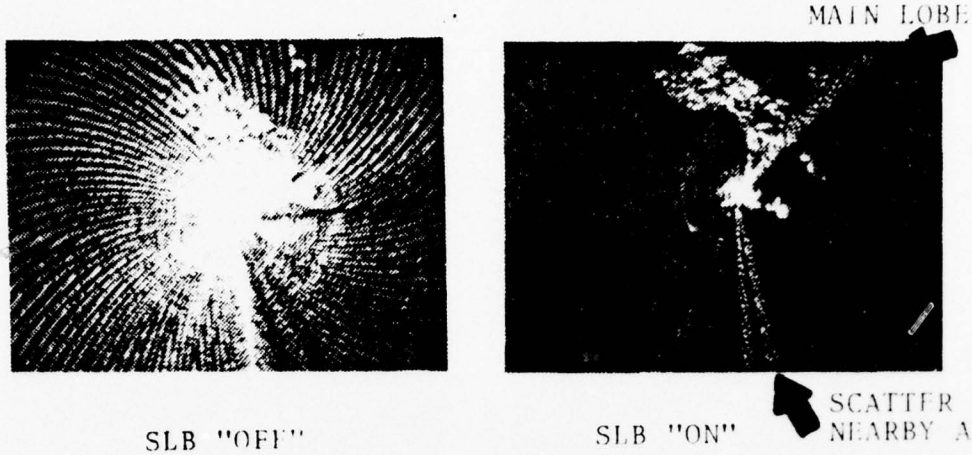

SLB "OFF" SLB "ON"

SLB "OFF" SLB "ON"

SLB "OFF" SLB "ON"

RADAR AN/SPS-12 VIDEO.PPI DISPLAYS WITH PULSE JAMMING,HIGH PASS VIDEO "ON" 10μsec JAMMING PULSES AT 3KHZ.(The radar prf was changed by 5 percent between each pair of pictures.)

FIG. VI-5

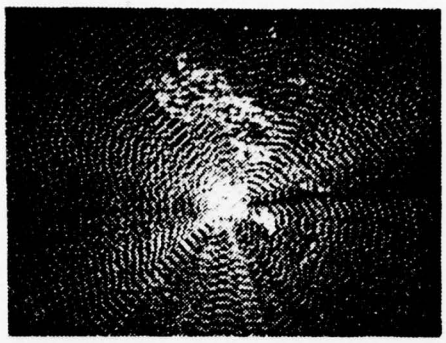

SLB "OFF"

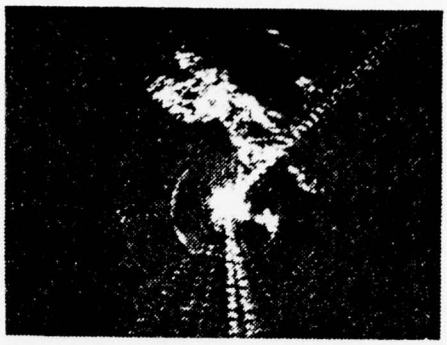

SLB "ON"

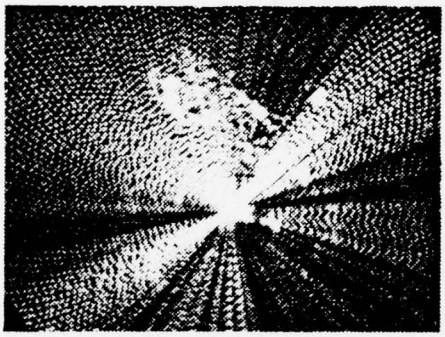

SLB "OFF"

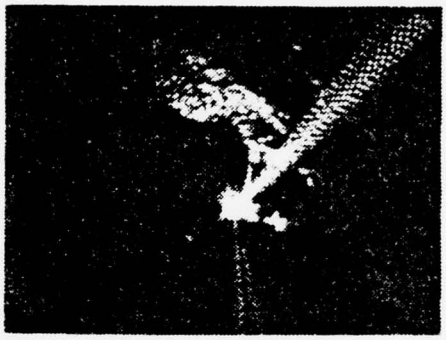

SLB "ON"

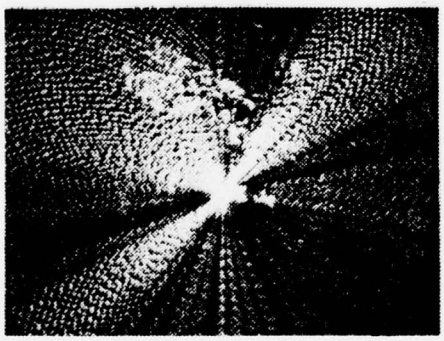

SLB "OFF"

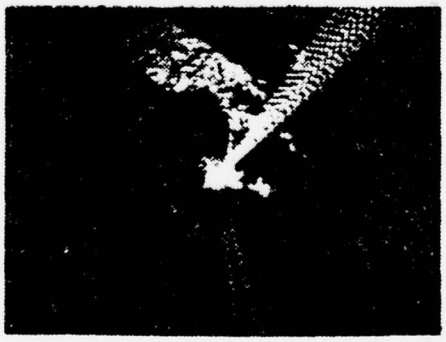

SLB "ON"

RADAR AN/SPS-12VIDEO.PPI DISPLAYS WITH PULSE JAMMING,HIGH PASS VIDEO "ON".17 μsec JAMMING PULSE AT 4 KHZ. (The radar prf was changed by 5 percent between each pair of pictures)

FIG. VI-6

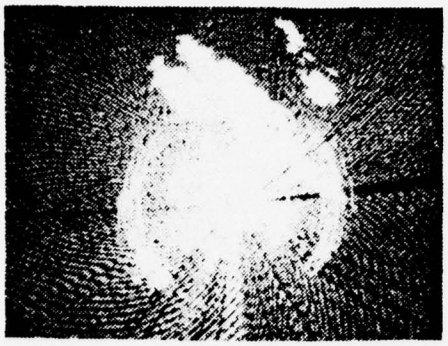

SLB "OFF"

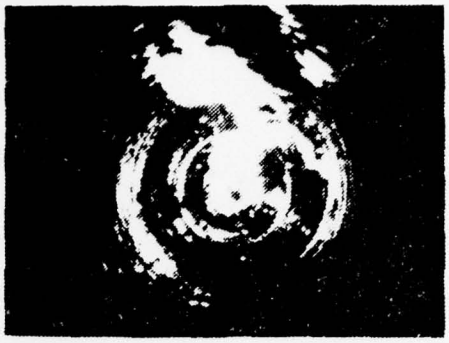

SLB "ON"

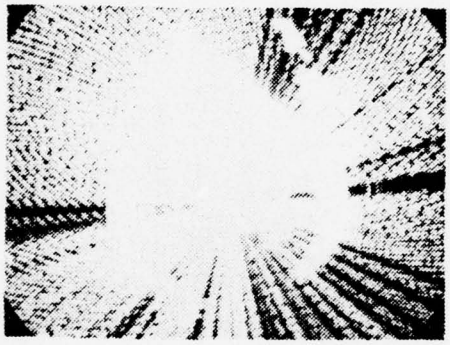

SLB "OFF"

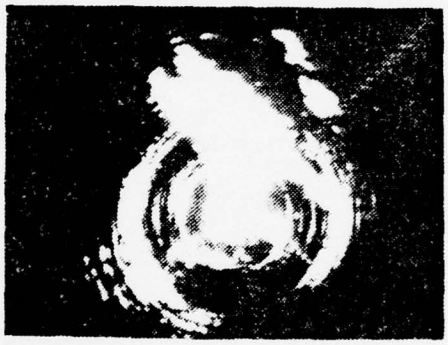

SLB "ON"

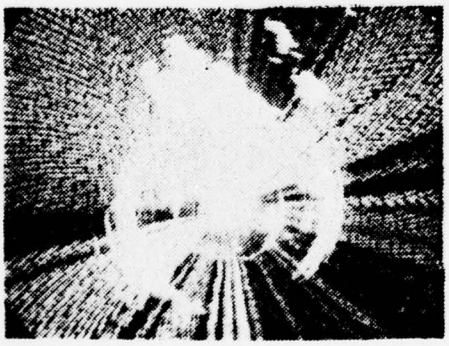

SLB "OFF"

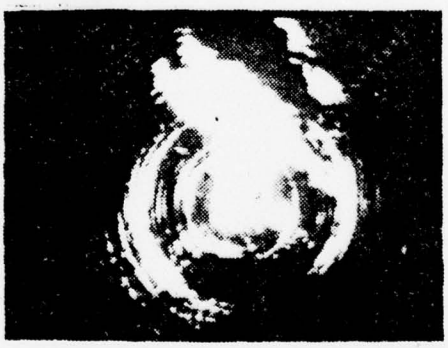

SLB "ON"

RADAR AN/SPS-12 NORMAL VIDEO.PPI DISPLAYS WITH PULSE JAMMING,HIGH PASS VIDEO "OFF". 17μsec JAMMING PULSES AT 4 KHZ. (The radar prf was changed by 5 percent between each pair of pictures)

FIG. VI-7

VII. CONCLUSIONS

The sidelobe blanking system designed was a success in preventing low-duty-cycle signals coming through the sidelobes of the radar antenna with no apparent loss in performance in detecting targets in the main lobe due to the presence of the sidelobe suppression system.

The results can be summarized as follows:

(1) When the jamming signal is in the radar main-beam it is not suppressed. (It is more difficult to detect targets in the direction of the jammer.)

(2) When the jamming signal arrives through the main antenna side lobes it is suppressed.

(3) A reduction in probability of detection with the jammer in the sidelobes was not observed in the tests made for duty cycles used. Detection probability was greatly reduced without the sidelobe blanking system in operation.

(4) It is shown in Appendix B that for strong jamming signals in the sidelobes and for jamming duty cycles small compared to one, the probability of detection in the main lobe is virtually one.

The antenna patterns shown in Fig. IV-4 indicate that with equal gain in the two channels, the system should be capable of blanking only the signals arriving through the back and secondary side lobes of the main antenna. If it is remembered that the losses in between the omnidirectional antenna and its receiver are 17 dB, compared with 1 dB

AD-A039 159 NAVAL POSTGRADUATE SCHOOL MONTEREY CALIF F/G 17/9
IMPLEMENTATION OF A SIDELOBE BLANKING SYSTEM ON THE AN/SPS-12 R--ETC(U)
MAR 77 P P ARANCIBIA

UNCLASSIFIED NL

2 OF 2
ADA
039159

END
DATE
FILMED
5-77

in the main channel from the radar antenna to its receiver, it can be expected that if the losses in the auxiliary channel are reduced to the same level as in the main channel, the system will be able to blank any signal which is not main-beam without introducing extra gain in the auxiliary receiver.

This is shown in Fig. VII-1 where the pattern of the omnidirectional antenna was increased by 16 dB.

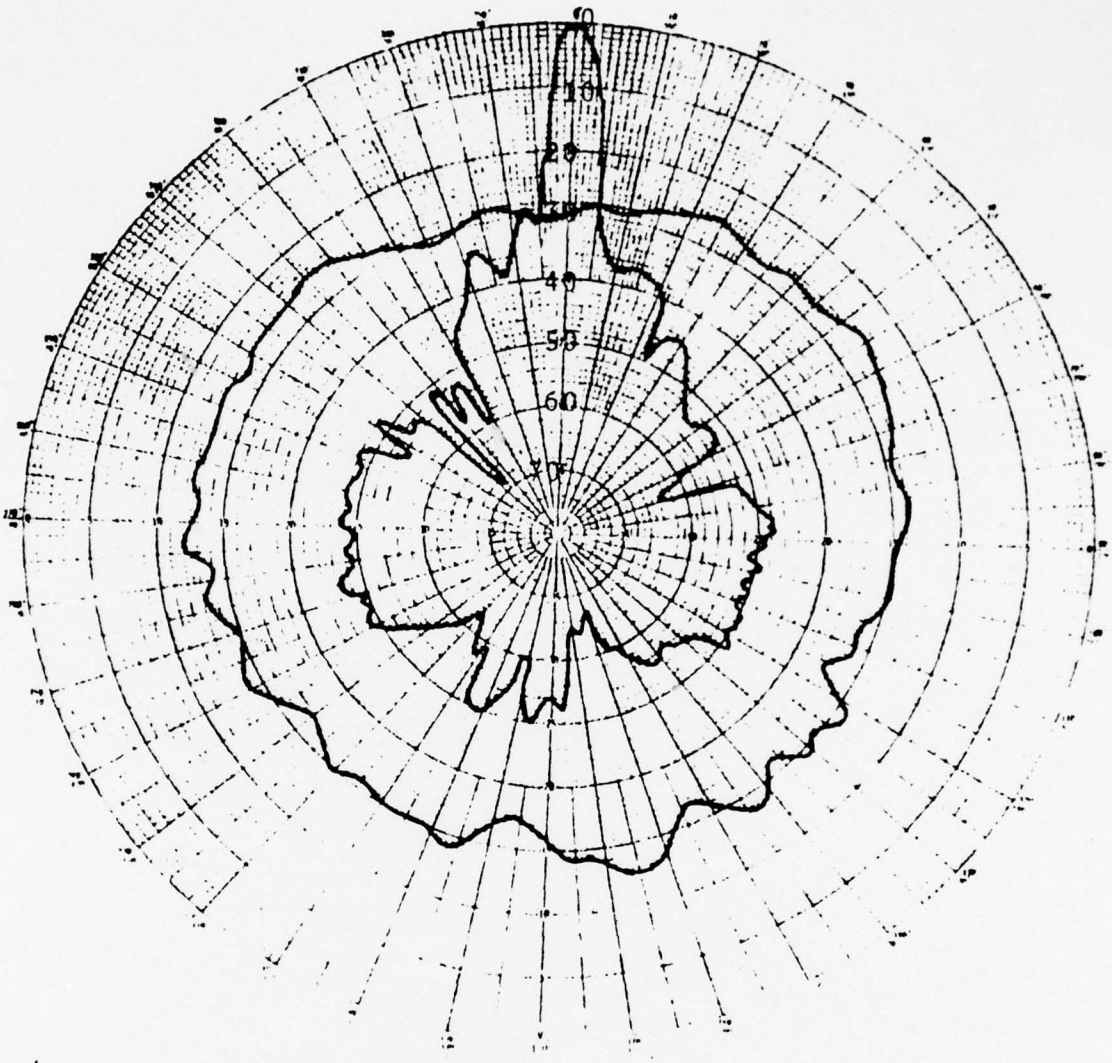

HORIZONTAL PATTERN
RADAR AND OMNIDIRECTIONAL ANTENNA(SUPERIMPOSED)
HORIZONTAL POLARIZATION
FRECUENCY : 1320 MHZ
(Scale in dB of attenuation to maintain constant output at the receivers, and normalized to 0 dB at the pattern peak for the radar antenna)

FIG. VII-1

APPENDIX A

SIDELOBE-CLUTTER BLANKING TECHNIQUE [REF 1]

One of the crucial problems affecting the success of AMTI radar systems, operating either over land or in proximity to a land mass, is the existence of very intense ground clutter patches or individual scattering objects. Such clutter signals may be strong enough to be detectable even when entering the antenna sidelobes.

Signals entering the sidelobes will in general have doppler velocities within the acceptance band of the MTI filter or filter bank. The result is an unacceptable frequency of false alarms. Therefore, sidelobe clutter can severely degrade the overland or near-land performance of airborne search radars.

The method of sidelobe clutter blanking is based on processing a sequence of outputs (radar returns) from both a sum and a monopulse difference channel. This dual output sequence is tested to determine whether the signal in any given resolution element arises from the antenna main beam or not. However with this technique there is a loss of detection sensitivity caused by the sidelobe blanking. The technique can be described as follows.

It is assumed that a scanned array antenna is used for both transmitting and receiving, and that different beams can be formed simultaneously by using different element

weights in the antenna's beam-forming circuitry. Beam forming can be done either at RF or video. Formation of symmetrical (sum) or anti-symmetrical (difference) beams at RF is accomplished by employing antenna-element weights. A sum beam is formed by using an even set of weights and a difference beam by using an odd set of weights, as shown in Fig. A-1.

Using three sets of element weights, two beams are formed at video. One set of elements weights is real, and is used to form a transmit beam directly along the antenna boresight. The other two sets of weights are complex (they include a phase shift from element to element) so that two receive-beams are formed, each squinted slightly off boresight.

The difference in azimuth between the peaks of the received beams is the beam separation (Fig. A-2).

After amplification by the receiver and passage through MTI or doppler filters, the outputs of the left and right beams are combined non-coherently to form sum and difference channels. The sum channel output is simply the sum of the magnitudes of the signals from the left and right beams.

The difference channel output is the difference in magnitudes of the signals from the left and right beams, divided by the sum channel. Due to this normalization to the sum channel, the difference channel can be referred to as the normalized difference channel.

As the main beam sweeps across a target, the sequence of pulses from the normalized difference channel follows a distinct pattern; typically that shown in Fig. A-3.

This pattern has the same shape that the difference beam has around boresight. Thus, if a signal comes from the main beam, rather than from a sidelobe, the sequence of pulses from the difference channel will be identical (neglecting receiver noise) with the shape of the difference beam.

To test whether or not a signal is from the main beam, a cross-correlation is made between the sequence of pulses emanating from the difference channel and the sequence which would eliminate due to a point target in the main beam. The output of this correlation is referred to as the correlated difference channel.

If a signal is in fact from a target in the main beam, the correlated difference channel will have a value near +1.

On the other hand, due to the gross difference in shape between the main beam and sidelobes, a signal coming through the sidelobes will seldom correlate with the response expected in the main beam, in which case the correlated difference channel will have a relatively low or negative output. Of course, because the sidelobes do occasionally resemble the main beam, occasional false alarms will still occur in the correlated difference channel.

To minimize this, conventional integration and detection is performed on the output of the sum channel.

Since the sidelobes of the sum beam are generally uncorrelated with those of the difference beam, false alarms seldom occur in both channels simultaneously, so the total system's false alarm performance is very good.

This technique of "sidelobe clutter Blanking" was studied and the entire AMTI radar system (radar system, radar aircraft, target/clutter environment), was simulated on a computer [Ref. 1].

A block diagram of the entire radar system is shown in Fig. A-4.

The elements necessary for an MTI search radar employing this proposed sidelobe clutter blanking technique are:

1. A Monopulse Antenna

The test as to whether or not a target is in the main beam is based on the fact that the sequence of outputs will have a different pattern according to whether a target is in the main beam or in the sidelobes.

In principle, the test could be performed without a monopulse antenna; however, performance would then be degraded for fluctuating targets (if the target fluctuation time was less than the total illumination time). This is the main reason for the monopulse feature.

If a phased array is used, the monopulse feature can be realized by conventional beam-forming methods.

The phased array has been chosen for this exposition, though there is no reason to believe that other monopulse systems would not work equally well.

In any case, two separate receiving beams, displaced from each other in azimuth, are utilized.

2. A Clutter Suppression System for Each of the Two Receive Beams

Best performance can be expected from a bank of doppler filters, since individual doppler cells could then be blanked, but for ease of implementation a 3-pulse canceller can be used for this function.

3. A Video Processor

This part of the system must perform the following operations:

(a) Form both the normalized difference channel and sum channel outputs. Specifically, let:

v_i^{ℓ} = output of the MTI after the ith pulse for the left receive channel

v_i^{r} = output of the MTI after the ith pulse for the right receive channel

S_i = sum channel output

D_i = difference channel output

Then from the envelopes of v_i^{ℓ} and v_i^{r} we have

$$S_i = |v_i^{\ell}| + |v_i^{r}|$$

$$D_i = \frac{|v_i^{\ell}| - |v_i^{r}|}{|v_i^{\ell}| + |v_i^{r}|} \qquad \text{if } S_i \geq \text{threshold}$$

$$D_i = 0 \qquad \text{if } S_i < \text{threshold}$$

(b) Quantizes the difference channel.

This can be done for processing simplicity. For example,

$$D_i^{*} = 1 \qquad \text{if } D_i > 0$$

$$D_i^{*} = -1 \qquad \text{if } D_i < 0$$

(c) Makes a cross-correlation.

For a sequence of N pulses between the normalized difference channel output and the (noise free) response predicted from the known monopulse main beam pattern.

N is an adjustable design parameter roughly equal to the number of pulses emitted during the time the main-beam of the monopulse pattern illuminates the target.

The normalized correlated difference channel output c_i^{d} is thus defined by

$$c_i^{d} = \frac{\sum_{j=1}^{N} W_j D_{i-j}}{\left[\left(\sum_{j=1}^{N} W_j^{2}\right)\left(\sum_{j=1}^{N} D_{i-j}^{2}\right)\right]^{1/2}}$$

where the weights W_j are

W_j = the expected responses, and,

D_{i-j} = a sequence of pulses from the normalized difference channel.

(d) Performs a conventional noncoherent integration of the sum channel.

This is accomplished by taking the running sum over N pulses. The integration interval N is identical to the cross-correlation interval of the normalized difference channel.

The integrated sum channel output c_i^s is thus:

$$c_i^s = \sum_{j=1}^{N} S_{i-j}$$

(e) Performs threshold test.

This is done on both the normalized correlated difference channel output c_i^d and the integrated sum channel output c_i^s. Detection requires the outputs of both channels to simultaneously surpass their respective thresholds.

Inclusion of the above listed components in a radar system can have many advantages. For example, the resulting clutter blanking technique not only discriminates against false alarms caused by clutter, but also against false alarms caused by receiver noise. This is because it

is very unlikely that N sequential pulses of noise in the difference channel will be highly correlated with the distinct shape of the difference-channel near main beam. As a result, the conventional sum channel threshold which eliminates noise-generated false alarms can be set very low.

The improved performance in a clutter environment provided by this technique is obtained at a cost of reduced performance in the absence of clutter. For example, a slight degradation of detection sensitivity occurs when the only interference is receiver noise. This is because noise in the normalized difference channel decreases the correlation between a true target return from the main beam and the expected noise-free pattern.

A target with low signal-to-noise ratio which could be detected by a conventional processor may be rejected because the correlated difference channel does not surpass its threshold.

Receiver noise will also degrade the accuracy of beam-splitting if it is performed on the correlated difference channel. Noise may cause the peak of the correlation to occur at an azimuth slightly different from the target azimuth. However, an improvement in overall beam-splitting accuracy is expected.

Summary

The principal results can be summarized as follows:

This technique represents a powerful method for eliminating false alarm caused by discrete sidelobe clutter. It is

effective against both scintillating and constant clutter echoes.

The reduction of false alarms is directly proportional to the threshold applied to the correlated difference (blanking) channel. Thus, the problem of ring-around encountered by many present AMTI radars in operation near or over land can be virtually eliminated by raising the blanking threshold.

However, this reduction of ring-around is offset by a degradation in target detection sensitivity in environments of distributed clutter or noise. This loss varies from 2 to 8 dB, depending on the environment, the system configuration, and the desired detection probability.

Results of this work show that a relatively high threshold in the correlated difference (blanking) channel is necessary to effectively blank discrete sidelobe clutter. However, a low threshold is adequate to blank distributed clutter.

A tradeoff therefore results between blanking discrete clutter and detecting targets in distributed clutter. The compromise depends critically on the environment.

If the radar is flown in environments with a large number of discrete scatterers, such as near a coastline backed by cliffs, then blanking may be a necessity, despite the slight loss in detection sensitivity.

Thus, the technique of sidelobe clutter blanking improves coastal surveillance techniques by enabling the radar bearing

aircraft to fly very close to shore and by reducing the ring-around which currently obscures targets near land.

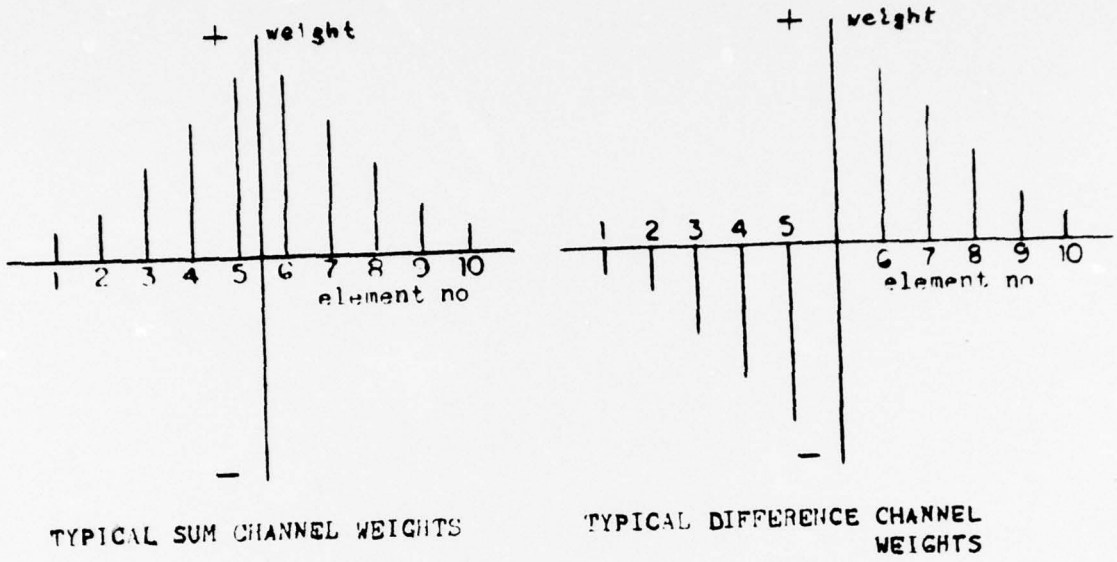

TYPICAL SUM CHANNEL WEIGHTS

TYPICAL DIFFERENCE CHANNEL WEIGHTS

TYPICAL ELEMENT WEIGHTS FOR RF BEAM FORMATION

FIG. A-1

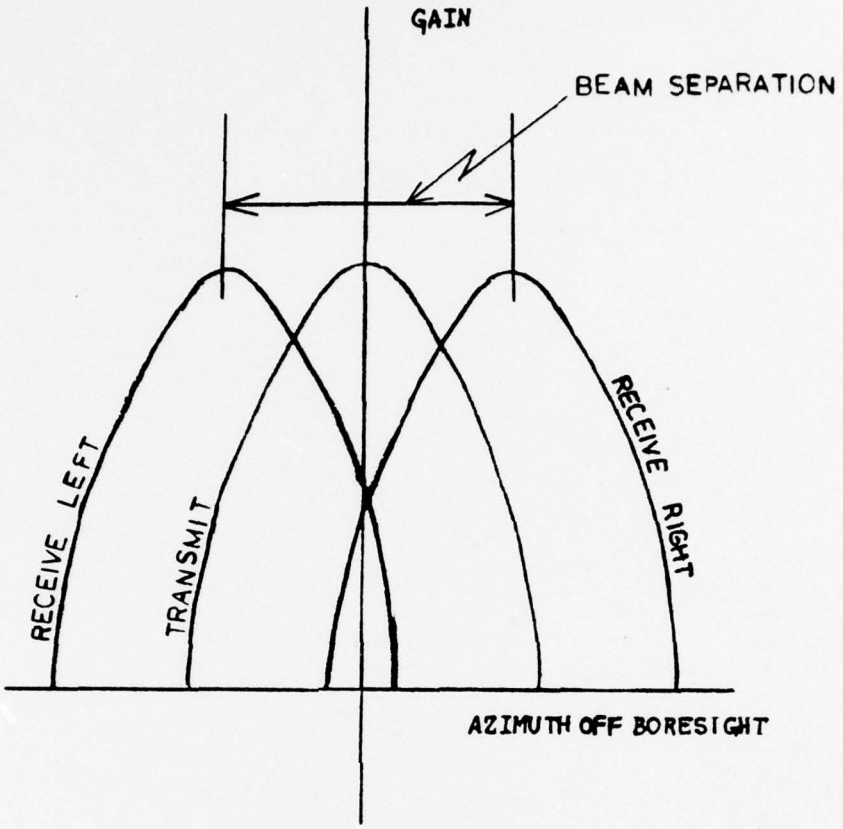

TRANSMIT AND RECEIVE BEAMS

FIG. A-2

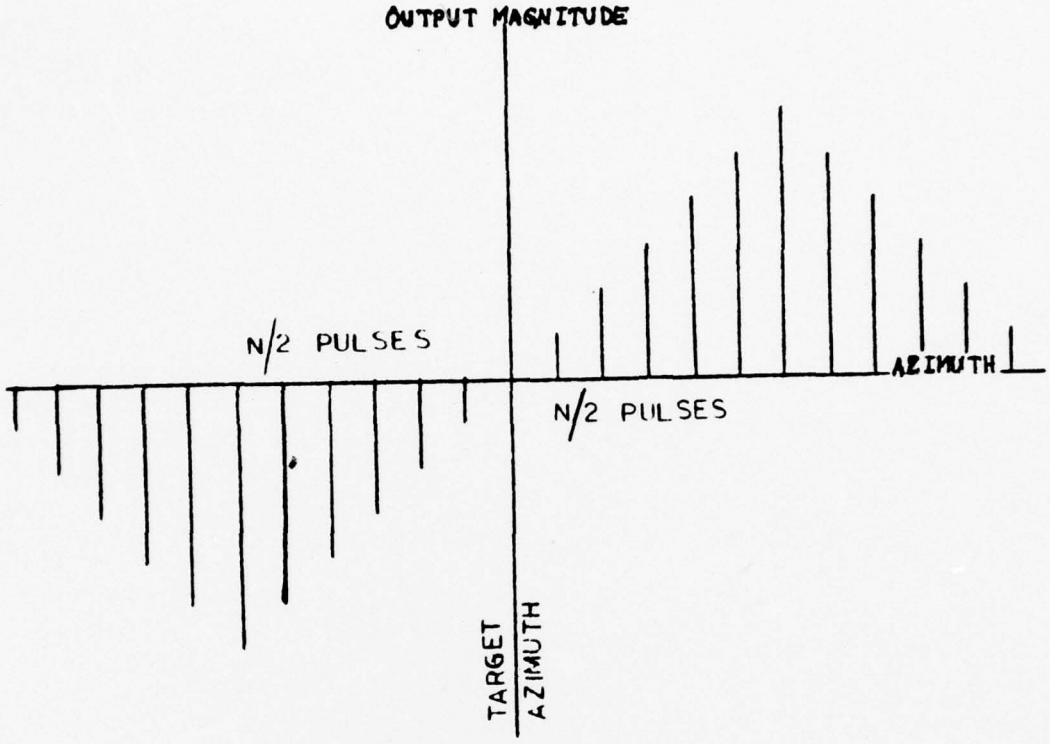

NORMALIZED DIFFERENCE CHANNEL OUTPUT

FIG. A-3

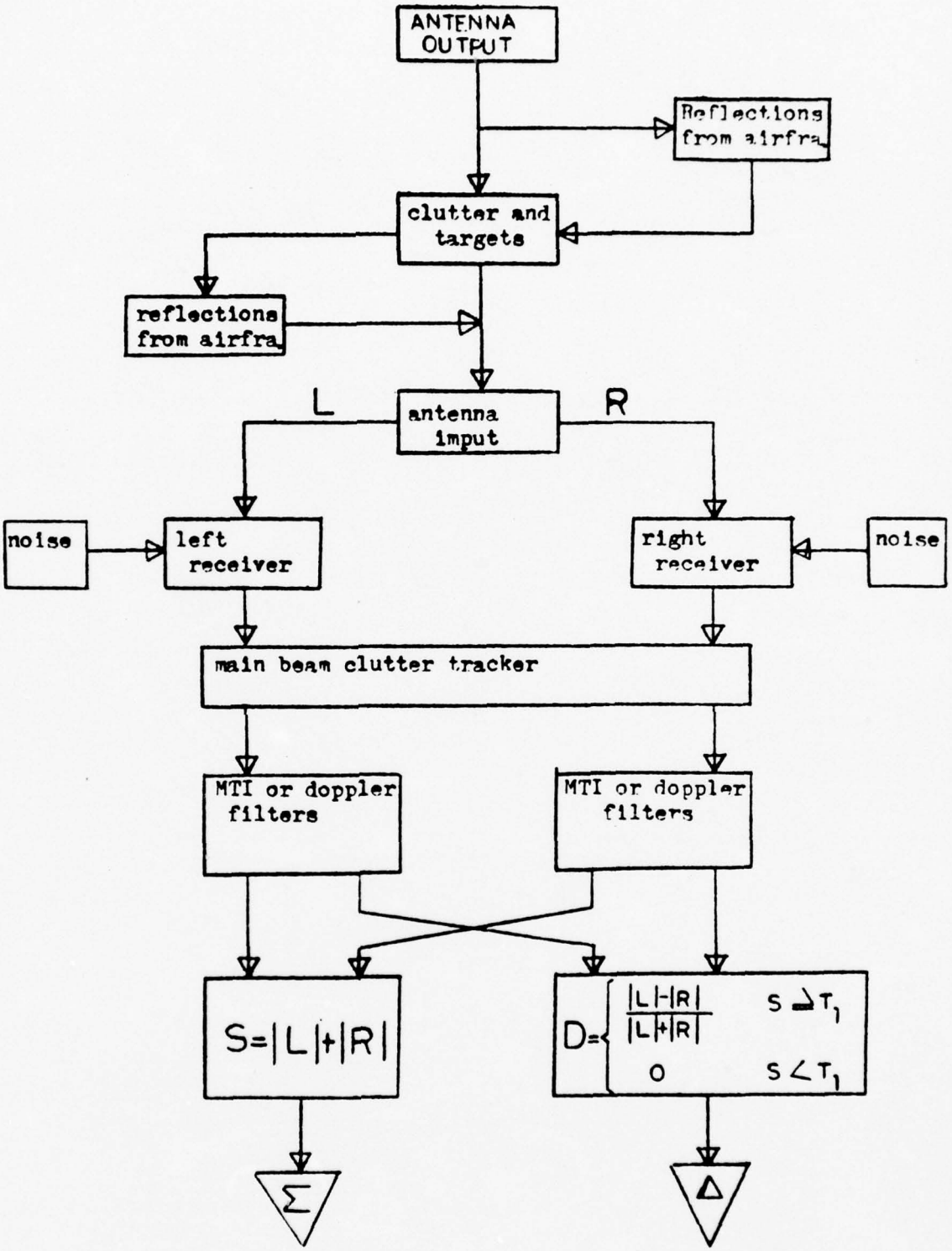

RADAR SYSTEM BLOCK DIAGRAM (REF. 1)

FIG A-4

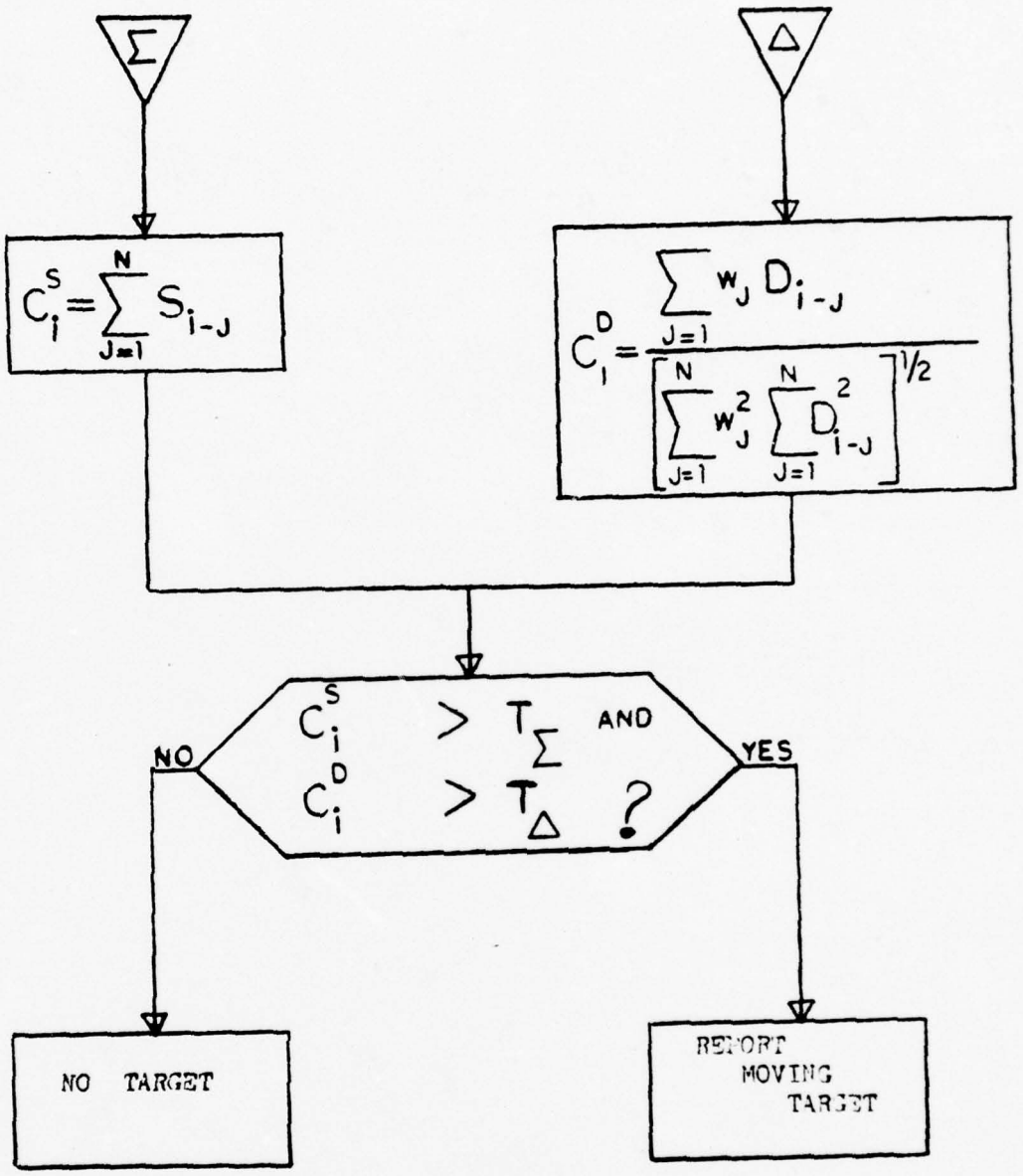

RADAR SYSTEM BLOCK DIAGRAM

FIG A-4 (cont.)

APPENDIX B

The Q function occurs frequently in radar detection theory and in problems involving the bivariate normal distribution. The Q function can be defined:

$$A(a,t) = \iint_{(x^2+y^2)>t^2} e^{-[(x-a)^2 + \frac{y^2}{2}]} \frac{dx\,dy}{2\pi} \qquad \text{[Ref. 9]}$$

$$Q(a,t) = 1 - \int_0^t u\, I_o(au)\, e^{-(u^2+a^2)/2}\, du$$

A recursive procedure which is well suited for rapid machine computation is as follows:

$$Q(a,t) = 1 - \int_0^t u\, I_o(au)\, e^{-(\frac{u^2+a^2}{2})}\, du \qquad (1)$$

where $I_o(au) = I_o(x) = J_o(ix)$ is the modified Bessel Function of first kind and of order zero given in series form by

$$I_o(x) = \sum_{n=0}^{\infty} (\frac{x}{2})^{2n} \frac{1}{(n!)^2} \qquad (2)$$

Substituting equation (2) in (1) yields

$$Q(a,t) = 1 - \int_0^t u \left[\sum_{n=0}^{\infty} \cdot \left(\frac{au}{2}\right)^{2n} \frac{1}{(n!)^2} \right] e^{-\left(\frac{u^2+a^2}{2}\right)} du \quad (3)$$

$$= 1 - \sum_{n=0}^{\infty} \left[\frac{1}{n!} \left(\frac{a^2}{2}\right)^n e^{-\frac{a^2}{2}} \right] \left[\frac{1}{2^n (n!)} \int_0^t u^{2n+1} e^{-\frac{u^2}{2}} du \right]$$

$$Q(a,t) = 1 - \sum_{n=0}^{\infty} k_n(a)\, g_n(t) = 1 - [k_o g_o + k_1 g_1 + k_2 g_2 + \ldots]$$

where

$$k_n(a) = \frac{1}{n!} \left(\frac{a^2}{2}\right)^n e^{-\frac{a^2}{2}} \quad (4)$$

and

$$g_n(t) = \frac{1}{2^n (n!)} \int_0^t u^{2n+1} e^{-\frac{u^2}{2}} du \quad (5)$$

substituting

$$u^2 = t^2 v \quad (6)$$

into equation (5) yields

$$g_n(t) = \frac{1}{2^n (n!)} \int_{u=0}^{u=t} (u^2)^n e^{-\frac{u^2}{2}} \frac{d(u^2)}{2}$$

$$= \frac{1}{2^{n+1} (n!)} \int_{v=0}^{v=1} (t^2 v)^n e^{-\frac{t^2 v}{2}} d(t^2 v)$$

$$g_n(t) = \left(\frac{t^2}{2}\right)^{n+1} \frac{1}{(n!)} \int_{v=0}^{v=1} v^n e^{-\frac{t^2 v}{2}} dv \qquad (7)$$

Note from equation (4) that

$$k_n(a) = \frac{1}{n(n-1)!} \left(\frac{a^2}{2}\right)^{n-1} \left(\frac{a^2}{2}\right) e^{-\frac{a^2}{2}} \qquad (8)$$

and

$$k_{n-1}(a) = \frac{1}{n(n-1)!} \left(\frac{a^2}{2}\right)^{n-1} e^{-\frac{a^2}{2}}$$

then

$$k_n(a) = \frac{a^2}{2n} k_{n-1}(a) \qquad (9)$$

Thus, the values of $k_n(a)$ can be obtained recursively,

$$k_o(a) = e^{-\frac{a^2}{2}}$$

$$k_1(a) = \frac{a^2}{2} k_o(a)$$

$$k_2(a) = \frac{a^2}{2 \cdot 2} k_1(a)$$

$$k_3(a) = \frac{a^2}{2 \cdot 3} k_2(a)$$

$$\vdots$$

$$k_n(a) = \frac{a^2}{2 \cdot n} k_{n-1}(a)$$

by the use of equation (9). Similarly, the values of $g_n(t)$ can be obtained recursively. Integrating

$$\int_0^1 v^n e^{-\frac{t^2 v}{2}} dv = \frac{v^n e^{-\frac{t^2 v}{2}}}{(-\frac{t^2}{2})} \Bigg|_0^1 - \frac{n}{(-\frac{t^2}{2})} \int_0^1 v^{n-1} e^{-\frac{t^2 v}{2}} dv$$

$$= -\frac{2}{t^2} e^{-\frac{t^2}{2}} + \frac{2n}{t^2} \int_0^1 v^{n-1} e^{-\frac{t^2 v}{2}} dv$$

Thus,

$$g_n(t) = (\frac{t^2}{2})^{n+1} \frac{1}{n!} [-\frac{2}{t^2} e^{-\frac{t^2}{2}} + \frac{2n}{t^2} \int_0^1 v^{n-1} e^{-\frac{t^2 v}{2}} dv]$$

$$= -\frac{1}{n!} (\frac{t^2}{2})^n e^{-\frac{t^2}{2}} + (\frac{t^2}{2})^n \frac{1}{(n-1)!} \int_0^1 v^{n-1} e^{-\frac{t^2 v}{2}} dv$$

$$g_n(t) = g_{n-1}(t) - \frac{1}{n!} (\frac{t^2}{2})^n e^{-\frac{t^2}{2}} \qquad (10)$$

Now from equations (7) and (10)

$$g_o(t) = \frac{t^2}{2} \int_0^1 e^{-\frac{t^2 v}{2}} dv = [-e^{-\frac{t^2 v}{2}}]_0^1 = 1 - e^{-\frac{t^2}{2}}$$

$$g_1(t) = g_o(t) - (\frac{t^2}{2}) e^{-\frac{t^2}{2}}$$

$$g_2(t) = g_1(t) - \frac{1}{2!} (\frac{t^2}{2})^2 e^{-\frac{t^2}{2}}$$

$$g_3(t) = g_2(t) - \frac{1}{3!}\left(\frac{t^2}{2}\right)^3 e^{-\frac{t^2}{2}}$$

$$\vdots$$

$$g_n(t) = g_{n-1}(t) - \frac{1}{n!}\left(\frac{t^2}{2}\right)^n e^{-\frac{t^2}{2}} \qquad (11)$$

Then for a specific pair of values a, and t,

$$Q(a,t) = 1 - k_o g_o - k_1 g_1 - k_2 g_2 - k_3 g_3 - \ldots - k_n g_n$$

where $k_n(a)$ is obtained from equation (8) and $g_n(t)$ is obtained from equation (11) for n = 0,1,2,... . (The function g_n is the incomplete gamma function divided by n factorial.)

After N iterations, the error in Q is given by the remainder term,

$$R_N = \sum_N^\infty g_n k_n$$

$$R_N = k_N \left(\frac{t^2}{2}\right)^{N+1} \sum_{m=0}^{\infty} \left[\frac{N!}{(N+m)!}\right]^2 \int_0^1 \left(\frac{a^2 t^2 u}{4}\right)^m u^N e^{-\frac{t^2 u}{2}}\, du$$

where $N!/(N+m)! < N^{-m}$.

Then replacing u in the first term of the integrand by one, its upper bound in the interval of integration. Then summing the series in m gives:

$$R_N < k_N g_N / (1 - \frac{a^2 t^2}{4N^2}) \quad \text{for} \quad N > \frac{at}{2}$$

The remainder bound can be calculated during each iteration, and the series for Q truncated when $N > \frac{at}{2}$ and R_N is less than the desired accuracy. $\frac{t^2}{2}$, $\frac{a^2}{2}$, $e^{-\frac{t^2}{2}}$, need only be computed once at the beginning of the iteration, so that the computation of successive terms in the series is very rapid.

To avoid computation of R_N during each iteration, an alternative bound can be used,

$$R_{N+1} = R_N - k_N g_N < k_N g_N / (\frac{4N^2}{a^2 t^2} - 1) \leq k_N g_N \quad \text{for} \quad N \geq \frac{at}{\sqrt{2}}$$

The summation can be terminated when $k_N g_N$ is smaller than the desired error bound and $N > at/\sqrt{2}$.

Figure B-1 shows the number of iterations required to satisfy the condition $k_N g_N < 10^{-3}$, and Figure B-2, the condition $k_N g_N < 10^{-5}$.

The convergence is very rapid, once the series approaches the correct value of Q. For example, at a = t = 6, increasing N from 25 to 30 improves the accuracy by a factor of 100.

For large values of (a·t) more iterations than indicated in the figures are required to satisfy the condition $N > (a \cdot t)/\sqrt{2}$.

This recursive method can be used to compute detection probabilities for a radar which integrates a train of pulses incoherently. When N samples of the envelope squared (output of square-law-second detector) are added and the sum compared with a threshold t, the detection probability is

$$P_D = e^{-\frac{Na^2}{2}} (Na^2)^{\left(\frac{1-N}{2}\right)} \int_t^\infty z^N e^{-\frac{z^2}{2}} I_{N-1}(aZ\sqrt{N})\, dZ$$

Again the modified Bessel function I_{N-1} is expanded in a power series and P_D is expressed as a series in which the successive terms are obtained by a recursive procedure.

Numerical results of P_D with threshold level, acquisition channel signal-to-noise ratio (SNR), and β^2 (ratio of sidelobe gain of the SLS antenna to the sidelobe gain of the acquisition antenna), for specified values of P_{fa} can be obtained using the following technique, which results in curves similar to Fig. II-5.

In calculating the probability of detection in the main lobe, r_o is taken to be zero. Therefore, in the main lobe:

$$P_{fa} = e^{-\frac{1}{2}\alpha_o} - \frac{e^{-\frac{1}{2}\alpha_o(1+F)}}{1+F}$$

$$P_D = Q(s_o, \sqrt{\alpha_o}) - \int_{\alpha_0}^\infty p_u(u)\, Q(0, \sqrt{Fu})\, du$$

which can be written as

$$P_{D_{ML}} = Q(s_o, \sqrt{\alpha_o}) - \frac{e^{\left[-\frac{s_o^2 F}{2(1+F)}\right]}}{1+F} \cdot Q\left(\frac{s_o}{\sqrt{1+F}}, \sqrt{\alpha_o(1+F)}\right)$$

$$P_{fa} = e^{-\frac{1}{2}\alpha_o} - \frac{1}{1+F} e^{-\frac{1}{2}\alpha_o(1+F)}$$

can be written in the form

$$P_{fa} = z - \frac{1}{1+F} z^{(1+F)}$$

where

$$z = e^{-\frac{\alpha_o}{2}} \qquad \alpha_o = -\ln z^2$$

let $$f(z) = z - \frac{1}{1+F} z^{(1+F)} - P_{fa} = 0$$

then

$$f'(z) = 1 - z^F$$

Newton's method can be used and iterates with

$$z_{n+1} = z_n - \frac{f(z_n)}{f'(z_n)} \qquad (n = 0,1,2,\ldots)$$

$$z_{n+1} = z_n - \left[\frac{z_n - \frac{1}{1+F} z_n^{(1+F)} - P_{fa}}{1 - z_n^F}\right]$$

$$= \frac{z_n(1 - z_n^F) - z_n + \frac{1}{1+F} z_n^{(1+F)} + P_{fa}}{1 - z_n^F}$$

$$z_{n+1} = \frac{-z_n^{(1+F)} + \frac{1}{1+F} z^{1+F} + P_{fa}}{1 - z_n^F}$$

$$z_{n+1} = \frac{P_{fa} - \frac{F}{1+F} z_n^{1+F}}{1 - z_n^F} \qquad (n=0,1,2,\ldots)$$

For example:

choosing $z_o = P_{fa}$ and $F = \beta^2$ $(r = 0)$ where $\beta = 0.25$, continuous iterations give:

For $P_{fa} = 0.001$ and $\beta = 0.25$

$F\ (r = 0)$	α_o	
$\beta^2 = 0.0625$	11.6987744	(a)
$0.629\beta^2 = 0.0393125$	10.79174229	(b)
$0.316\beta^2 = 0.01975$	9.318982595	(c)
$0.159\beta^2 = 0.0099375$	7.700747859	(d)

Then, the probabilities of detection in the main lobe will be

$$P_D = Q(s_o, 3.420347117) - \frac{e^{-s_o^2(0.0294117647)}}{1.0625} Q\left(\frac{s_o}{1.030776406}, 3.525613\right) \qquad (a')$$

$$P_D = Q(s_o, 3.285078734) - \frac{e^{-s_o^2(0.0187969924)}}{1.0390625} Q\left(\frac{s_o}{1.019344152}, 3.348625796\right) \qquad (b')$$

$$P_D = Q(s_o, 3.052700869) - \frac{e^{-s_o^2(0.009683746)}}{1.01975} Q\left(\frac{s_o}{1.009826718}, 3.082698899\right) \quad (c')$$

$$P_D = Q(s_o, 2.775022137) - \frac{e^{-s_o^2(0.0049198589)}}{1.0099375} Q\left(\frac{s_o}{1.004956467}, 2.788776442\right) \quad (d')$$

and so on for different values of P_{fa} and β given a value for s_o.

For calculating the probability of detection in the sidelobes, r_o is different from zero, and then a numerical integration must be done.

From

$$P_D = Q(s_o, \sqrt{\alpha_o}) - \int_{\alpha_o}^{\infty} p_u(u)\, Q(r_o, \sqrt{Fu})\, du$$

where

$$p_u(u) = \frac{1}{2} e^{-\frac{1}{2}(u + s_o^2)} I_o(s_o\sqrt{u})$$

a numerical integration method of the form of "global Simpson's 3/8 Rule" assumes a cubic fit to (x_i, f_i) $(i = 0,1,2,3)$ and another cubic fit to (x_i, f_i) $(i = 3,4,5,6)$, etc.

In the sidelobes P_D could be evaluated in this manner.

Choosing some small increment $\Delta u = h$, and letting

$$f(u) = p_u(u)\, Q(r_o, \sqrt{Fu}) = \frac{1}{2} e^{-\frac{1}{2}(u+s_o^2)} I_o(s_o\sqrt{u})\, Q(s_o, \sqrt{Fu})$$

(in the sidelobes $r_o = \beta s_o$)

then with $u_o = \alpha_o$

$$f_o = f(u_o) = f(\alpha_o)$$

$$f_1 = f(u_1) = f(u_o+h) = f(\alpha_o+h)$$

$$f_2 = f(u_2) = f(u_o+2h) = f(\alpha_o+2h)$$

$$f_3 = f(u_3) = f(u_o+3h) = f(\alpha_o+3h)$$

$$f_4 = f(u_4) = f(u_o+4h) = f(\alpha_o+4h)$$

$$\vdots$$

$$f_n = f(u_n) = f(u_o+nh) = f(\alpha_o+nh)$$

and then

$$P_D = Q(s_o, \sqrt{\alpha_o}) - \frac{3h}{8} [f_o + 3f_1 + 3f_2 + 2f_3 + 3f_4 + 3f_5 + 2f_6 + 3f_7 + 3f_8 + 2f_9 + \ldots]$$

and the process may be stopped when $\left|\frac{3h}{8} f_n\right| < \varepsilon$ for some value of n.

Using the recursive procedure developed for the Q function and the incomplete gamma function g_n, a computer program was constructed to obtain the false-alarm probability and the main-lobe-detection probability with the following

parameters; predetection output of the radar receiver (A), threshold detector of the sidelobe blanking system (TH), and the ratio of sidelobe gain of the sidelobe suppression antenna to the sidelobe of the radar antenna (F).

For the values

A = 5.0 volts

TH = 0.25 volts below detection output (measured)

F = 1.1 from Fig. III-1

the false-alarm probability and main-lobe-detection probability for the system turn out to be

$$P_{fa} = 0.09$$

$$P_D = 1.0 \quad .$$

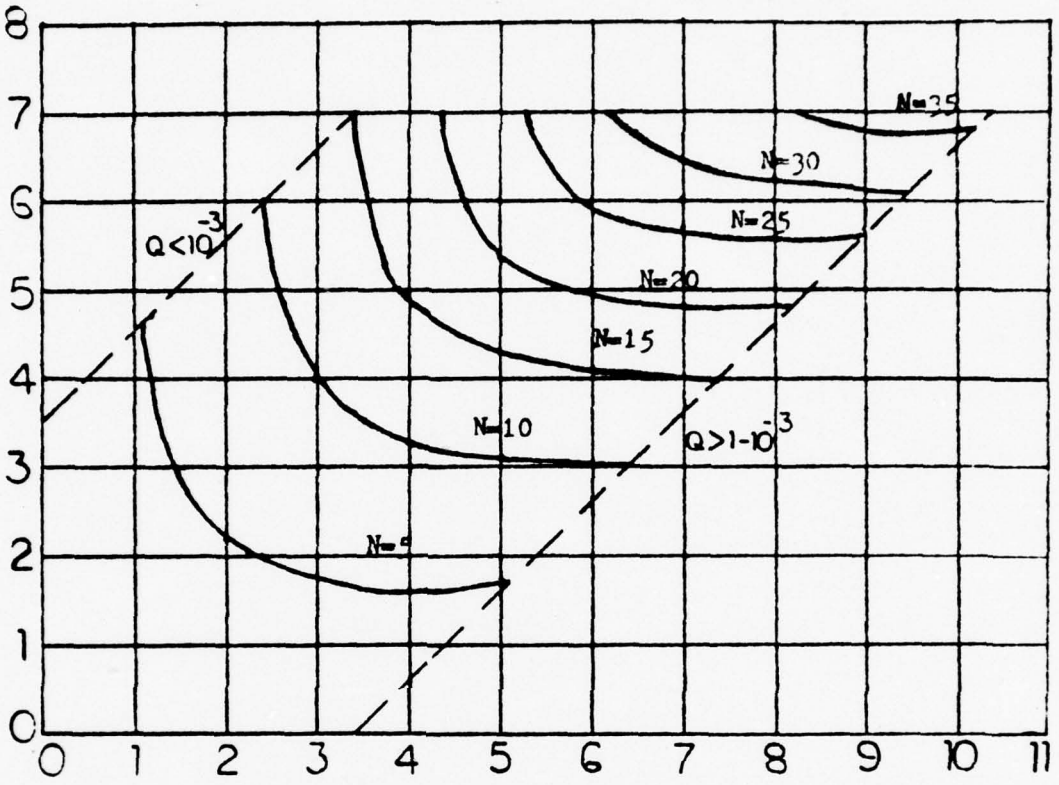

Number of iterations required for $K_N G_N < 10^{-3}$

FIG. B-1

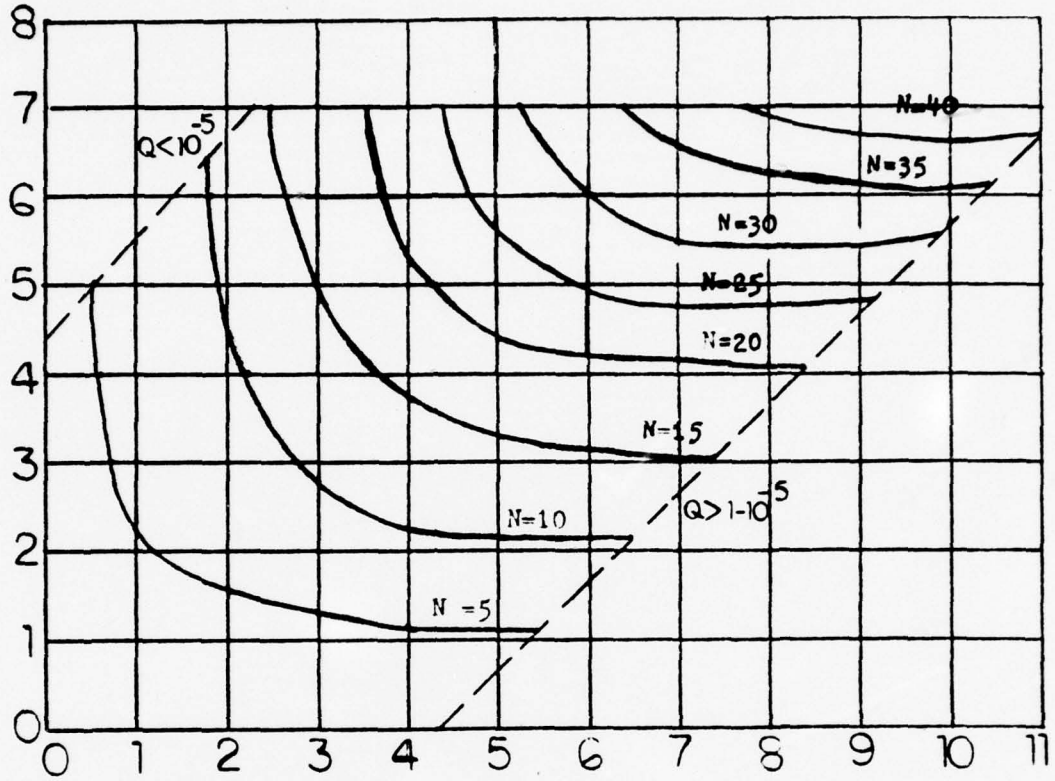

Number of iterations required for $K_N G_N < 10^{-5}$

FIG. B-2

COMPUTER PROGRAM FOR CALCULATING THE FALSE-ALARM PROBABILITY AND THE MAIN-LOBE-DETECTION PROBABILITY

```
      A=SO,  DETECTION OUTPUT OF RADAR RECEIVER
      TH = THRESHOLD DETECTOR SLB, SYSTEM
      F = SIDELOBE GAIN SLS ANT. / SIDELOBE GAIN RADAR ANT.
      E = DESIRED ACCURACY
      PFA = PROBABILITY OF FALSE ALARM
      PD = PROBABILITY OF DETECTION IN THE MAIN LOBE

      A = 5.0
      TH = 4.75
      F = 1.1
      E = 0.00001

      T = SQRT (TH)
      PFA = EXP(-TH/2.0)-((1.0/(1.0+F))*EXP((-TH/2.0)*(1.0+F))
      PRINT, PFA

   55 J = 0
      J = J + 1

      B = (A*T)/SQRT(2.0)
      CO = EXP(A**2/(-2.0))
      GO = 1.0 - EXP(T**2/(-2.0))
      COGO = CO*GO
      QQ = 1.0 - CO*GO
      IF ((0.0.GT.B ).AND.( COGO.LT.E )) GO TO 100

      W = 1.0
      N = 0
   10 N = N + 1
      W = (1.0/FLOAT(N)) * W
      S = W
      CN = W
      CN = S*(((A**2/2.0)**N)*(EXP(A**2/(-2.0))))

      R = 1.0
      R = ((1.0/FLOAT(N))*R
      TT = R
      G = R
      IF (N.GT.1) GO TO 20
      GN = 0.0
   20 G = -TT*(((T**2/2.0)**N)*(EXP(T**2/(-2.0)))) + GN
      IF (N.GT.1) GO TO 30
      GG = GO + G
      GN = GG
      IF (N.EQ.1) GO TO 15
   30 GN = G

   15 CNGN = CN*GN
      IF (N.GT.1) GO TO 40
      Q1 = QC-CNGN
      QQ = Q1
      B = 0.0
      IF ((N.GT.B).AND.(CNGN.LT.E)) GO TO 100
      GO TO 10
   40 QA = QC + B
      QN = QA - CNGN
      B = QN
      CO = 0.0
      IF ((N.GT.B).AND.(CNGN.LT.E)) GO TO 100
      GO TO 10

  100 WRITE (6,500) N,CO,GO,GN,QN
  500 FORMAT (//,I4,5X,F14.7,5X,F14.7,5X,F14.7,5X,F14.7)
      IF (J.EQ.2) GO TO 65

      QNEIRS = QN
      ASEC = A/SQRT (1.0+F)
      A = ASEC
      TSEC = T*SQRT (1.0+F)
      T = TSEC
      IF (J.EQ.1) GO TO 55

   65 A = 5.0
      QNSEC = GN
      PD = QNEIRS - (EXP(A**2*F/(-2.0*(1.0+F)))) * QNSEC

      WRITE (6,600) PD
  600 FORMAT (////,F14.7)
      STOP
      END
```

```
 0.8976555E-01

 8          0.9069955          0.9999967        -22.3527500          1.0014280

 2          0.9931773          0.2177823          0.8742910          0.0374069

  1.0013740
```

APPENDIX C

COMPARATOR - SWITCHING - MIXER, TECHNICAL DATA

1. Technical data, comparator

Dual voltage comparator LM 319

(a) General Description

The LM 319 voltage comparator is a high speed dual comparator fabricated on a single monolithic chip. It is designed to operate over a wide range of supply voltages down to a single 5-volt logic supply and ground. Further, it has high gain and low input current.

The uncommitted collector of the output stage makes the LM 319 compatible with RTL, DTL and TTL as well as capable of driving lamps and relays at currents up to 25 mA.

(b) Features

- Typically 80 nsec response time at ±15 Volts
- Minimum fan-out of 2 each side
- Maximum input current of 1 µA over full temperature range
- Inputs and outputs can be isolated from system ground
- High common mode slew rate
- Operating temperature 0°C to +70°C

(c) Transistor 2N 3437

Silicon field effect ransistor - N channel

- Maximum Coll. Diss. at 25°C 300 mW
- f_{ab} 4.8 MHz
- h_{fe} 20

2. Technical data, switch

a) General Description

The CD 4016 is a quad bilateral switch which utilizes P-channel and N-channel complementary MOS (CMOS) circuits to provide an extremely high "OFF" resistance and low "ON" resistance switch. The switch will pass signals in either direction.

b) Features

- High noise immunity .45 V_{CC} typ.
- High degree of linearity .5% distortion typ. @ f_{is} = 1 kHz
- Transmits frequencies up to 10 MHz
- Extremely low "OFF" switch leakage resulting in very low offset current and high effective "OFF" resistance
  10 pA typ. @ $V_{DD} - V_{ss}$ = 10 V, T_A = 25°C
- Extremely high control input impedance (control circuit isolated from signal circuit) -10^{12} Ω typ.
- Low crosstalk between switches (-50 dB typ. @ f_{is} = 0.9 MHz, R_L = 1 kΩ)
- Matched control-input to signal-output capacitances
  Reduces output signal transients
- Supply voltage range 3V to 15V
- Range of digital and analog levels ±7.5 V peak
- Matched switch characteristics ΔRON = 40 Ω typ.

3. Technical data, mixer Microwave balanced mixer ZMA-2

a) General description

To convert an incoming RF signal to a lower frequency IF output in the radar front end. The incoming RF signal (R) is combined with a high-level oscillator signal (L.O.) and the desired IF sideband is selected at the output by appropriate filters.

b) Features

Four specially selected Schottky-barrier diodes combined with two carefully balanced wideband transformers considerably reduce the amount of RF and L.O. signals appearing at the IF output; the more effective the balance, the less stringent the demand on the IF filter.

- Frequency range, GHz L.O. 1 - 2.5
  RF 1 - 2.5
  IF DC - 0.15

- Conversion Loss, dB		Typ	Max
1.4 - 2 GHz		7.0	8.5
1.0 - 2.5 GHz		8.0	9.0

- Isolation, dB		Typ	Min
1.0 - 1.5 GHz	LO-RF	25	20
	LO-IF	50	35
1.5 - 2.0 GHz	LO-RF	22	17
	LO-IF	40	30
2.0 - 2.5 GHz	LO-RF	20	15
	LO-IF	35	25

- Signal 1 dB compression +2 dBm typ.
- Total input power 50 mW

- Total input, current peak 40 mA
- Operating and storage temperature -55°C to +100°C
- Standard LO level +7 dBm

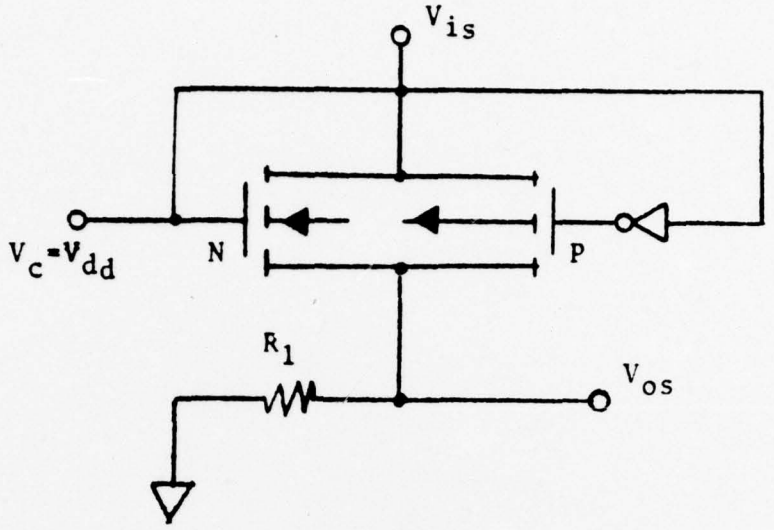

SWITCH CD 4016

FIG. C-1

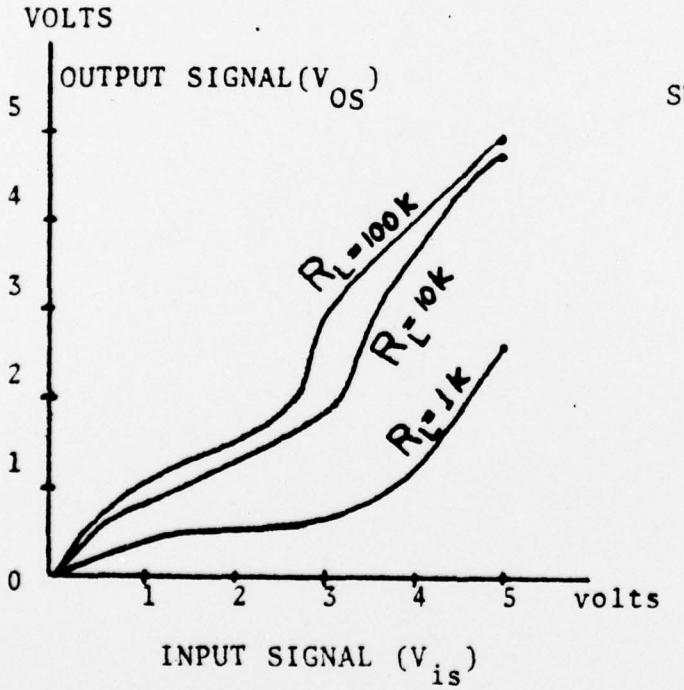

SUPPLY VOLTS V_{DD} = +5
V_{SS} = 0
T_A = 25 °C

TYP. "ON" CHARACTERISTIC FOR 1 OF 4 SWITCHES
WITH V_{DD} = +5 VOLTS, V_{SS} = 0 volts

FIG. C-2

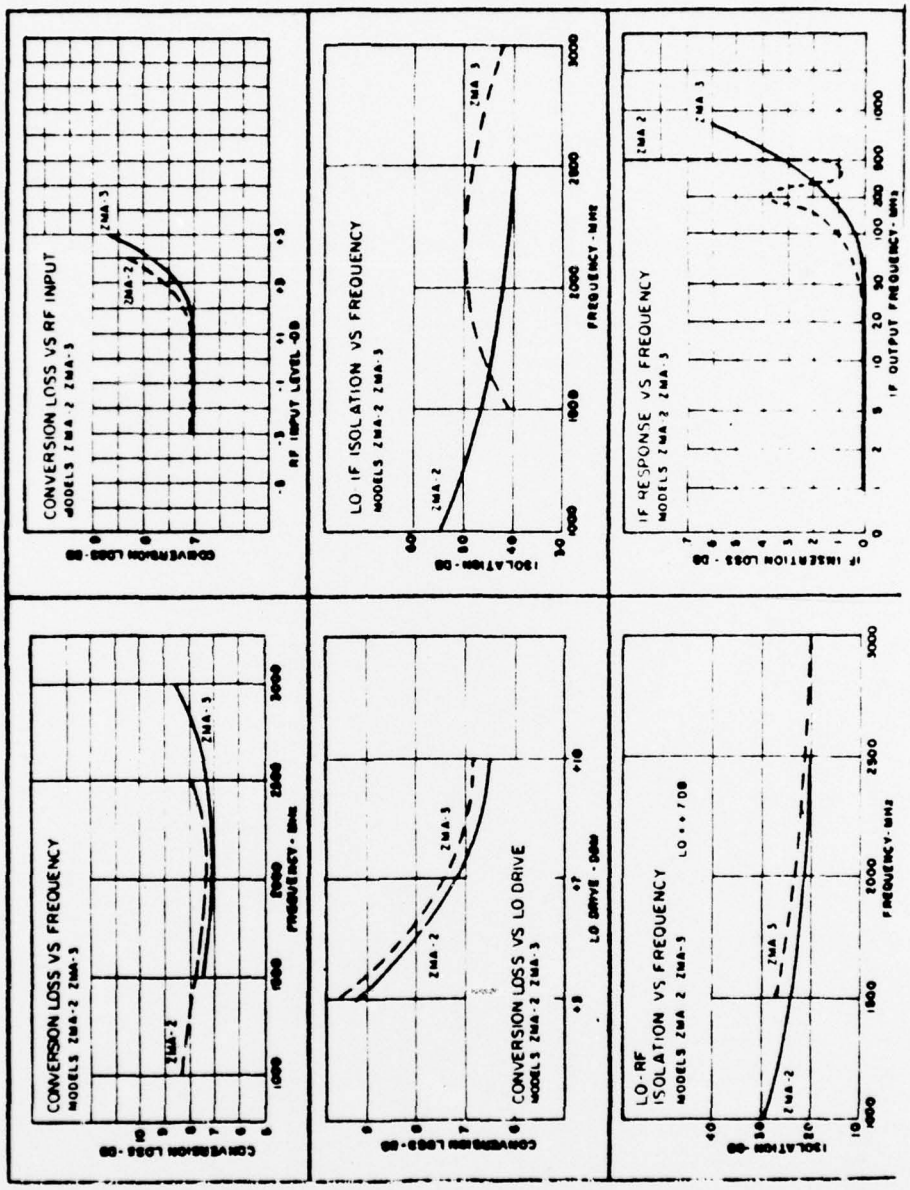

MICROWAVE BALANCED MIXER ZMA-2

FIG. C-3

APPENDIX D

The horizon range limit is given by,

$$R_h \approx \begin{cases} 4.15 \left(\sqrt{h_r} + \sqrt{h_t} \right) & \text{[km (h in meters)]} \\ 1.23 \left(\sqrt{h_r} + \sqrt{h_t} \right) & \text{[naut. mi. (h in feet)]} \end{cases}$$

[Ref. 10]

where h_r = radar antenna height, and h_t = target height. These are the conventional values based on the 4/3 earth's curvature approximation. More accurate coverage estimates for targets at all altitudes can be made using range-height-angle charts, based on ray tracing through the exponential reference atmosphere.

The average range near the horizon can be increased by directing the beam axis nearer the horizon, but the depth of nulls will be greater and they will extend further into the high-angle coverage.

Apart from lobing problems, heavy illumination of the ground can introduce intolerable clutter at short range, both from fixed objects and from moving clutter. To maintain visibility of aircraft at high elevation angles, it may be necessary to direct substantial energy into these regions while using a pattern which cuts off rapidly below the horizon.

The cosecant-squared antenna pattern has been designed to meet this requirement. With a cosecant-squared antenna

it is possible to maintain approximately constant altitude coverage at shorter range, but the gain must be greatly reduced at low angles or the cosecant-squared antenna directs much power toward the ground.

A typical vertical pattern radiation for such an antenna is shown in Fig. D-1 in which, for example, an air-surveillance radar provides coverage to 30000 ft (10 km) at 80 mi. (150 km) [Ref. 4].

Below 3°, the antenna gain peaks and falls off to its half-power point approximately at the horizon. Normally the effect of a small increase in atmospheric attenuation is included in calculating the antenna coverage at low angles, and the effect of lobing is shown as a series of lobes whose spacing depends on antenna height. The average range near the horizon can be increased by directing the beam axis nearer the horizon, but the depth of nulls will be greater and they will extend further into the high-angle coverage.

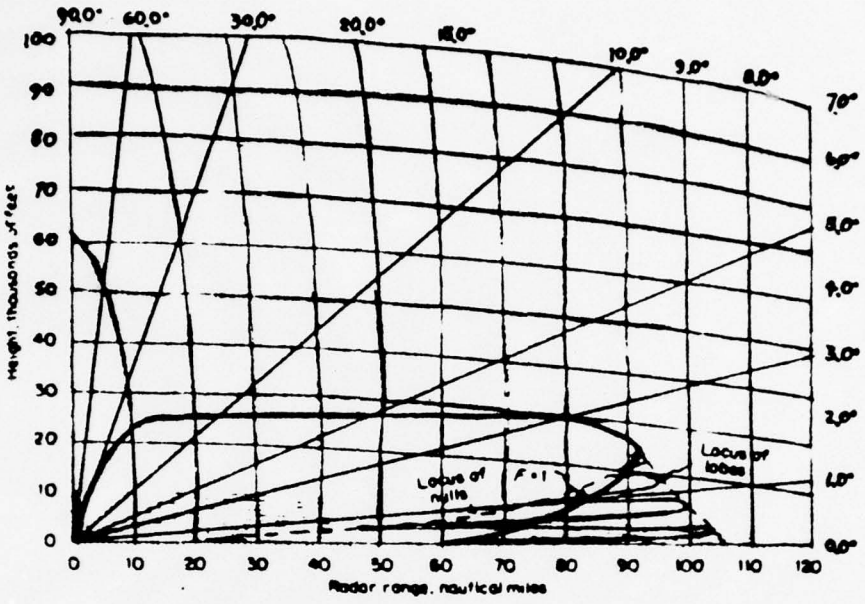

COSECANT-SQUARED AIR-SEARCH COVERAGE

FIG. D-1

APPENDIX E

SUMMARY

The whole purpose of the sidelobe blanker system can be stated as the ability to produce the maximum percent sidelobe blanking with the least system sensitivity loss. This was achieved with the signal coming from the sidelobe antenna being processed in the same manner as the signal in the radar main channel. When the SLB signal level exceeds the level in the main beam as it would for targets in the main antenna sidelobes, target detection is inhibited or blanked. When the main beam signal is greater, a target detection is reported.

The criteria for evaluating performance of the sidelobe blanker can be sensitivity reduction and percent blanking. Sensitivity reduction is defined as the increase in signal-to-noise ratio necessary for a given target to achieve the same detection probability as without the blanker. Percent blanking is defined as the percentage of sidelobe signals, uniformly distributed in angle, which are inhibited from being processed as targets.

In general comparison of the main signal and blanker antenna outputs with equal channel gains would not result in the required blanking due to transmission line losses. For this reason, normally the sidelobe blanker channel gain must be increased so that sidelobe signals produce a larger

response at the blanker channel output than the normal radar antenna channel and result in the required blanking.

The presence of the sidelobe blanker reduces the probability of detection of a target in the main beam. This is because of the finite probability that thermal noise at the blanker channel output will have a larger amplitude than signal plus noise at the receiver radar antenna output. This results in non-detection of a signal which has successfully exceeded the conventional constant false-alarm-rate threshold. Sensitivity reduction is specifically defined as "the increase in target average signal-to-noise ratio for a given target necessary to achieve the same detection probability as would be obtained with no blanker in the system." [Ref. 8]

This effect of the sidelobe blanker on system sensitivity can be better explained using Figures E-1, E-2, and E-3. Figure E-1 shows a sidelobe target producing a larger signal out of the receiver radar antenna than out of the blanker channel. This results if the blanker channel gain is too low and results in a sidelobe target which is not suppressed.

Figure E-2 is of the same sidelobe target which is successfully blanked due to an increase in blanker channel gain.

Figure E-3 shows a small target (low SNR) which is blanked even though it is in the main beam direction because blanker channel noise exceeds signal plus noise in the receiver radar antenna.

It is this latter phenomenon that reduces the P_D and must be accounted for in reassessing system detection performance with the sidelobe blanker.

An alternate measure of system sensitivity reduction can be in terms of system fractional range reduction. Specifically, the system range reduction can be defined as that percent reduction in range for a given target necessary to achieve the same probability of detection as would be obtained with no sidelobe blanker system. (With the same probability of false alarm.)

In this case, system range reduction is related to sensitivity reduction according to the equation [Ref. 8]

$$\text{Percent range reduction} = 100(10^{\frac{\Delta\overline{x}}{40}} - 1)$$

where $\Delta\overline{x}$ is the sensitivity reduction in dB.

Graphs of P_D versus target SNR with blanker channel gain as a parameter can be given in the form shown in Fig. E-4 [Ref. 8]. For a specified P_D the target SNR must increase as blanker gain increases. Sensitivity loss is measured as the increase in target SNR to maintain 95% probability of detection. The situation where blanker channel gain and receiver radar antenna gain are equal (G = 0 dB) coincides with the blanker channel G = 1 dB curve. As an example (see Fig. E-4), the sensitivity loss due to a blanker channel gain of 6 dB is about 2.2 dB for a constant $P_D = 0.95$. Depending on the constant false alarm threshold

of the radar the system can have different sensitivity losses (normally a higher CFAR threshold will have much smaller sensitivity losses).

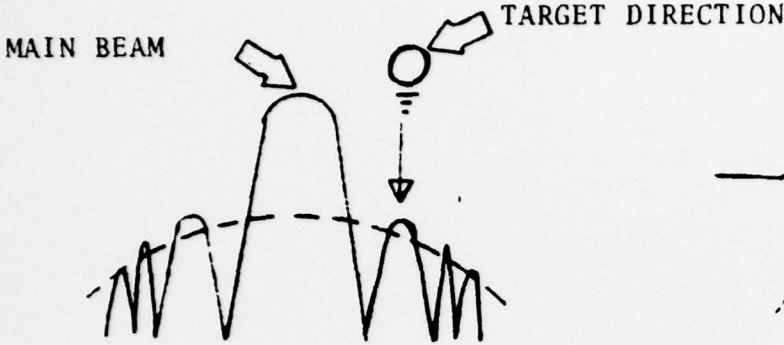

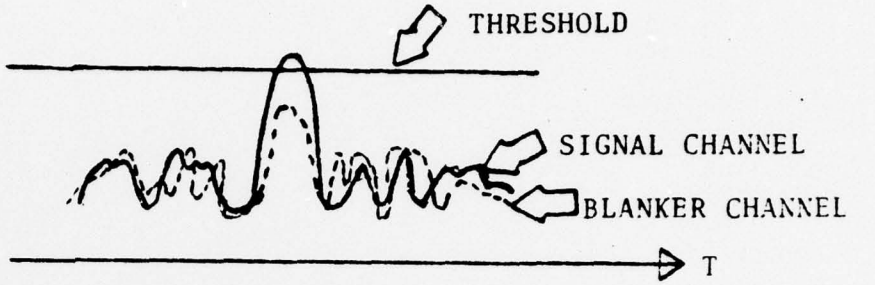

FIG. E-1

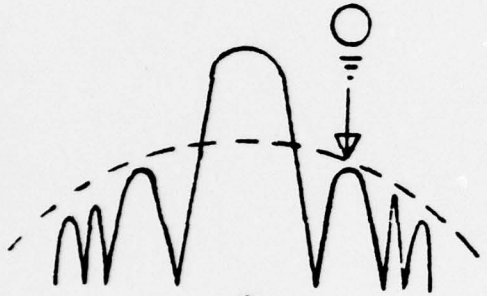

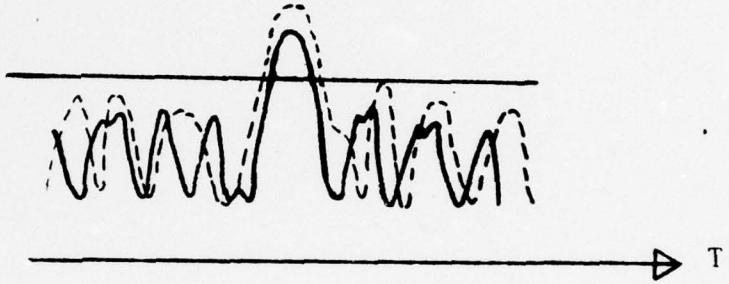

FIG. E-2

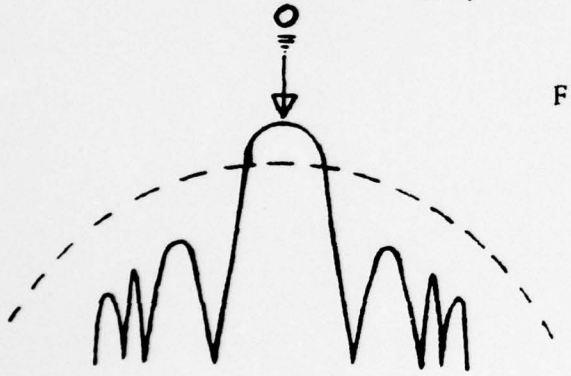

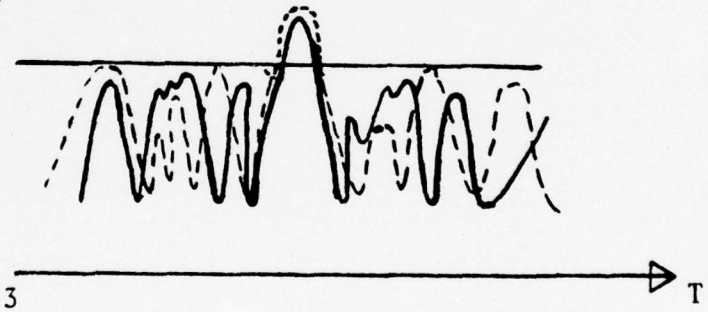

FIG. E-3

SENSITIVITY REDUCTION

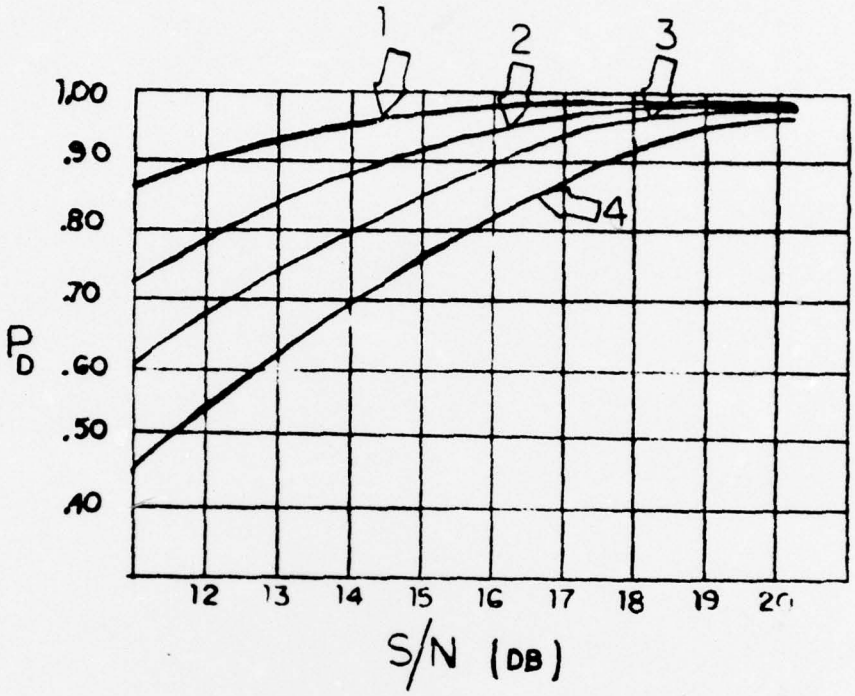

1....G=1dB
2....G=6dB
3....G=8dB
4....G=10dB

BLANKER CHANNEL
GAIN SIGNAL CURVES

PROBABILITY OF DETECTION VS. TARGET SNR
(Constant False Alarm Rate threshold=6.04dB)

FIG. E-4

BIBLIOGRAPHY

1. Technology Service Corporation, PD-016-8, January 1969, PD-016-11, April 1970.

2. Louis Maisel, "Performance of Sidelobe Blanking Systems", IEEE Trans. Aerospace and Electronics Systems, March 1967.

3. J.I. Marcum, "A Statistical Theory of Target Detection by Pulse Radar: Mathematical Appendix," April 1960.

4. Technical Manual for Radar Set AN/UPS-1, NAVSHIPS 94122.

5. Technical Manual for Radar Set AN/SPS-12, NAVSHIPS 91949(A).

6. R.H. DuHamel and D.E. Isbell, "Broadbank Logarithmically Periodic Antenna Structures," 1957 I.R.E. National Convention Record.

7. H. Jasik, "Antenna Engineering Handbook", MacGraw-Hill 1961.

8. D. Duval, A. Sinsky, D. Weber, "The AN/FPS-85 Sidelobe Blanker", Bendix Communications Division, Baltimore, Maryland.

9. I.E. Brenna, I.S. Reed, "A Recursive Method of Computing the Q Function", IEEE Trans. on Information Theory, April 1965.

10. "Electronics Engineers' Handbook", MacGraw-Hill, 1975.

11. D.K. Barton, "Radar Principles".

INITIAL DISTRIBUTION LIST

		No. Copies
1.	Defense Documentation Center Cameron Station Alexandria, Virginia 22314	2
2.	Library, Code 0142 Naval Postgraduate School Monterey, California 93940	2
3.	Department Chairman, Code 67 Department of Aeronautics Naval Postgraduate School Monterey, California 93940	1
4.	Professor David B. Hoisington, Code 62 Hs Department of Electrical Engineering Naval Postgraduate School Monterey, California 93940	1
5.	Associate Professor John M. Bouldry, Code 62 Bo Department of Electrical Engineering Naval Postgraduate School Monterey, California 93940	1
6.	Department Chairman, Code 62 Deparment of Electrical Engineering Naval Postgraduate School Monterey, California 93940	1
7.	Commandancia De La Aviacion Naval Base Aeronaval "El Belloto" Correo Naval – Valparaiso Chile	1
8.	Direccion de Armamentos de La Armada Departamento de Electronica Correo Naval – Valparaiso Chile	1
9.	Escuela de Electronica de La Armada Correo Naval – Valparaiso Chile	1
10.	LT Pedro P. Arancibia Comandancia Aviacion Naval Base Aeronaval "El Belloto" Correo Naval – Valparaiso Chile	1